INL/EXT-10-19803

Studies Related to the Oregon State University High Temperature Test Facility: Scaling, the Validation Matrix, and Similarities to the Modular High Temperature Gas-Cooled Reactor

Richard R. Schultz
Paul D. Bayless
Richard W. Johnson
Glenn E. McCreery
William Taitano
James R. Wolf

September 2010

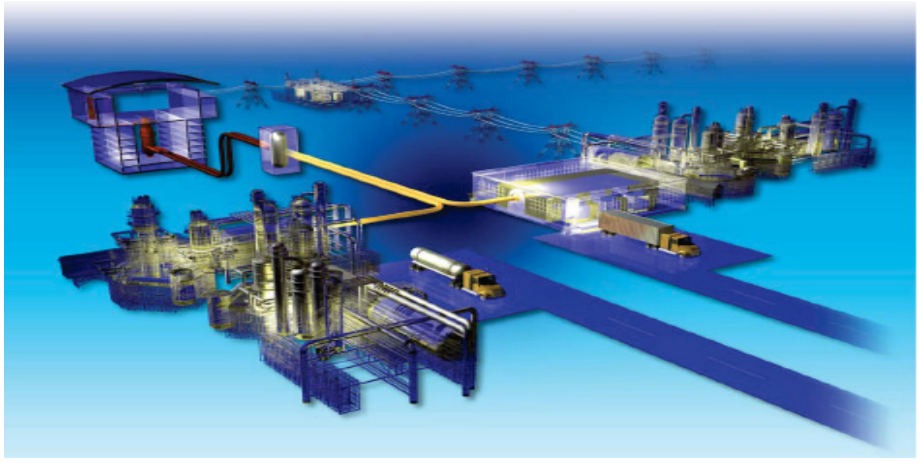

The INL is a U.S. Department of Energy National Laboratory
operated by Battelle Energy Alliance

Idaho National Laboratory

INL/EXT-10-19803

Studies Related to the Oregon State University High Temperature Test Facility: Scaling, the Validation Matrix, and Similarities to the Modular High Temperature Gas-Cooled Reactor

Richard R. Schultz, Paul D. Bayless, Richard W. Johnson, Glenn E. McCreery, William Taitano, and James R. Wolf

September 2010

Idaho National Laboratory
Next Generation Nuclear Plant Project
Idaho Falls, Idaho 83415

Prepared for the
U.S. Department of Energy
Office of Nuclear Energy
Under DOE Idaho Operations Office
Contract DE-AC07-05ID14517

Next Generation Nuclear Plant Project

Studies Related to the Oregon State University High Temperature Test Facility: Scaling, the Validation Matrix, and Similarities to the Modular High Temperature Gas-Cooled Reactor

INL/EXT-10-19803
Revision 0

September 2010

Approved by:

Hans D. Gougar for Richard Schultz — 9/23/2010

Richard R. Schultz
Author

Date

Hans D Gougar — 9/23/2010

Hans D. Gougar
VHTR TDO Technical Deputy Director

Date

Jack Simonds for — 9/23/2010

Diane V Croson
VHTD TDO Deputy Director

Date

SUMMARY

The Oregon State University (OSU) High Temperature Test Facility (HTTF) is an integral experimental facility that will be constructed on the OSU campus in Corvallis, Oregon. The HTTF project was initiated, by the U.S. Nuclear Regulatory Commission (NRC), on September 5, 2008 as Task 4 of the 5-year High Temperature Gas Reactor Cooperative Agreement via NRC Contract 04-08-138. Until August, 2010, when a DOE contract was initiated to fund additional capabilities for the HTTF project, all of the funding support for the HTTF was provided by the NRC via a cooperative agreement.

The U.S. Department of Energy (DOE) began its involvement with the HTTF project in late 2009 via the Next Generation Nuclear Plant (NGNP) project. Because the NRC's interests in HTTF experiments were only centered on the depressurized conduction cooldown (DCC) scenario, NGNP involvement focused on expanding the experimental envelope of the HTTF to include steady-state operations and also the pressurized conduction cooldown (PCC).

Since DOE has incorporated the HTTF as an ingredient in the NGNP thermal-fluids validation program, several important outcomes should be noted:

1. The reference prismatic reactor design that serves as the basis for scaling the HTTF, became the modular high temperature gas-cooled reactor (MHTGR). The MHTGR has also been chosen as the reference design for all of the other NGNP thermal-fluid experiments.
2. The NGNP validation matrix is being planned using the same scaling strategy that has been implemented to design the HTTF, i.e., the hierarchical two-tiered scaling methodology developed by Zuber in 1991. Using this approach, a preliminary validation matrix has been designed that integrates the HTTF experiments with the other experiments planned for the NGNP thermal-fluids verification and validation project.
3. Initial analyses showed that the inherent power capability of the OSU infrastructure, which only allowed a total operational facility power capability of 0.6 MW, is inadequate to permit steady-state operation at reasonable conditions.
4. To enable the HTTF to operate at more representative steady-state conditions, DOE recently allocated funding via a DOE subcontract to HTTF to permit an OSU infrastructure upgrade such that 2.2 MW will become available for HTTF experiments.
5. Analyses have been performed to study the relationship between HTTF and MHTGR via the hierarchical two-tiered scaling methodology which has been used successfully in the past, e.g., APEX facility scaling to the Westinghouse AP600 plant. These analyses have focused on the relationship between key variables that will be measured in the HTTF to the counterpart variables in the MHTGR with a focus on natural circulation, using nitrogen as a working fluid, and core heat transfer.
6. Both RELAP5-3D and computational fluid dynamics (CD-Adapco's STAR-CCM+) numerical models of the MHTGR and the HTTF have been constructed and analyses are underway to study the relationship between the reference reactor and the HTTF.

The HTTF is presently being designed. It has 1/4-scaling relationship to the MHTGR in both the height and the diameter. Decisions have been made to design the reactor cavity cooling system (RCCS) simulation as a boundary condition for the HTTF to ensure that (a) the boundary condition is well defined; and (b) the boundary condition can be modified easily to achieve the desired heat transfer sink for HTTF experimental operations.

This report summarizes the work identified in Items 1 through 6 above.

Studies to date have shown that the HTTF should have the capability to give a reasonable representation of the MHTGR, although some HTTF design compromises will exist. Work is continuing to identify and quantify the design compromises as a function of the final design.

CONTENTS

SUMMARY v

1. INTRODUCTION 1

2. SUMMARY OF THE SCALING STRATEGY AND THE REFERENCE REACTOR DESIGN 3
   - 2.1 Hierarchical Two-Tiered Scaling Methodology 3
   - 2.2 Summary Description of Reference Plant Design 4

3. DESCRIPTION OF NGNP THERMAL-FLUIDS VALIDATION MATRIX AND THE ROLE OF THE HTTF EXPERIMENTS 9

4. HTTF TO MHTGR SCALING RATIOS 19

5. USING NITROGEN AS THE HTTF WORKING FLUID TO BETTER MATCH MHTGR OPERATIONAL CONDITIONS 23

6. STUDY OF DUAL-CHANNEL NATURAL CIRCULATION DURING A PCC SCENARIO 32
   - 6.1 Assumptions 32
   - 6.2 Up-flow in Channel 1 33
   - 6.3 Down-flow in Channel 2 33

7. INVESTIGATION OF TEMPERATURE DISTRIBUTION IN HTTF CORE FOR ASYMMETRIC UNIT CELLS 35

8. STUDIES OF STEADY-STATE BEHAVIOR IN MHTGR AND HTTF USING RELAP5-3D AND CFD 43
   - 8.1 MHTGR Modeling and Analysis 43
     - 8.1.1 RELAP5-3D Input Model Description 43
     - 8.1.2 Base Transient Simulations 47
     - 8.1.3 Sensitivity Calculations 50
   - 8.2 HTTF Modeling and Analysis 53
     - 8.2.1 Scoping Analyses Using the MHTGR Model 53
     - 8.2.2 Scoping Analyses Using HTTF Models 59
   - 8.3 Summary 69

9. References 70

Appendix A Computer Code Quality Assurance 74

FIGURES

Figure 2-1. MHTGR module (DOE 1986).....5

Figure 2-2. Plan view of reactor vessel and internals in an elevation through the core region (DOE 1986).....6

Figure 2-3. Isometric view through MHTGR reactor building (DOE 1986) 7

Figure 2-4. RCCS cooling system and air cooling panels. 8

Figure 3-1. A validation pyramid approach is the basis for constructing the NGNP thermal-fluids validation matrix.....9

Figure 3-2. Thermal hydraulic phenomena: experiment planning.....11

Figure 3-3. The HTTF integral experiment: a 1/4-scale experiment based on the MHTGR. The experiment will be located at Oregon State University. 12

Figure 3-4. The RCCS facility is located at Argonne National Laboratory. The facility is 1/2-scale to the MHTGR and is capable of operating at representative conditions for the scenarios of interest. 13

Figure 3-5a. Upper plenum portion of the P2P experiment. 14

Figure 3-5b. Lower plenum portion of P2P experiment. 14

Figure 3-6. Lower plenum mixing experiment conducted in the MIR facility. 15

Figure 3-7a. The MIR bypass experiment was designed to represent scaled interstitial passages between three prismatic blocks as shown. To the left a plan view of three prismatic blocks is shown.....16

Figure 3-7b. The MIR prismatic bypass test section.....16

Figure 3-8. The air ingress isothermal test apparatus. 17

Figure 5-1. Comparison of unchoking time for nitrogen and helium as a function of break area to volume ratio.....28

Figure 6-1. Geometry considered for natural circulation dual-channel behavior analysis. 32

Figure 7-1. OSU preliminary alternate HTTF core layout.....36

Figure 7-2. Alternate core design nodalization.....37

Figure 7-3. The original design showing four cells where each heater rod transfers heat to six coolant channels. H indicates heater, C indicates coolant channel.....38

Figure 7-4. Calculated final temperature profile for original design. 39

Figure 7-5. Normalized temperature distribution for original design. 40

Figure 7-6. Calculated final temperature profile for alternate design for a cell surrounded by four coolant channels. 41

Figure 7-7. Calculated final temperature profile for alternate design for a cell surrounded by six coolant channels. 42

Figure 8-1. RELAP5-3D nodalization of the MHTGR reactor vessel.....44

Figure 8-2. Cross section of the MHTGR reactor vessel in the core region. 45
Figure 8-3. Cross section of the RELAP5-3D model of the MHTGR reactor vessel. 45
Figure 8-4. RELAP5-3D modeling of the MHTGR central reflector outer ring. 46
Figure 8-5. Unit cell for the core rings in the RELAP5-3D MHTGR model. 46
Figure 8-6. Peak fuel temperatures for the MHTGR base case DCC and PCC simulations..... 48
Figure 8-7. Reactor vessel temperatures for the MHTGR base case DCC and PCC simulations. 49
Figure 8-8. RCCS heat removal for the MHTGR base case DCC and PCC simulations. 49
Figure 8-9. Peak fuel temperatures for the base and PCC pressure sensitivity cases. 51
Figure 8-10. DCC transient peak fuel temperatures for the base and bypass flow sensitivity calculations. 51
Figure 8-11. PCC transient reactor vessel temperatures for the base and bypass flow sensitivity calculations. 52
Figure 8-12. PCC transient reactor vessel temperatures for the base and bypass flow sensitivity calculations. 52
Figure 8-13. Peak fuel temperatures for the DCC base and 10% power cases. 54
Figure 8-14. Peak fuel temperatures for the PCC base and 10% power cases. 55
Figure 8-15. Reactor vessel temperatures for the DCC base and 10% power cases. 56
Figure 8-16. Reactor vessel temperatures for the PCC base and 10% power cases..... 56
Figure 8-17. DCC transient peak fuel temperatures for the scaled MHTGR model. 58
Figure 8-18. DCC transient reactor vessel temperatures for the scaled MHTGR model. 59
Figure 8-19. RELAP5-3D nodalization of the HTTF reactor vessel. 61
Figure 8-20. Cross-section of the RELAP-3D model of the HTTF reactor vessel. 62
Figure 8-21. Unit cells used in the RELAP5-3D model of the HTTF reactor vessel. 62
Figure 8-22. Cross section of the STAR-CCM+ HTTF model for three control rod hole configurations. 63
Figure 8-23. Lower block axial mesh of the STAR-CCM+ HTTF model (1.27-cm mesh height). 63
Figure 8-24. Calculated HTTF temperatures near the core midplane for the 2.0 MW base case. 65
Figure 8-25. Calculated HTTF temperatures near the core midplane for the 2.0 MW control rod hole sensitivity case. 66
Figure 8-26. Calculated HTTF temperatures in the bottom portion of the core for the 2.0 MW base case. 66
Figure 8-27. Calculated HTTF temperatures in the bottom portion of the core for the 2.0 MW control rod hole sensitivity case. 67
Figure 8-28. Calculated HTTF temperatures near the core midplane for the 2.2 MW base case. 67
Figure 8-29. Calculated HTTF temperatures near the core midplane for the 2.2 MW control rod hole sensitivity case. 68

Figure 8-30. Calculated HTTF temperatures in the bottom portion of the core for the 2.2 MW base case. 68

Figure 8-31. Calculated HTTF temperatures in the bottom portion of the core for the 2.2 MW control rod hole sensitivity case. 69

TABLES

Table 3-1. Summary of NGNP experiments, key phenomena, and experiments. 18

Table 4-1. Relationships between MHTGR and HTTF primary variables. 20

Table 4-2. Relationships between MHTGR and HTTF non-dimensional quantities. 20

Table 4-3. Relationships between MHTGR and HTTF primary heat transfer variables. 21

Table 4-4. Relationships between MHTGR and HTTF quantities specific to DCC and PCC scenarios. 22

Table 5-1. Properties used in scaling calculations. 23

Table 8-1. Desired and calculated MHTGR steady state conditions. 47

Table 8-2. Calculated MHTGR steady state structure average temperatures at 350 and 35 MW. 54

Table 8-3. Calculated steady state structure temperatures for the scaled MHTGR model. 57

Table 8-4. Calculated steady state Reynolds numbers for the scaled MHTGR model. 58

Table 8-5. Calculated HTTF steady state values for the control rod hole sensitivity at 2.0 MW. 65

Table 8-6. STAR-CCM+ calculated HTTF steady state values for the control rod hole sensitivity at 2.2 MW. 65

Table A-1. Quality assurance information for the computer codes used for the computer simulations. 73

ACRONYMS

CFD	computational fluid dynamics
DCC	depressurized conduction cooldown
DOE	Department of Energy
H2TS	hierarchical, two-tiered scaling
HTGR	High Temperature Gas-cooled reactor
HTTF	High Temperature Test Facility
INL	Idaho National Laboratory
JAEA	Japan Atomic Energy Agency
LOCA	loss of coolant accident
LOFA	loss of flow accident
LWR	light water reactor
MHTGR	Modular High Temperature Gas-Cooled Reactor
MIR	Matched Index of Refraction
NGNP	Next Generation Nuclear Plant
NIST	National Institute of Standards and Technology
NRC	Nuclear Regulatory Commission
NSTF	Natural Convection Shutdown Test Facility
OECD	Organization for Economic Co-operation and Development
OSU	Oregon State University
P2P	plenum-to-plenum
PCC	pressurized conduction cooldown
PIRT	phenomena identification and ranking table
PSID	Preliminary Safety Information Document
RCCS	reactor cavity-cooling system
V&V	verification and validation
VHTR	Very High Temperature Reactor

Studies Related to the Oregon State University High Temperature Test Facility: Scaling, the Validation Matrix, and Similarities to the Modular High Temperature Gas-Cooled Reactor

1. INTRODUCTION

The High Temperature Test Facility (HTTF), to be located at Oregon State University in Corvallis, Oregon, is presently being designed. Although the design isn't finalized, the first hardware configuration of the HTTF will be 1/4-scale in both the height and radial dimensions to the Modular High Temperature Gas-Cooled Reactor (MHTGR), as described in the Preliminary Safety Information Document for the Standard MHTGR (DOE 1986).

The MHTGR is a prismatic block reactor design that uses graphite as a moderator in the form of prismatic graphite blocks in its core. It has an air-cooled reactor cavity-cooling system (RCCS) and its power conversion is provided by a Rankine cycle via a once-through steam generator.

The HTTF is one ingredient of the U.S. Nuclear Regulatory Commission (NRC) High Temperature Gas Reactor cooperative agreement that began on September 5, 2008 via NRC Contract 04-08-138. This NRC Contract is a 5-year agreement and the HTTF was originally designed to only address the depressurized conduction cooldown (DCC) scenario.

The HTTF was recently included as a member of the set of thermal-fluids experiments that will be used to generate validation data for the Next Generation Nuclear Plant (NGNP) experimental verification and validation (V&V) program. As such, U. S. Department of Energy (DOE) funding is being used to: (a) study the scaling of the HTTF in its present form, (b) define modifications that will expand the experimental envelope of the HTTF from a facility that is designed primarily to address the DCC scenario to include additional scenarios such as the pressurized conduction cooldown (PCC) scenario and also representative steady-state conditions; and (c) ensure the HTTF experiments are compatible with the other experiments in the set of experiments that will be used to create the NGNP validation matrix for the prismatic high temperature gas-cooled reactor (HTGR).

Presently the NGNP intends to perform experiments in conjunction with the NRC until the NRC's contract expires in 2013. Thereafter, NGNP plans to continue OSU HTTF experiments to include tests of specific interest to the DOE program.

Sections 2 through 8 in this report give overviews of:

Section 2	The set of experiments that will be used by NGNP to generate the NGNP validation matrix. The HTTF will be discussed from the perspective of how it is compatible with the other planned and ongoing NGNP validation experiments.
Section 3	The scaling criteria, i.e., the two-tiered hierarchical approach together with a short summary of the reference plant (MHTGR) hardware configuration.
Section 4	The scaling ratios that will be used to link the HTTF data to the MHTGR behavior.
Section 5	The use of nitrogen as a working fluid to enable the HTTF to operate at steady-state conditions that are more representative of the MHTGR steady-state conditions than would be possible using helium as a working fluid.
Section 6	A short analysis of dual channel natural circulation characteristics such as might occur during a PCC scenario.

Section 7 A preliminary comparison of an alternate HTTF core design with the baseline HTTF design.

Section 8 A summary of steady-state calculations performed to characterize the behavior of the MHTGR and the HTTF using RELAP5-3D and using the STAR-CCM+ computational fluid dynamics (CFD) numerical models.

The software used for the analyses summarized herein are listed in Appendix A together with the software's V&V status, operating system, version number, and the approach for ensuring the software algorithms are current.

2. SUMMARY OF THE SCALING STRATEGY AND THE REFERENCE REACTOR DESIGN

The experiments that will be used to generate data for the NGNP thermal-fluids validation matrix will be related to a specified reference reactor via rigorous scaling relationships. The scaling methodology used to define the scaling relationships is documented in Zuber 1991 and is known as a hierarchical, two-tiered scaling methodology. The prismatic reference reactor is the MHTGR. A pebble-bed reference reactor is not presently defined. Therefore, all of the discussion in this report will be confined to only the MHTGR and the experiments that are being defined to generate data for the validation matrix that will be used to validate numerical models specific to the MHTGR design. The following two subsections give summaries of the hierarchical two-tiered scaling methodology and the MHTGR reference reactor.

2.1 Hierarchical Two-Tiered Scaling Methodology

The hierarchical, two-tiered scaling (H2TS) methodology was formulated to define the scaling relationships between scaled experiments and prototypical systems for problems of organized complexity which have the following characteristics:

- The component parts of the system are too few in number to permit a statistical approach
- The cost of the prototypical system imposes an economic limitation that restrains the problem to an approach that is centered on scaled systems
- The component parts have intractably complex interactions between one another such that experimentation and/or computer simulations of the prototypical system alone are not sufficient.

Problems of organized complexity are addressed in Weinberg (1975), where he breaks down the problem of having to analyze systems behavior into three classes: (1) problems of organized simplicity, i.e., small-number simple systems, (2) problems of organized complexity, i.e., problems characterized by having a number of components that are too few to permit statistical solutions but too many to permit simple solutions; and (3) problems of disorganized complexity (which permit statistical solutions). Thus, the H2TS methodology addresses Weinberg's class (2) problems.

Creating experimental matrices that will serve as the basis for validating complex numeric models such as systems analysis software (e.g., RELAP5-3D) and computational fluid dynamics software (STAR-CCM+) is a problem of organized complexity because it's a reactor system that consists of component parts where the working fluid is acted upon in different, often complex manners in (potentially) each component part (e.g., regions in the reactor vessel where mixing occurs, energy is added to the fluid, energy is removed from the fluid, the fluid interacts with the solid structures, the fluid expands and contracts, frictional pressure drops occur, pressure rises occur during pumping, and so forth). The actions that occur in one component are a boundary condition for adjacent, linked components such that together the combined actions dictated the overall system behavior trajectory for a given scenario. The many phenomena that are represented in the thermal-fluids behavior field equations interact with one another to dictate the overall behavior obtained by using discretized control volumes that (taken together in an integrated sense) represent the overall fluid behavior of the system.

The H2TS methodology is comprised of 4 elements (Zuber 1991):

1. System decomposition: For example the system is divided into convenient sub-volumes; the sub-volumes are divided into constituents (e.g., different gases); the constituents are divided into geometrical configuration, (e.g., a gas that fully occupies a volume or a series of stratified gases).

2. Scale identification: The volumetric and area concentrations are identified; the residence and process times are identified.

3. Top-down/system scaling analysis: The conservation equations are defined together with the scaling groups and characteristic time ratios. From this step follows the scaling hierarchy and the important processes that should be addressed in bottom-up process scaling analyses.

4. Bottom-up/process scaling analysis: Detailed scaling analyses of important processes are identified and the important scaling groups are derived and validated.

The H2TS methodology, as applied to the OSU HTTF, is shown in great detail in Woods et al. (2009) and is followed in performing the scaling analyses for the other experiments for the NGNP validation matrix. Note that the H2TS methodology has shown great success in designed scaled facilities for the light water reactors (LWR) and the methodology is equally applicable to gas-cooled reactors.

2.2 Summary Description of Reference Plant Design

The reference prismatic reactor system is the MHTGR as defined in the PSID (1986). The MHTGR is designed to use tri-isotropic (TRISO) fuel in a hexagonal prismatic cylindrical block that is quite similar to the Ft. St. Vrain design. The reactor is designed to deliver 350 MWt with a power density of 5.9 W/cc. The working fluid is helium on the primary side. The operating pressure is 6.4 MPa where the helium inlet temperature is 259°C and the helium exit temperature is 687°C, i.e., a total temperature rise of 428°C.

Power conversion occurs via a secondary system that operates on the Rankine cycle using light water as the working fluid. The operating pressure is 17.3 MPa with an exit steam temperature of 541°C—which is over 180°C superheated.

The primary and secondary (steam generator) vessels, and the relationships to one another, are shown in Figure 2-1. The reactor vessel is designed such that helium intended to enter the core enters the reactor vessel via an annular passage in the cross duct and proceeds upward through annular-type passages, divided into distinct coolant inlet channels that exist between the peripheral duct wall of the core region and the inner diameter of the reactor vessel wall. The helium then flows into the upper plenum which houses the control rod drives. These flow passages may be viewed in Figure 2-2 which shows a plan view of the reactor vessel taken in the core region at a plane that is perpendicular to both the axis of the reactor vessel and the direction of the flowing helium. As the helium moves into the upper plenum it changes direction 180 degrees and enters the annular core and inner and outer reflector regions and flows downward. The helium exits into the lower plenum and is gathered into a single stream which flows through the cross duct to the steam generator.

The steam generator consists of a large number of helical tubes that contain water that is boiled and then superheated. The steam outlet nozzle is shown on the side of the steam generator vessel.

The reactor vessel and steam generator vessel are housed in a confinement as shown in Figure 2-3. The confinement is cooled by a continuous circulation of air inside the confinement and also by radiation heat transfer to the reactor cavity cooling heat exchanger—the air panels identified in Figure 2-4. Via the air panels, cooling is administered using environmental air that enters through passages shown in the RCCS inlet/exhaust structure shown in Figure 2-3.

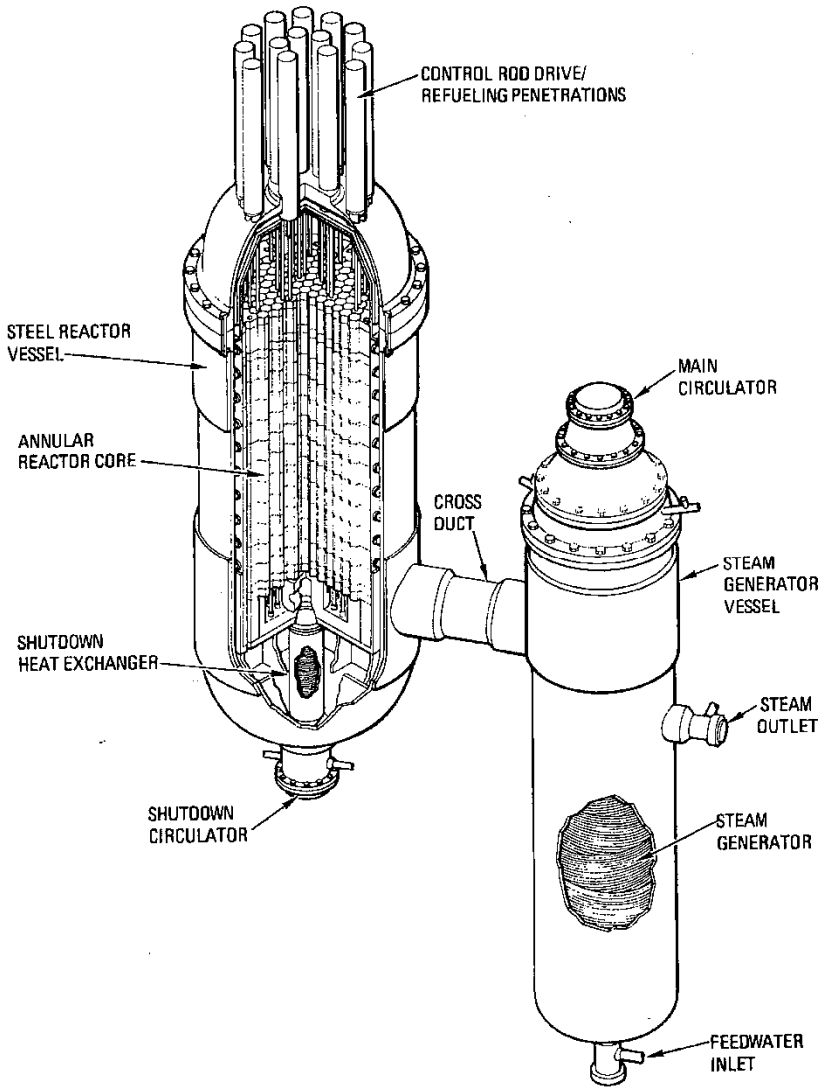

Figure 2-1. MHTGR module (DOE 1986).

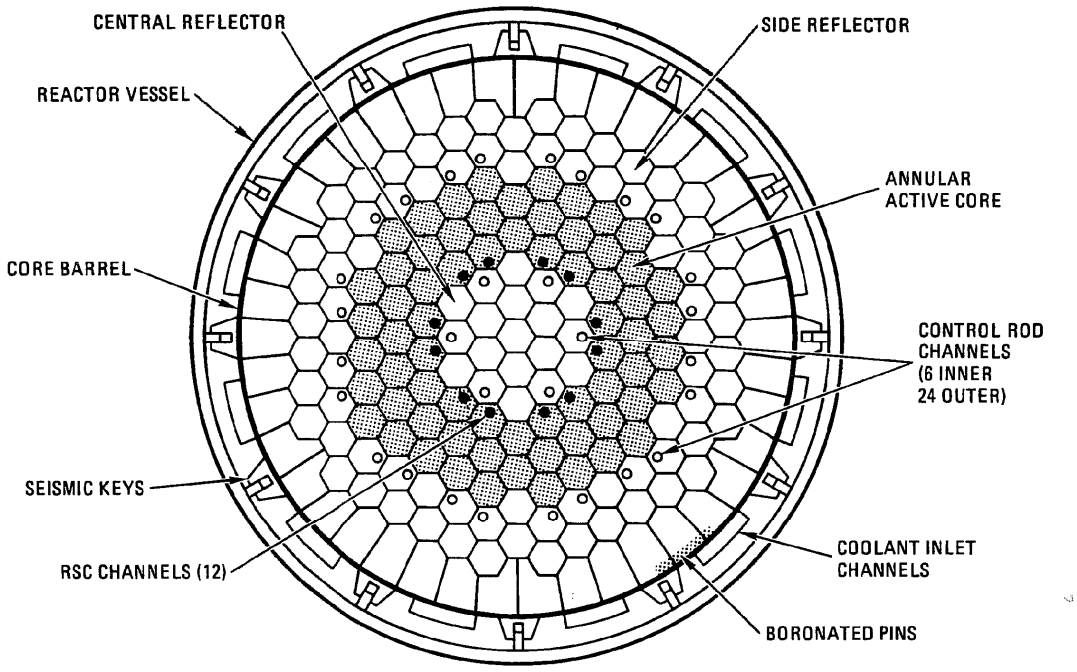

Figure 2-2. Plan view of reactor vessel and internals in an elevation through the core region (DOE 1986).

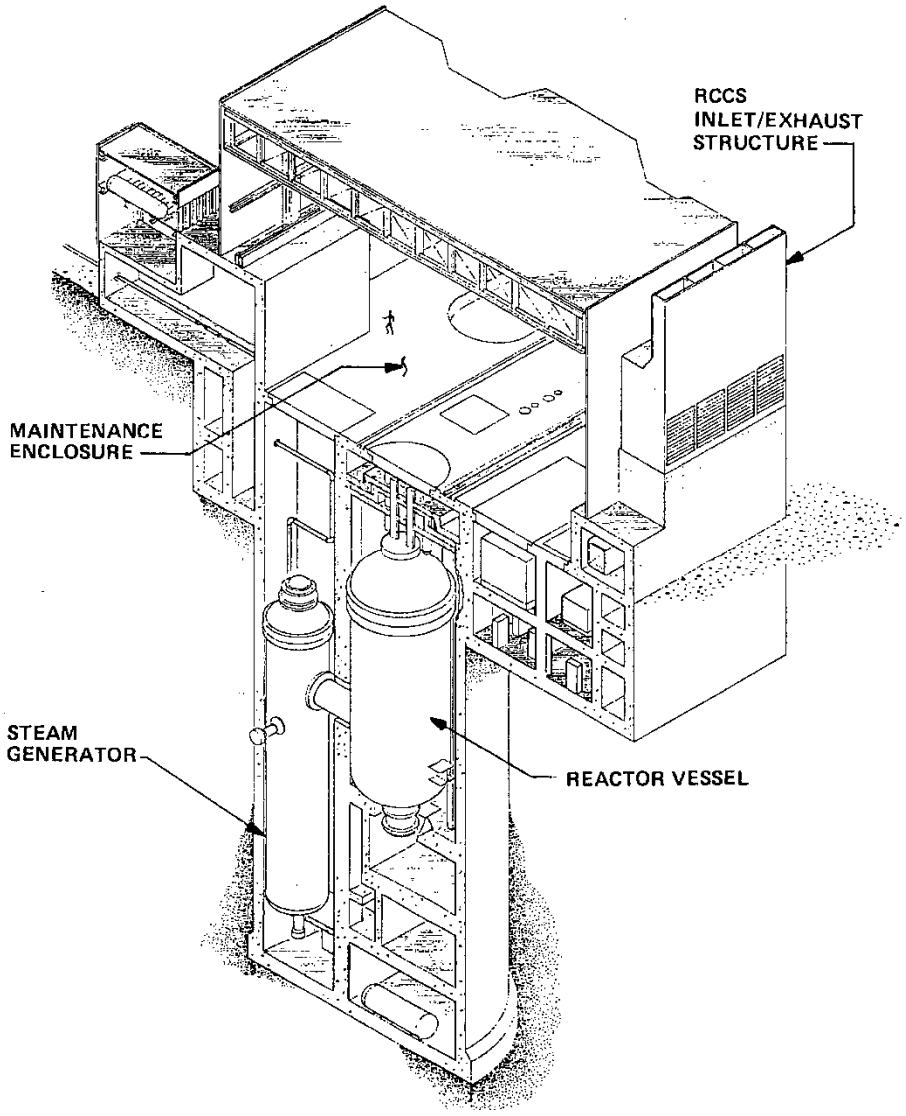

Figure 2-3. Isometric view through MHTGR reactor building (DOE 1986).

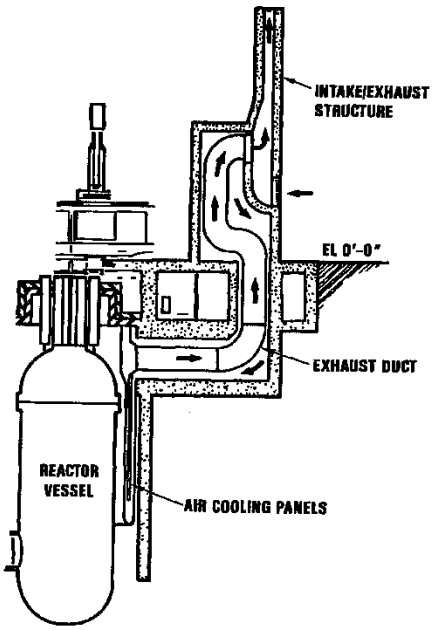

Figure 2-4. RCCS cooling system and air cooling panels.

3. DESCRIPTION OF NGNP THERMAL-FLUIDS VALIDATION MATRIX AND THE ROLE OF THE HTTF EXPERIMENTS

The HTTF that will be constructed at Oregon State University in Corvallis, Oregon is the integral reactor vessel experimental facility that will be used to generate validation data for the NGNP thermal-fluids tools development. As such, the NGNP methods expectations are that experiments performed in the HTTF will provide data for validating both systems analysis and CFD software for a majority of the challenging HTGR scenarios that must be studied—as indicated by the phenomena identification and ranking studies—that are identified presently or in future phenomena identification and ranking table (PIRT) efforts over the course of the NGNP project.

The HTTF is the centerpiece of the NGNP thermal-fluids experimental matrix that includes six other large experiments plus a number of to-be-specified fundamental experiments that together will provide the data for the validation matrix for the NGNP thermal-fluids behavior analysis numeric models. As such, a consistent design approach is being taken to ensure that the set of NGNP thermal-fluids experiments are complementary and are all related to the reference reactor design via the scaling laws.

The experiments that are being used to construct the validation matrix are defined on the basis of a validation pyramid (Figure 3-1) approach. That is, the foundation of the pyramid is made up of validation data from basic experiments designed to study fundamental phenomena which are ideal for the university environment. A basic experiment, in the context of the mixing between numerous gas jets, would be the behavior of a single jet and then the interaction between only two jets. A relatively large number of basic experiments will be performed as determined during the NGNP experimental program once the reactor design has been better identified.

Resting upon the framework formed by basic experiments are separate effects experiments which may represent the thermal-fluid behavior that occurs within a component or region of the NGNP. Such experiments may be designed to examine the behavior in the core region or in one of the plena of the reactor.

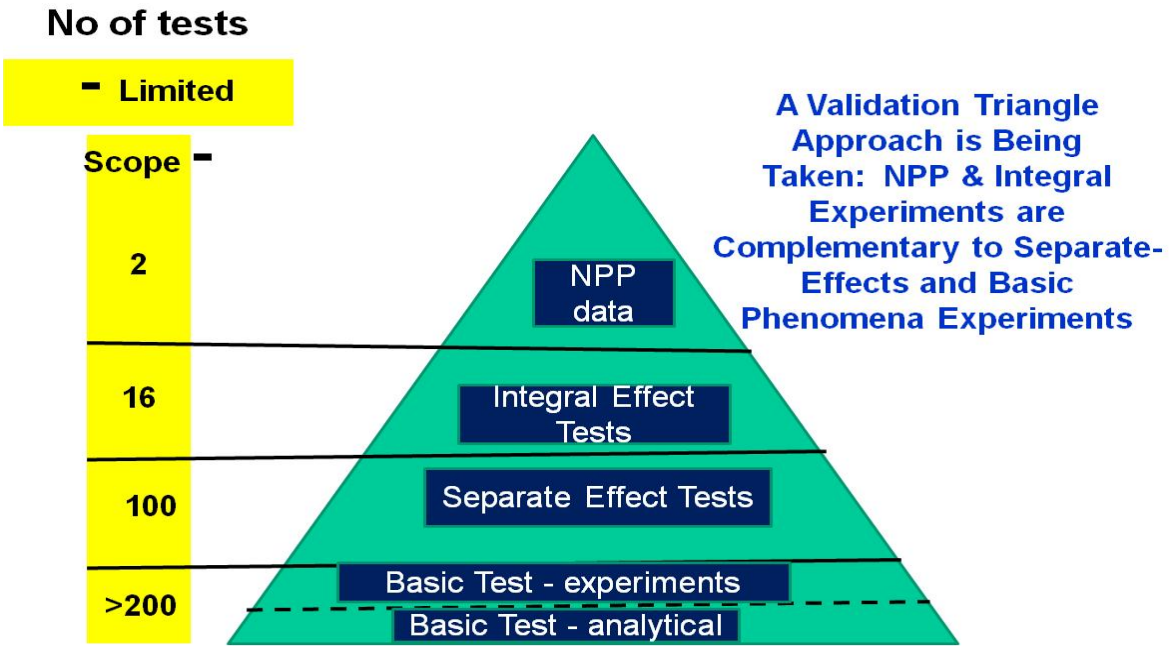

Figure 3-1. A validation pyramid approach is the basis for constructing the NGNP thermal-fluids validation matrix.

Integral effects experiments are designed to enable researchers to explore the overall behavior of the system and the interactions between the various phenomena for scenarios of interest. Data from plants form the uppermost level where examples for the prismatic reactor are Ft. St. Vrain and the High Temperature Test Reactor (HTTR) in Tokai, Japan.

The experiments defined, based on the validation pyramid approach, are shown in Figure 3-2 together with a sampling of the thermal-fluids behavior that is addressed by each. Figure 3-2 shows three representative scenarios of interest in the left-most column (i.e., operational conditions, the pressurized conduction cooldown (PCC) scenario, and the depressurized conduction cooldown (DCC) scenario. The center column for Figure 3-2 shows the defined experiment spectrum. The defined experiment spectrum includes:

- Integral facility: the HTTF
- Integral Reactor Cavity Cooling System (RCCS) experiment: the Natural Convection Shutdown Test Facility (NSTF)
- Lower plenum mixing experiment facility
- Plenum-to-plenum experiment
- Core heat transfer facility
- Matched Index of Refraction (MIR) experiments
- Air ingress experiments.

The arrows indicate the types of scenarios where data may be taken. For example, the integral facility experiments (the HTTF and the RCCS experiments) should have the capability for measuring data applicable to all three scenarios: steady-state operations, PCC, and DCC. However, the air ingress experiment will only give data for the air ingress phase of the DCC scenario. On the right of Figure 3-2 a schematic of a typical prismatic design shows the various regions of the HTGR: upper plenum, lower plenum, core, reflectors, and reactor cavity. A short description of each of the above experiments follows.

1. ***Integral facility:*** An integral facility is one that is scaled directly to the reference reactor and which can be used to study the majority of the phenomena for the scenarios of interest including the phenomena interactions for each phase of the scenario. For example, during steady-state operations the core power distribution influences the exit helium temperature distribution entering the lower plenum. Therefore, this influences the potential for mixing in the lower plenum and the potential for having “hot streaking” that could translate to large temperature gradients in the gas velocity profiles leaving the reactor vessel and entering downstream heat exchangers or power conversion equipment. Thus phenomena in the core are related to the phenomena in the lower plenum and downstream equipment. These phenomena interact with one another. For NGNP, the reference prismatic reactor is the MHTGR. Based on the MHTGR, an HTTF is being designed and will be constructed at a facility at Oregon State University. The HTTF is 1/4-scaled to the MHTGR and will have an electrically-heated core (Figure 3-3). The first HTTF configuration is prismatic; however, subsequent HTTF configurations may be pebble-bed depending on the need.

- **Normal operation at full or partial loads**
  - Coolant flow and temperature distributions through reactor core channels ("hot channel")
  - Mixing of hot jets in the reactor core lower plenum ("hot streaking")
- **Loss of Flow Accident (LOFA or "pressurized cooldown")**
  - Mixing of hot plumes in the reactor core upper plenum
  - Coolant flow and temperature distributions through reactor core channels (natural circulation)
  - Rejection of heat by natural convection and thermal radiation at the vessel outer surface
- **Loss of Coolant Accident (LOCA or "depressurized cooldown")**
  - Prediction of reactor core depressurized cooldown - conduction and thermal radiation
  - Rejection of heat by natural convection and thermal radiation at the vessel outer surface

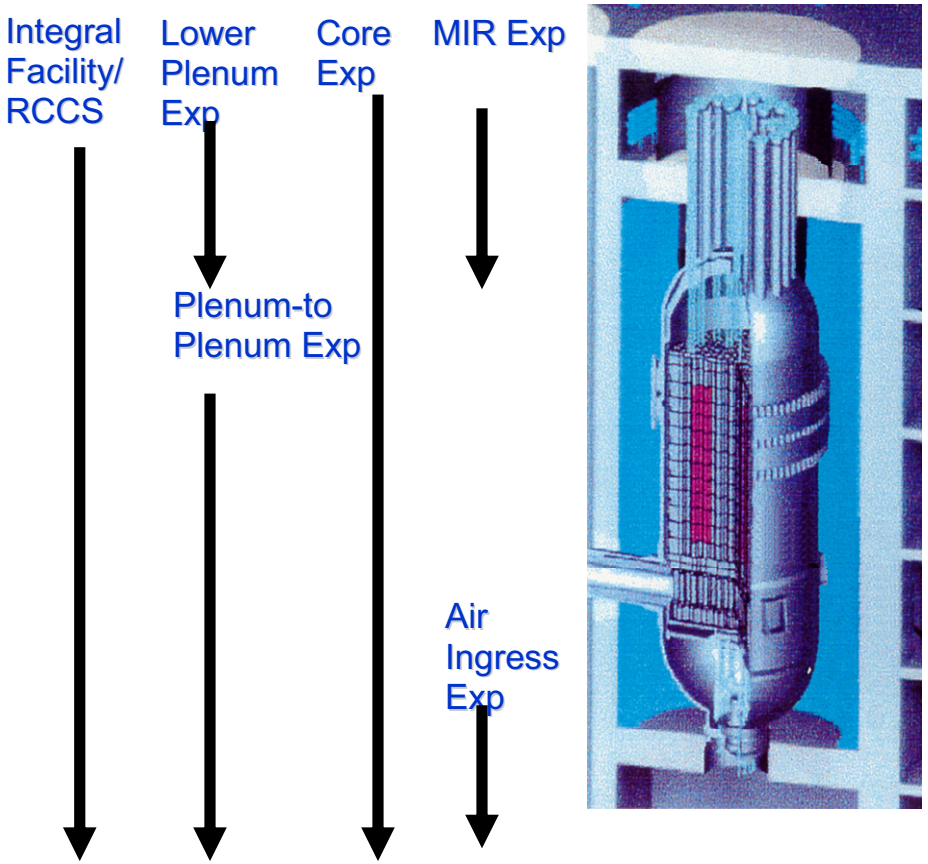

Figure 3-2. Thermal hydraulic phenomena: experiment planning.

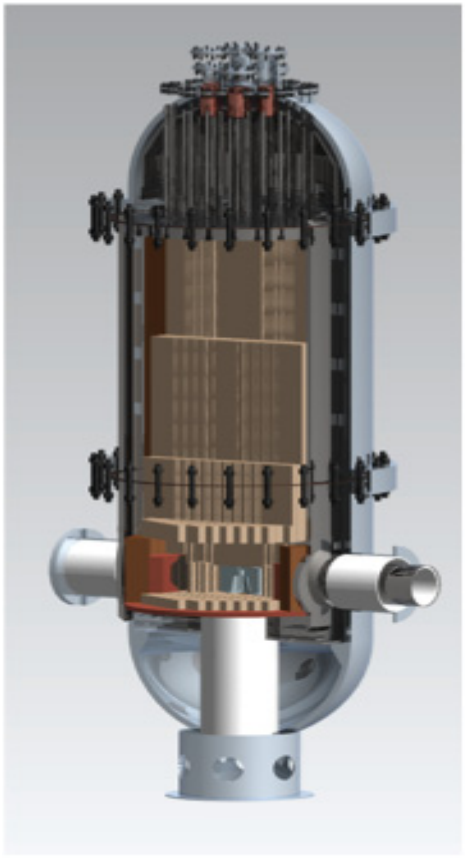

Figure 3-3. The HTTF integral experiment: a 1/4-scale experiment based on the MHTGR. The experiment will be located at Oregon State University.

2. ***Reactor cavity cooling system (RCCS) integral facility:*** The RCCS integral facility is at Argonne National Laboratory in Argonne, IL. The RCCS integral facility will be 1/2-scale of the MHTGR and will represent the confinement together with its cooling system and the outer skin of the reactor vessel. The RCCS integral facility is shown in Figure 3-4. Typical conditions in the confinement will be simulated in the RCCS facility.

Figure 3-4. The RCCS facility is located at Argonne National Laboratory. The facility is 1/2-scale to the MHTGR and is capable of operating at representative conditions for the scenarios of interest.

3. ***Lower plenum mixing experiment facility:*** This experiment has not been designed yet. However, the objective is to record data that detail the mixing of hot gases in the lower plenum at operational conditions (representative temperatures and pressures). The objective is to examine the influence of a range of large thermal gradients on structures caused by considerable variations in exit gas temperature jets from the core into the lower plenum. The large temperature distributions of the jets will be caused by potentially large asymmetrical core power distributions. The structures affected are the lower plenum structures, the hot duct, and downstream structures that may be exposed to unacceptably large thermal gradients. This experiment is intended to develop a pattern-factor approach for specifying acceptable thermal gradients for downstream power conversion equipment such as intermediate heat exchangers and turbines. The experiment would be a scaled representation of a portion of the HTGR lower plenum, hot duct, and a mock-up of a portion of selected power conversion equipment.
4. ***Plenum-to-plenum experiment:*** The plenum-to-plenum (P2P) experiment is designed to study the natural convection heat transfer that will occur during the DCC or PCC scenarios. A schematic of the P2P experiment is shown in Figure 3-5. Operational conditions cannot be studied using the P2P experiment.

   Once natural circulation is achieved during the DCC and PCC scenarios, the upward flowing gases (helium for PCC and helium/air for DCC) will appear as plumes in the upper plenum with the location and intensity of the plumes a function of the core power distribution. With hot plumes impinging on the ceiling of the upper plenum and the control rod drive mechanisms, there exists the potential for unacceptably large thermal gradients and temperatures to occur that may result in structural cracking of the upper plenum structure.

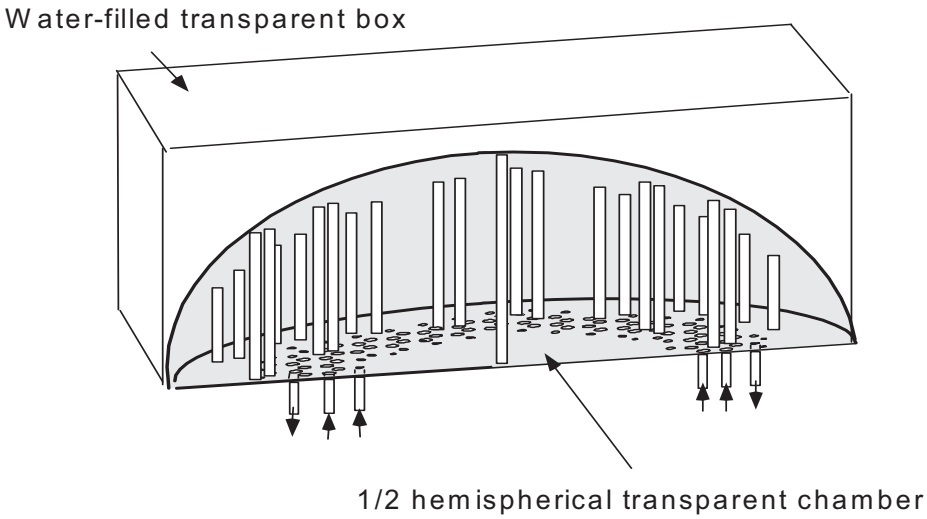

Figure 3-5a. Upper plenum portion of the P2P experiment.

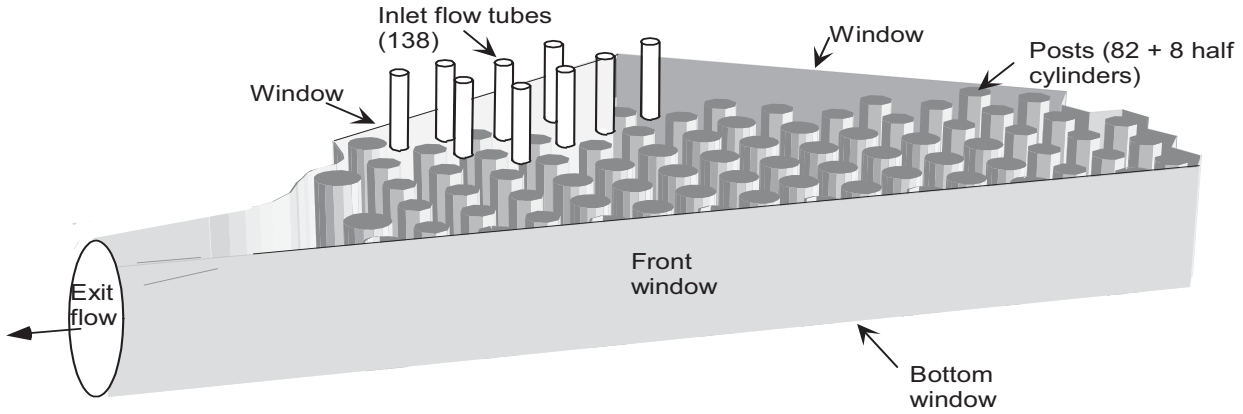

Figure 3-5b. Lower plenum portion of P2P experiment.

The P2P experiment is designed to use an isothermal approach (different density fluids) that examines the plume behavior as a function of the simulated core power distribution. The initial P2P experiment configuration is shown in Figure 3-5 where the lower plenum and the upper plenum are modeled separately. The experimental envelope would be designed to cover a spectrum of conditions that encompass the expected scaled operational range of the reference reactor.

5. ***Core heat transfer facility:*** This facility has not been designed yet. The purpose of the experiment is to study the detailed heat transfer in the core for either the prismatic or pebble-bed reactor. Because detailed data will be taken, it is envisioned that the core heat transfer facility will be scaled to study a localized region of the core with representative inlet and outlet conditions. Instrumentation will be sufficient to study (in detail) the localized heat transfer for both operational and natural convection conditions at temperature and pressure.

6. ***Matched-index-of refraction (MIR) experiments:*** The MIR is operational and has performed preliminary mixing studies in the lower plenum. The MIR is being used during FY-10 to study the detailed flow behavior that will occur in the bypass regions in a prismatic core. Because the MIR experiments are performed using mineral oil at room temperature, the experiment is isothermal and can only be used to study momentum-dominated phenomena which are not affected by fluid density

gradients. Thus the MIR can be used to study thermal-fluid behavior for operational conditions but not for natural convection conditions that will exist during the PCC and DCC scenarios.

Figure 3-6 shows the MIR experiment as used to model mixing in the lower plenum. Figure 3-7 shows the MIR hardware that will be used to study flow in the interstitial bypass regions of a prismatic reactor. The arrows indicate the relevance of the experiment to the reference reactor. A variation of the MHTGR is shown on the left of the figure. A plan view of the lower plenum is shown at top-center. The MIR experiment was designed to simulate the conditions in the portion of the lower plenum identified by the black rectangle. The quartz test section, scaled to represent the chosen region in the lower plenum is shown in the upper right. The test section was placed in the MIR experimental loop shown in the lower right. Data were obtained in the form of velocity vector profiles for the flow in the test section; as shown in the lower center portion of the figure.

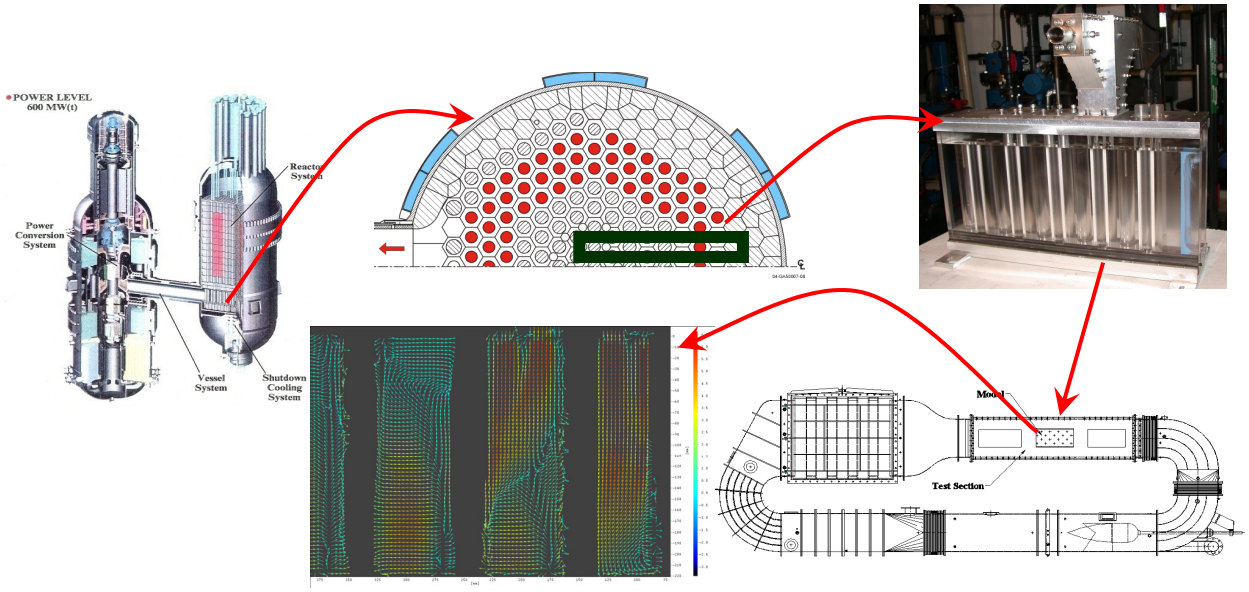

Figure 3-6. Lower plenum mixing experiment conducted in the MIR facility.

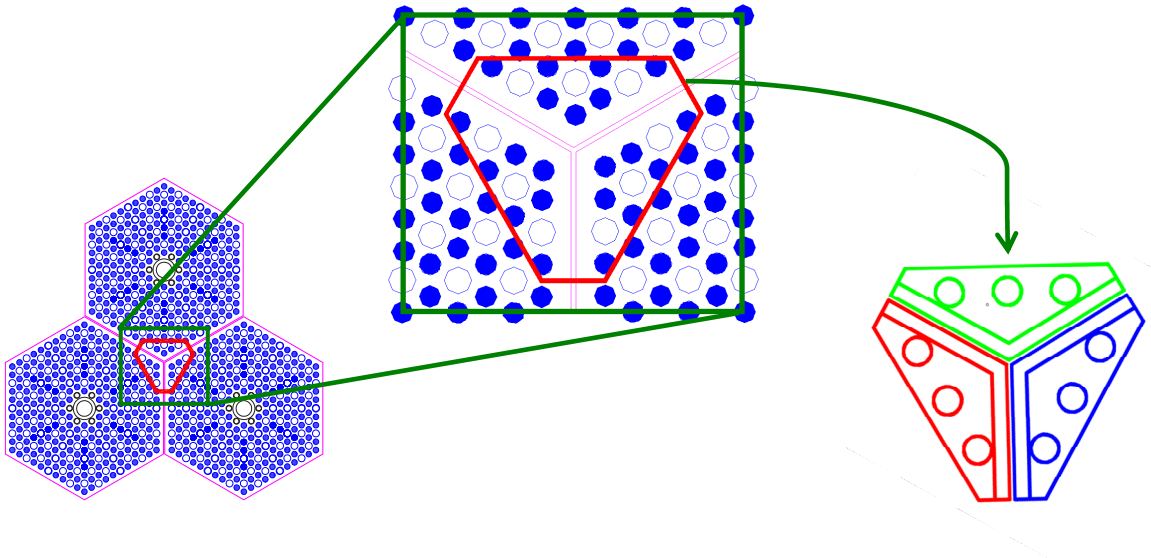

Figure 3-7a. The MIR bypass experiment was designed to represent scaled interstitial passages between three prismatic blocks as shown. To the left a plan view of three prismatic blocks is shown.

The MIR experiment focuses on the region enclosed by the red line. An important flow region of interest is the interactions between the three gaps and the vertex that connects the blocks.

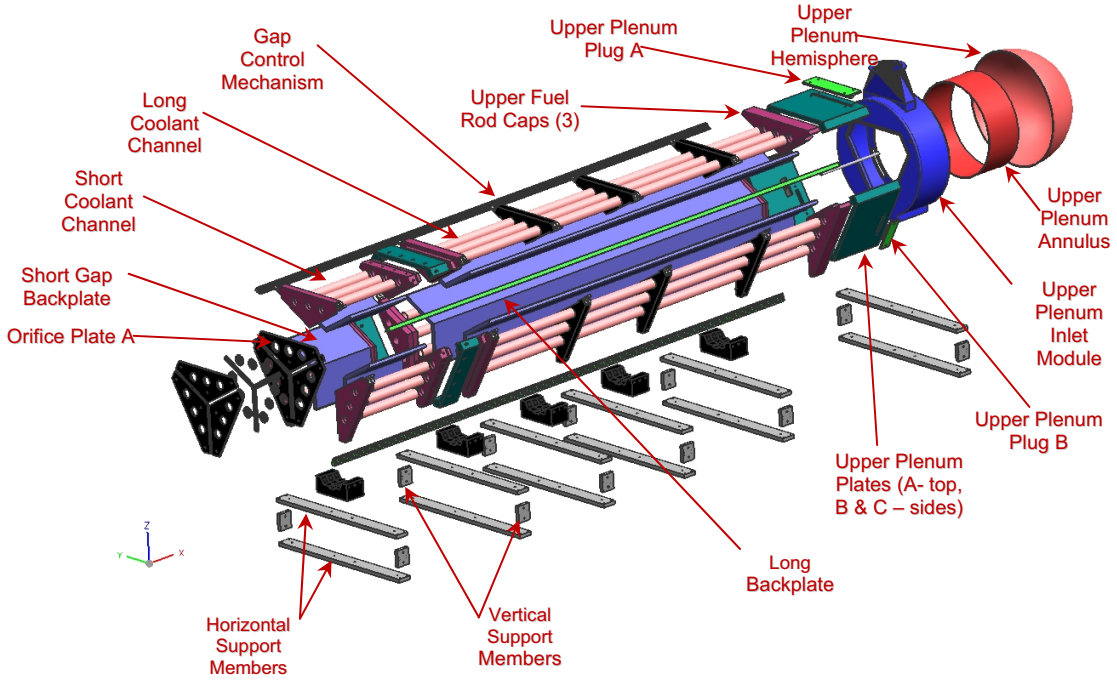

Figure 3-7b. The MIR prismatic bypass test section.

7. ***Air ingress experiments:*** Air ingress into the reactor vessel must be considered if a helium leak from the reactor vessel to the confinement develops. The effect of the reactor vessel helium leakage will be to: (a) potentially allow entry of oxygen (air) into the reactor vessel, (b) pressurize the confinement, and (c) potentially cause the confinement blowout panels to open and allow gas and fission product communication to the adjacent rooms of the plant.

Presently air ingress experiments are designed to study stratified flow into the reactor vessel through various leak locations and sizes using different density liquids. Future air ingress experiments will be designed to study air ingress using the HTTF, stratified flow between rooms (between the confinement and adjacent rooms), and gas mixing from leakage jets into the confinement. Figure 3-8 shows the ongoing air ingress test apparatus for experiments at Idaho National Laboratory (INL). Initially light liquid (or gas such as helium) is introduced in the leftmost cylinder and a heavier liquid (or gas such as air) is introduced in the rightmost cylinder. The two liquid or gas volumes are separated by a gate valve. The experiment is initiated by opening the gate valve and measuring the progression of the light gas to the right and the heavier gas to the left.

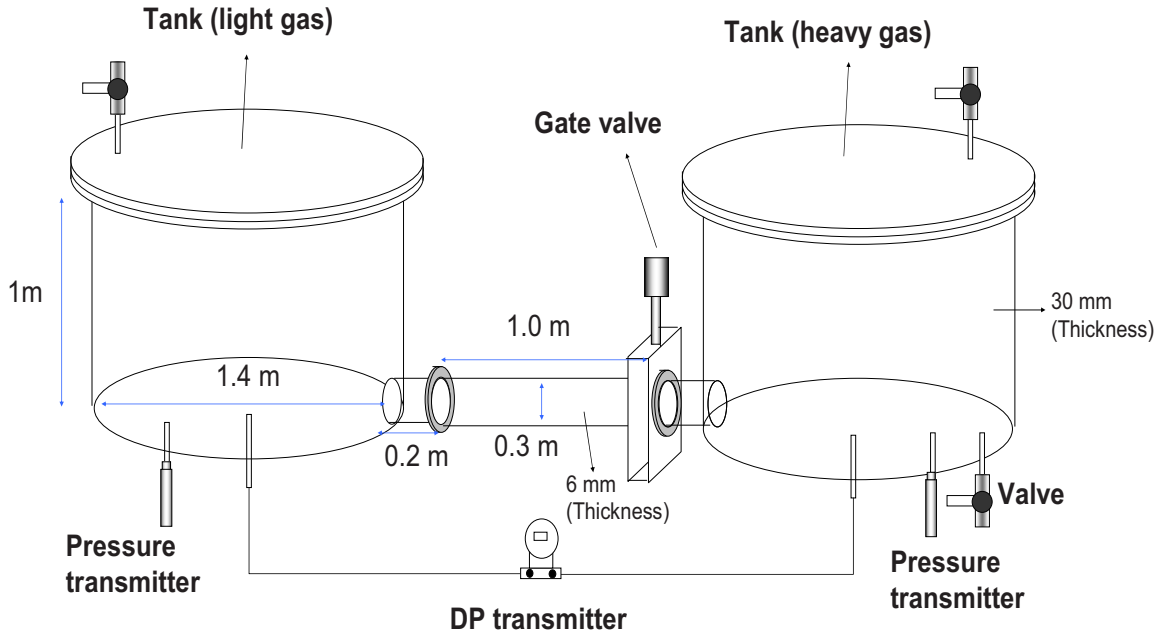

Figure 3-8. The air ingress isothermal test apparatus.

The above spectrum of experiments leads to the NGNP validation matrix that is displayed in Table 3-1 in preliminary form. The NGNP validation matrix is given in the familiar format of the Organization for Economic Co-Operation and Development (OECD) validation matrices and is organized with the experimental facility which is the source of validation data in the leftmost column. The columns to the right are arranged according to type: scenario, phenomena, and in-vessel and ex-vessel applicability. The capability of an experimental facility to deliver validation data applicable to a particular scenario relevant to phenomena of interest and for a specific region of the reference reactor is indicated by a "--." Thus the validation table gives guidance on either available data or data which may become available as the experimental test program progresses. Details regarding specific experiments, experiment hardware configurations, and experimental procedures are given in support documentation that is specific to each experiment from each experimental facility. The validation matrix displayed in Table 3-1 will (when complete) give a validation data matrix that is the basis for validating the Evaluation Model software tools such that the validated calculational envelope encompasses the NGNP operational and accident envelope.

Table 3-1. Summary of NGNP experiments, key phenomena, and experiments.

Facility	Program or Nation	Reactor Type	Scenario									Phenomena												In-Vessel							Ex-Vessel				
			Operational Conditions	Pressurized Conduction Cooldown	Depressurized Cooldown	Air Ingress	Water Ingress	Control Rod Withdrawal	ATWS	Load Change	Process-Heat Side Transient	Convective Heat Transfer	Conduction Heat Transfer	Radiation Heat Transfer	Flow Distribution	Thermal Mixing	Pressure Drop	Bypass Flow	Thermal Striping	Molecular Diffusion	Stratified Flow	Natural Circulation	Bulk CO Reaction	Graphite Oxidation	Risers	Upper Plenum	Control Rod Drives	Core & Reflectors	Fuel	Lower Plenum	Hot Duct	Vessel Outer Wall	Reactor Cavity	Downcomer Piping & Headers	Heat Exchanger	Chimney
High Temperature Test Facility	NGNP	Both	–	–	–	–				–		–	–	–	–		–	–	–	–	–	–	–	–	–		–		–	–					
Lower Plenum @ Operational Conditions		Both	–	–						–					–	–	–		–											–	–					
Lower Plenum Matched-Index-of-Refraction (MIR)		Pris	–							–					–				–											–						
Modular Core Heat Transfer Experiment		Pris	–	–	–							–	–	–	–	–	–	–				–						–								
Bypass Gap Flow Behavior: MIR		Pris	–																																	
Plenum-to-Plenum Natural Circulation		Both		–						–					–			–										–							
Air Ingress Experiments: Isothermal & Heated		Both			–	–	–								–	–				–	–	–	–	–							–					
Reactor Cavity Cooling System Experiments: ANL		Both	–	–	–					–	–	–	–	–	–	–	–															–	–	–	–	–
High Temperature Test Reactor	JAEA	Pris	–	–				–	–			–	–	–	–	–	–	–	–	–		–			–	–	–	–	–	–	–	–	–	–	–	–

4. HTTF TO MHTGR SCALING RATIOS

The HTTF facility is a 1/4 geometric length scale, 1/2 time scale, representation of the MHTGR design. The facility will operate at full-scale temperature using helium as the working fluid at reduced pressure. The scaling analysis presented by Woods, et al. (2009) indicates that HTTF will simulate the following phenomena:

- Core conduction and radiation heat transfer
- Vessel radiation heat transfer
- Core temperature profiles
- Air-ingress by lock-exchange
- Air-ingress by molecular diffusion
- Single-phase air natural circulation.

In addition, the HTTF is capable of limited primary side blow-downs and PCC studies at an operating pressure of 8 bars.

In general, MHTGR behavior of a quantity as a function of time may be predicted by multiplying the same measured quantity in HTTF by a scaling factor and expanding the time scale by a factor of two. If the quantity is dimensionless and scaling is preserved in HTTF (e.g., Power/initial Power, Pressure/initial Pressure, etc.) then it is equivalent to the HTTF data in the MHTGR as a function of scaled time. If a dimensional quantity (e.g., convection heat transfer coefficient) or non-dimensional parameter (e.g., Reynolds number or Nusselt number) is distorted from prototypical then an assessment of the distortion is required to predict MHTGR conditions from HTTR data. A preliminary list of plots of predicted MHTGR behavior that may be generated from HTTF data and the associated scaling relationships is given in Table 4-1 to Table 4-4.

Although some scaling parameters and scaling distortions may be estimated from the basic scaling relationships of the HTTF facility (such as scaled Reynolds number as a function of scaled velocity and scaled diameter), some more complicated distortions (such as heat transfer relationships that are a function of several variables), will require analysis of HTTF data to accurately quantify. Also, some scaling parameters (such as those that relate to core heat transfer) await the final design choice before they may be quantified.

Steps required to predict MHTGR behavior from HTTF data include:

1. Collection of HTTF data
2. Assessment of HTTF data validity and data uncertainties
3. Assessment of scaling distortions in HTTF data: The scaling distortion assessment will be a function of the choice of materials and the fundamental material properties of these materials relative to the MHTGR materials
4. Scaling HTTF data to MHTGR using basic scaling relationships and incorporating scaling distortions from Item 3
5. Assessment of uncertainties of scaled MHTGR behavior.

Table 4-1. Relationships between MHTGR and HTTF primary variables.[ab]

Time Scale	
Time = t	$t_{MHTGR} = 2\,t_{HTTF}$
Dimensional Quantities	
Temperature = T	$T_{MHTGR} = T_{HTTF}$
Differential temperature increase across core = ΔT	$\Delta T_{MHTGR} = \Delta T_{HTTF}$
Pressure = P	$P_{MHTGR} = P_{HTTF}$
Differential pressure across core = ΔP	$\Delta P_{MHTGR} = \Delta P_{HTTF}$
Density = ρ	$\rho_{MHTGR} = \rho_{HTTF}$
Velocity = V	$V_{MHTGR} = V_{HTTF} * 2$
Mass flow rate = $\dot{M}$	$\dot{M}_{MHTGR} = \dot{M}_{HTTF} * (A_{MHTGR} / A_{HTTF}) * 2$
Heat flux to atmosphere = q	$q_{MHTGR} = q_{HTTF} / 2.11$ (subject to final design)
Core heat flux = q_{core}	$q_{c-MHTGR} = q_{c-HTTF} * (A_R L_R^{1/2}) = 1/30.9$
Convection heat transfer coefficient = h	$h_{MHTGR} = h_{HTTF} * f(\mathrm{Re})$ [c]

Table 4-2. Relationships between MHTGR and HTTF non-dimensional quantities.[d]

Non-dimensional Quantities and Scaling Ratios	
$P/P_{initial}$	$P/P_{initial-MHTGR} = P/P_{initial-HTTF}$
$T/T_{initial}$	$T/T_{initial-MHTGR} = T/T_{initial-HTTF}$
$Power/Power_{initial}$	$Power/Power_{initial-MHTGR} = Power/Power_{initial-HTTF}$
$Core\ \Delta P/P$	$Core\ \Delta P/P_{MHTGR} = Core\ \Delta P/P_{HTTF}$
Radial temperature profile	$(T - T_{outside-radius}) / (T_{center} - T_{outside\text{-}radius})$ v. $Radius/outside\text{-}Radius$ determined by final design
Axial temperature profile	$(T - T_0)/(T_{\max} - T_0)$ v. z/L determined by final design
Thermal striping	$\dfrac{(T\max - T\min)_{Hot-duct}}{(Thot - Tcold)_{core\ exit\ channels}}$ unknown functions of mixing and therefore of Reynolds number
$\dfrac{(T\max - T\min)_{Hot\ duct}}{\overline{T}_{Hot\ duct}}$	Same as thermal striping
Re	$\mathrm{Re}_{MHTGR} = \mathrm{Re}_{HTTF} * (V_{MHTGR}/V_{HTTF}) * (D_{MHTGR}/D_{HTTF})$

a. Subscripts indicate whether variable pertains to HTTF or MHTGR.

b. All HTTF data may be shown as a function of either *tHTTF* or $t^* = 2tHTTF = tMHTGR$. In some cases HTTF data and ratios may be shown as a function of other variables for analysis or characterization purposes.

c. Re = Reynolds number.

d. All HTTF data may be shown as a function of either t_{HTTF} or $t^* = 2t_{HTTF} = t_{MHTGR}$. In some cases HTTF data and ratios may be shown as a function of other variables for analysis or characterization purposes, e.g., radial temperature profile.

Table 4-3. Relationships between MHTGR and HTTF primary heat transfer variables.[e]

Core Conduction Heat Transfer	
Biot modulus[f] = Bi	Bi = $Bi_{HTTF}(h_{MHTGR}/h_{HTTF})(D_{MHTGR}/D_{HTTF})/(K_{MHTGR}/K_{HTTF})$
Core Fourier modulus[g] = Fo	$Fo_{MHTGR} = Fo_{HTTF}(\alpha_{MHTGR}/\alpha_{HTTF})*32$
Convection Heat Transfer	
Nusselt number[h] = Nu	$Nu_{MHTGR} = Nu_{HTTF} * (h_{MHTGR}/h_{HTTF}) * (D_{MHTGR}/D_{HTTF})$
Heat Flux Ratios	
$q_{convection}/q_{total}$	$q_{convection}$ is a function of Re and Gr[i]
$q_{radiation}/q_{total}$	q_{total} is a function of Re, Gr, and emissivity

e. All HTTF data may be shown as a function of either *tHTTF* or *t* = 2tHTTF = tMHTGR.* In some cases HTTF data and ratios may be shown as a function of other variables for analysis or characterization purposes.

f. K = thermal conductivity of core material.

g. α = Kcore/(Cp ρ).

h. *D* = characteristic diameter.

i. Gr = Grashof number.

Table 4-4. Relationships between MHTGR and HTTF quantities specific to DCC and PCC scenarios.[j]

DCC Specific Quantities	
Mass ratio[k]	$M(t)_{system}/M(t_{initial})_{system}$
Pressure ratio	$P/P_{initial}$ v. $M/M_{initial}$
Mass ratio with respect to M_{MHTGR}	$M_{MHTGR} = M_{HTTF}(Volume_{MHTGR}/Volume_{HTTF})$
$\dot{m}_{break} = dm/dt$	$\dot{m}_{MHTGR} = \dot{m}_{HTTF}(Volume_{MHTGR}/Volume_{HTTF})$ $where,\ \dot{m}_{MHTGR} = dm_{MHTGR}/dt*$
$P(t)$	with individual curves for each break size
M_{air}/M_{total}	$(M_{air}/M_{total})_{MHTGR} = (M_{air}/M_{total})_{HTTF}$
Height of air ingress level = H	$H_{MHTGR} = H_{HTTF} * 4$
Froude number for air ingress = Fr	$Fr_{MHTGR} = Fr_{HTTF}$
Densimetric Froude number[l] = Fr_D	$(Fr_D)_{MHTGR} = (Fr_D)_{HTTF}$
Air mole fraction = mf	at various non-dimensional elevations (H/H_{max}) for either stratified flow or diffusion
Mole fraction on basis of MHTGR	$mf_{MHTGR} = mf_{HTTF}\ at\ (L_R)^2 = mf_{HTTF}\ \ at\ 16t$
PCC Specific Quantities	
Loop natural convection velocity = V	$V_{MHTGR} = V_{HTTF} * 2$
In-core natural convection	Dependent on final choice of channel diameter. See Section 6 on in-core natural convection.
Bypass flow	Dependent on final core design.

j. All HTTF data may be shown as a function of either *tHTTF* or *t* = 2tHTTF = tMHTGR.* In some cases HTTF data and ratios may be shown as a function of other variables for analysis or characterization purposes.

k. *M(t)* = mass of system as a function of time.

l. Densimetric Froude number = g' = (g Δρ)/ρair where g = gravitational acceleration and Δρ = ρair – ρhelium.

5. USING NITROGEN AS THE HTTF WORKING FLUID TO BETTER MATCH MHTGR OPERATIONAL CONDITIONS

Scaling of nitrogen flow in HTTF experiments to represent helium flow at higher pressure was investigated; and the results of the study are presented in this chapter. The NRC PIRT described in Woods, et al. (2009), Section 4-1, specified six general categories of postulated accident scenarios for an HTGR. Nitrogen flow may plausibly be considered to represent higher pressure helium flow for two of these scenarios, which are, (1) pressurized conduction cooldown (PCC); and (2) depressurized conduction cooldown (DCC) prior to air ingress.

It is assumed for the scaling calculations described here that the maximum temperature in HTTF is 700°C and the maximum pressure is 0.69 MPa. Under these conditions the density of nitrogen gas at 700°C and 0.69 MPa equals the density of helium at 700°C and 4.84 MPa. The physical properties of nitrogen and helium at 700ºC and the above two pressures are chosen to investigate the scaling of MHTGR to HTTF under forced and natural convection conditions.

For a scaled system using nitrogen flow, it is assumed that in HTTF:

- Velocity nitrogen gas at 700°C, 0.69 MPa = velocity helium at 700°C, 4.84 MPa
- Mass flow rate of nitrogen gas = mass flow rate of helium (since the densities and velocities are equal)
- Core outlet temperature of nitrogen = core outlet temperature of helium = 700$^{\circ C}$
- Core differential temperature for nitrogen flow = core differential temperature for helium flow.

Fluid properties used in scaling calculations*:* All properties used in subsequent calculations were taken from the National Institute of Standards and Technology (NIST) Webbook, http://webbook.nist.gov and are listed in Table 5-1.

Table 5-1. Properties used in scaling calculations.

	Density —ρ (kg/m^3)	Kinematic viscosity —ν (m^2/s)	Dynamic viscosity— μ (kg/m s)	Thermal conductivity —K (W/m K)	Specific heat— C_P (kJ/ kg-K)	Specific Heat— C_v (kJ/kg-K)	C_P/C_v	Thermal diffusivity $K/\rho C_p$ (m^2/s)	Prandtl number Pr = $C_p\mu/K$
Helium 700°C, 4.84 MPa	2.3820	1.903 10^{-5}	4.533 10^{-5}	0.3563	5.1907	3.1161	1.6658	0.0288	0.660
Nitrogen 700°C, 0.69 MPa	2.3820	1.717 10^{-5}	4.0895 10^{-5}	0.0646	1.1624	0.8651	1.3437	0.0233	0.735
Property ratio N2/He	1.00	0.902	0.902	0.1813	0.2239	0.278	0.8066	0.8095	1.114

The calculations presented in this section were performed using the MathCad 2001 Professional computer program (Math Soft, Inc., 2001).

Core power scaling: Core power will need to be adjusted to provide the scaled core flow outlet temperature and core differential temperature for initial forced flow conditions. The core power that is transferred to core flow may be calculated from,

$$\dot{q}_{channels} = \dot{M} C_p \Delta T$$

where,

$\dot{q}_{channels}$ = *heat transfer rate to core channels*

$\dot{M}$=*mass flow rate* = $\rho_{avg,core} w_{avg,core} a_{avg,core}$

ΔT = *core differential temperature*

$w_{avg,core}$ = *core average velocity*

$a_{avg,core}$ = *core average cross section area*

Since $\dot{M}$ *and* ΔT are maintained in the nitrogen flow scaled system,

$$\dot{q}_{channels-N2} / \dot{q}_{channels-He} = Cp_{N2} / Cp_{He} = 0.224$$

The above scaling ratio is not the same as for total core power. Since bulk fluid temperatures for scaled nitrogen flow are the same as for the higher pressure helium flow, environmental heat losses will represent a larger fraction of the total core power for nitrogen flow than for helium flow in HTTF. Total core power will need to be specified and the resultant core temperature distribution determined by using a systems code such as RELAP5. It may be necessary to reduce heat transfer to the RCCS (by reducing RCCS coolant flow) to satisfy the temperature scaling requirements.

Loop natural convection flow: Scaling of loop natural convection flow during a PCC event may be specified by employing Equation 354 in Woods, et al. (2009), for core channel velocity,

$$w_{avg,core} = \left(\frac{\beta_{g,vessel} \dot{q}_{core} L}{\rho_{avg,core} a_{core} C_{p,avg,core} \Pi_F} \right)^{1/3} =$$

$$\left(\frac{\beta_{g,vessel} \rho_{avg,core} w_{avg,core} a_{avg,core} C_{p,avg,core} \Delta T_{core} L}{\rho_{avg,core} a_{core} C_{p,avg,core} \Pi_F} \right)^{1/3}$$

$$w_{avg,core} = \left(\frac{\beta_{g,vessel} \rho_{avg,core} a_{avg,core} C_{p,avg,core} \Delta T_{core} L}{\rho_{avg,core} a_{core} C_{p,avg,core} \Pi_F} \right)^{1/2}$$

where,

β = *thermal expansion coefficient = 1/T for ideal gas*

L=*core channel length*

a_{core} = *core cross-section area*

Π_F = *resistance number*

Inserting the appropriate ratios,

$$\frac{w_{MHTGR,core}}{w_{HTTF,core,N2}} = \left(\frac{16 * 4}{16} \right)^{1/2} = 2.0$$

This is a favorable result since it corresponds to the ideal velocity scaling relationship for both forced and natural convection.

Break mass flow rate during a DCC scenario: Break flow may be subdivided into a choked flow regime, which will occur when vessel pressure is above about twice that of the reactor cavity pressure; and an unchoked flow regime which will occur at lower pressures. Break mass flow rate $(\dot{m})$ is given in Woods, et al. (2009) Equation 60, as:

$$\dot{m}_{Brk,0,i} = \left(C_D G_{Brk,0} \alpha_{Brk}\right)$$

where,

$C_D =$ discharge coefficient

$\alpha_{Brk} =$ break area

$G_{Brk,0} =$ mass flux

For choked flow, equation 61 in Woods, et al., 2009,

$$G_{Brk,0} = \frac{P_{vessel,0}}{\left((ZR)_{g,vessel} T_{vessel,0}\right)^{1/2}} \left[\gamma_{g,vessel,0} \left(\frac{2}{\gamma_{g,vessel,0}+1}\right)^{n}\right]^{1/2}$$

where,

$Z =$ compressibility factor ≈ 1

R= gas constant = $C_p - C_v$

$\gamma_{g,vessel,0} = C_p / C_v$

$$n = \frac{\gamma_{g,vessel,0}+1}{\gamma_{g,vessel,0}-1}$$

After the break unchokes, the mass flux is a function of both the upstream and downstream pressures, (Woods, et al., 2009, Equation 84),

$$G_{Brk,T} = \sqrt{2\rho_{Brk,T}(P_{vessel,T} - P_{cavity,T})}$$

The exact critical pressure ratio (cavity pressure/vessel pressure) below which the break will unchoke is given by Shapiro (1953, p. 84, Equation 4.15b). Using Woods, et al. (2009) notation, the critical pressure ratios are,

$$\frac{P_{cavity,T}}{P_{vessel,T}} = \left(\frac{2}{\gamma+1}\right)^{\frac{\gamma}{\gamma+1}}$$

$$\left(\frac{P_{cavity,T}}{P_{vessel,T}}\right)_{N_2} = 0.538$$

$$\left(\frac{P_{cavity,T}}{P_{vessel,T}}\right)_{He} = 0.5027$$

$$P_{vessel,T-unchoke N_2} = 0.188 MPa$$

$$P_{vessel,T\text{-}unchoke He} = 0.202 MPa$$

where cavity pressure is assumed to be atmospheric pressure = 0.1 MPa.

The density ratio at which the break flow will unchoke may be determined from the ideal gas law ($P = \rho RT$) under the assumption of equal upstream temperature as,

$$\frac{\rho_{N2}}{\rho_{He}} = \frac{P_{N_2} R_{He}}{P_{He} R_{N2}} = \frac{P_{vessel,T-unchoke_{N_2}} (C_p - C_v)_{He}}{\mathrm{P}_{\mathrm{vessel,T\text{-}unchoke_{He}}} (C_p - C_v)_{N2}} = 6.526$$

The ratios of choked and initial unchoked mass fluxes for nitrogen flow compared with higher pressure helium flow, are calculated from the above two equations for $G_{Brk,0}$ and $G_{Brk,T}$ as,

$$G_{Brk,0R} = 0.362$$

and,

$$G_{Brk,TR} = 2.380$$

Since these values of mass flux ratios differ from each other and from the ideal scaling value of 1.0, then either the choked flow regime or the unchoked regime must be chosen for scaling. The scaled break flow area would then equal the inverse of the mass flux ratio,

$$\alpha_{R-\text{choked flow}} = 2.762$$

$$\alpha_{R-unchoked} = 0.420$$

For a break in which the system quickly depressurizes to below the critical pressure ratio, the unchoked flow value could be chosen to scale the break area, and for a small break, in which the vessel pressure spends on a significant period of time above the critical pressure ratio, the choked flow ratio could be used to scale the break area.

Choked flow depressurization transient: The simplified model presented in Lewis (1979) for depressurization of a gas-cooled system may be used to estimate the time to unchoke the break for either nitrogen or helium and to compare the two systems. The model assumes that temperature is constant since (Lewis argues), heat stored in the core and vessel walls causes the coolant in the primary system to remain close to its original temperature during depressurization. The model for pressure (P) at time t (s) is:

$$P(t) = P(t=0)e^{-t/\tau}$$

where the time constant τ (s) is,

$$\tau = \frac{\mathrm{V}}{\mathrm{A}_{\mathrm{break}} \sqrt{2RT}\psi_{\max}}$$

V = volume (m^3)

$\mathrm{A}_{\mathrm{break}}$ = break flow area (m^2)

R = gas constant (J/kg - K)

$$\psi_{\max} = \sqrt{\frac{\gamma}{2}\left(\frac{2}{\gamma+1}\right)^{\frac{\gamma+1}{\gamma-1}}}$$

$$\gamma = \mathrm{C_p}/C_v$$

For nitrogen, the time to unchoke the break starting from 0.69 MPa is,

$$t_{unchoke-N_2} = 0.158\frac{V}{A_{break}\sqrt{2T}}\ (s)$$

and for helium starting from 4.84 Mpa

$$t_{unchoke-he} = 0.135\frac{V}{A_{break}\sqrt{2T}}\ (s)$$

The time to unchoke versus the ratio of A_{break}/V for an initial temperature of 700°C and the above pressures are shown in Figure 5-1. Although the time to unchoke for the same size break is quite similar for nitrogen and helium, the mass flow rates differ as stated above. If the break area is increased for nitrogen flow by the above factor of 2.762 to account for break mass flow rate scaling, then the nitrogen system will unchoke more rapidly than helium by a factor of:

$$\frac{t_{unchoke-N_2}}{t_{unchoke-He}} = \frac{0.158}{0.135 * 2.763} = 0.424$$

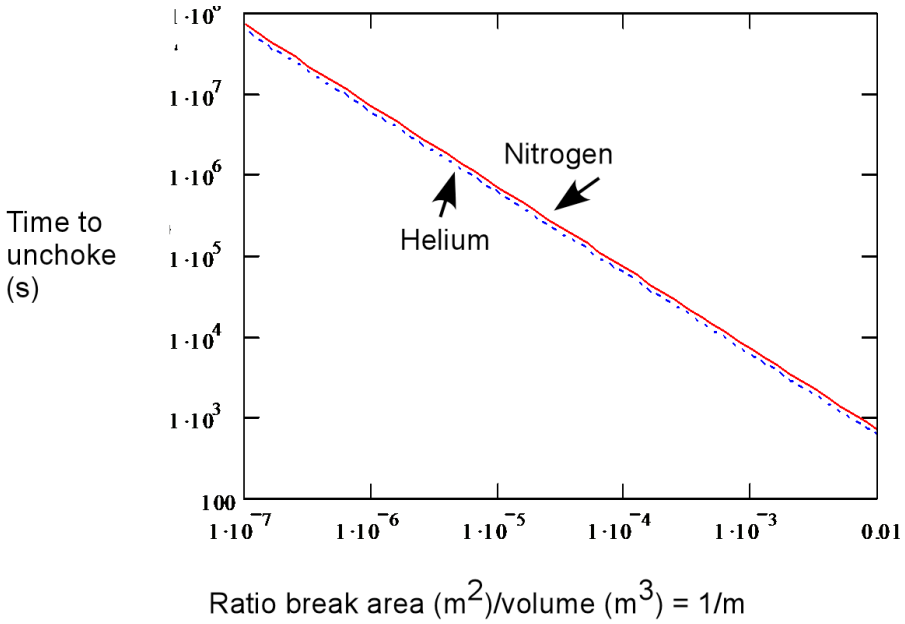

Figure 5-1. Comparison of unchoking time for nitrogen and helium as a function of break area to volume ratio.

Forced flow and loop natural convection heat transfer scaling: Forced convection or loop natural convection heat transfer scaling may be investigated by employing a typical heat transfer correlation such as the Dittus-Boelter (1930) correlation for turbulent flow,

$$Nu = hD/K = 0.021\mathrm{Re}^{0.8}\,\mathrm{Pr}^{0.4}$$

where

h = convection heat transfer coefficient

D = channel diameter

K = thermal conductivity

Re = Reynolds number = VD/ν.

For core channel flow the ratios of Reynolds numbers and convection heat transfer coefficients in an MHTGR core channel compared with HTTF using nitrogen flow are,

$$\mathrm{Re}_R = \mathrm{Re}_{MHTGR}/\,\mathrm{Re}_{HTTF} = \left(\frac{\nu_{He}}{\nu_{N2}}\right)\left(\frac{w_{MHTGR}}{w_{HTTF}}\right) = 2.217$$

w = velocity

$$Nu_R = \mathrm{Re}_R^{\,0.8}\,\mathrm{Pr}_R^{\,0.33} = 1.810$$

$$h_R = \frac{K_{He}}{K_{N2}}\left(\mathrm{Re}_R\right)^{0.8}\left(\frac{\mathrm{Pr}_{He}}{\mathrm{Pr}_{N2}}\right)^{0.4} = 10.004$$

where it is assumed that,

$$\frac{D_{channel-HTTF}}{D_{channel-MHTGR}} = 1$$

and,

$$V_{MHTGR}/V_{HTTF} = 2$$

A similar approach may be taken for laminar core channel flow and for flow in other components.

Free convection heat transfer scaling: Free convection heat transfer in, for example, the upper plenum may be investigated by employing a suitable correlation. Most correlations, such as those given in Kreith (1958) formulate Nusselt number as a function of Grashoff number (Gr) and Prandtl number (or Rayleigh number, the product of Gr and Pr), where,

$$Gr = \frac{g\beta\left(T_{bulk} - T_{surface}\right)L^3}{\nu^3}$$

The ratios of Gr and Pr for prototypical MHTGR conditions compared with those for nitrogen flow in HTTF are,

$$Gr_R = \frac{L_R^3}{\nu_R^2} = 78.66$$

$$\mathrm{Pr}_R = 0.898$$

If free convection flow in both the prototype and in HTTF are laminar then, for vertical plates or cylinders, the convection coefficient is proportional to vertical distance to the ¼ power (Kreith, 1958). A simple correlation for the average Nusselt number is given by Kreith (1958) as,

$$N\bar{u}_L = \frac{\bar{h}_L L}{K} = 0.480\ Gr_L^{1/4}$$

and the ratios of MHTGR values divided by HTTF values are,

$$N\bar{u}_{L_R} = Gr_R^{1/4} = 2.978$$

$$\bar{h}_R = N\bar{u}_R \frac{K_R}{L_R} = 4.113$$

If the flow is turbulent in both the prototype and in HTTF then a simple free convection correlation given by McAdams (1951) may be used,

$$N\bar{u}_L = 0.13(Gr\ \mathrm{Pr})^{1/3}$$

and the ratios are,

$$N\bar{u}_{L_R} = 1.033$$

$$\bar{h}_R = N\bar{u}_R \frac{K_R}{L_R} = 1.434$$

The free convection laminar-turbulent transition Grashoff number is approximately $Gr=10^9$ (Kreith, 1958). Therefore, because Gr is more than a factor of 78 times larger in the prototype, free convection flow in HTTF is likely to be laminar whereas the corresponding flow in the prototype is turbulent. In this case the actual values of Gr will need to be calculated for the components in question and the appropriate correlations employed in order to determine the convection coefficients and the ratios. In other words, there is no simple and direct way to scale prototypical free convection heat transfer conditions from HTTF; a systems code such as RELAP5 will need to be employed.

Core channel-to-channel natural circulation scaling: Although a channel-to-channel natural circulation scaling relationship may be derived from the simplified model presented in section 6, in-core natural circulation is largely determined by the core temperature distribution, which needs to be determined from a more thorough analysis using a systems or CFD code. However, if nitrogen is employed in HTTF to simulate only the initial period of a transient or accident then in-core natural circulation will not come into play.

Concluding remarks: Nitrogen flow in HTTF may be used to represent helium flow at higher pressure during either a loss of forced flow PCC event or during a limited period of a loss of forced flow DCC event (but before air ingress). The use of nitrogen produces the desired velocity scaling ratio of 1/2 in HTTF as compared with the prototype MHTGR under corresponding loop natural convection conditions. Nitrogen flow also results in higher Reynolds numbers under forced and loop natural convections conditions than for helium flow experiments in HTTF, which is a favorable result. However, because of varying heat transfer mechanisms and flow regimes in HTTF, there is no direct scaling method to relate heat transfer in HTTF to the prototype. Heat transfer and core power requirements must be first investigated by use of a systems code such as RELAP5 in order to determine the scaling factors and to specify core power and RCCS heat transfer requirements. The use of nitrogen in HTTF is more likely to scale well to the initial period of a PCC event rather than later when three dimensional aspects of heat

transfer, such as core temperature distribution driving in-core natural circulation, will become significant. For a DCC event, the large difference in break mass flow rate scaling ratios for choked flow versus unchoked flow precludes modeling both regimes in a well-scaled single experiment. If either choked flow or unchoked flow is chosen to scale the DCC experiment then the break flow area may be adjusted to provide the correct scaled mass flow rate for that flow regime but not the other.

The simple scaling analyses presented indicate that there are aspects of using lower pressure nitrogen flow to represent higher pressure helium flow that will scale well to the prototype and other aspects that will not scale well. It is recommended that a series of calculations using a systems code such as RELAP5 be used to determine the flow and heat transfer response of using nitrogen in HTTF. The calculations would be used to help determine core power and RCCS heat transfer requirements and flow and heat transfer scaling ratios.

6. STUDY OF DUAL-CHANNEL NATURAL CIRCULATION DURING A PCC SCENARIO

Consider natural circulation within two circular cross-section channels of the core, consisting of a representative hot channel and a representative cool channel. The heat input to the hot Channel 1 is Q_1 (J/s) and the heat removed from cooler Channel 2 is Q_2. Heat removed from the upper plenum per hot channel is Q_{out} and:

β = thermal expansion coefficient (1/K)

ρ = density (kg/m^3)

μ = dynamic viscosity (kg/m-s).

The configuration considered is shown in Figure 6-1.

6.1 Assumptions

- No lower plenum heat transfer
- Heat is primarily removed through upper plenum
- Linear density and temperature profiles in Channels 1 and 2 with thermal centers at same elevation
- Boussinesq approximation is applicable (fluid properties are constant except density in buoyancy terms)
- Steady-state 1-D flow
- Acceleration pressure changes are neglected.
- No flow in hot duct or upcomer.

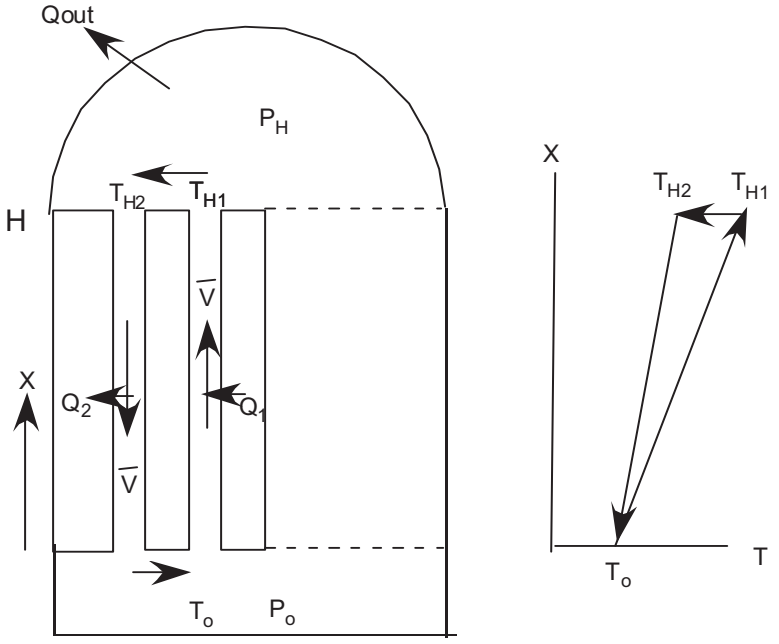

Figure 6-1. Geometry considered for natural circulation dual-channel behavior analysis.

Pressure change between the lower plenum at pressure P_o and the upper plenum at pressure P_H is assumed to be a balance between hydrostatic pressure and frictional pressure loss. This is the typical approach for analyzing natural convection involving a core and a heat exchanger at a higher elevation. However, in this case, the core heat source and the core heat sink are at similar elevations and it is assumed that the primary heat removal sink driving natural circulation is heat transfer from the upper plenum to the atmosphere.

6.2 Up-flow in Channel 1

$$P_o = P_H + \int_0^H (\bar{\rho} g x - \bar{\rho} g \beta (T_x - T_o))dx + f \frac{H}{2D} \bar{\rho} \bar{V}^2$$

where,

$$T_x - T_o = (T_H - T_o)(x / H)$$

$$P_o - P_H = \bar{\rho} g H - g \frac{H}{2} \beta \bar{\rho} (T_{H1} - T_o) + f \frac{H}{2D} \bar{\rho} \bar{V}^2$$

$$T_{H1} - T_o = \frac{Q_1}{\dot{m} C_P}$$

6.3 Down-flow in Channel 2

$$P_o - P_H = \bar{\rho} g H - g \frac{H}{2} \beta \bar{\rho} (T_{H2} - T_o) - f \frac{H}{2D} \bar{\rho} \bar{V}^2$$

$$T_{H2} - T_o = \frac{Q_2}{\dot{m} C_P}$$

$$T_{H1} - T_{H2} = \frac{Q_{out}}{\dot{m} C_P}$$

$$Q_1 = Q_{out} + Q_2$$

Equating the two equations for P_o - P_H

$$-g \frac{H}{2} \beta \bar{\rho} \frac{Q_1}{\dot{m} C_P} + f \frac{H}{2D} \bar{\rho} \bar{V}^2 = -g \frac{H}{2} \beta \bar{\rho} \frac{Q_1 - Q_2}{\dot{m} C_P} - f \frac{H}{D} \bar{\rho} \bar{V}^2$$

substituting

$$\dot{m} = \bar{\rho} \bar{V} \frac{\pi D^2}{4}$$

solve for $\bar{V}$

$$\bar{V} = \left| \frac{4 g \beta Q_{out}}{f C_p \pi \bar{\rho} D} \right|^{1/3} \qquad \textit{units} \quad \left(\frac{m/s^2 \;\; 1/K \;\; \text{J/s}}{\text{J/kg-K} \;\; \text{m} \;\; \text{kg/m}^3} \right)^{1/3} = \text{m/s}$$

This equation assumes that f is constant and therefore that flow is turbulent. If flow is laminar then,

$$f = \frac{64}{\mathrm{Re}} = \frac{64\mu}{\bar{\rho}\bar{V}D}$$

$$\bar{V} = \left| \frac{g\beta Q_{out}}{16\mu C_P \pi} \right|^{1/2}$$

Scaling considerations: Since core power density in HTTF is twice that of the prototype (from Eq. 442 in the OSU scaling document, Woods, et al. 2009[m]) and the channel diameter is expected to be similar to that of the prototype, then natural circulation velocity in HTTF is expected to be slightly higher than in the prototype from the above equations. Ideally, the velocity would be half that of the prototype to be consistent with the overall scaling rationale.

[m] Equation 442 in Woods et al. gives the Loop Core Power Number (LCPN). Given that the desired result is to have the HTTF LCPN equal the MHTGR LCPN, then following cancelation of equal quantities on both sides of the equality, the remaining ratios on both sides of the equality are the products of the core power density and the length between the thermal centers divided by the flow rate for the HTTF and the MHTGR respectively. Because the HTTF flow rate to the MHTGR flow rate is 1/2 and the distance between the thermal centers of the HTTF to that of the MHTGR is 1/4, then the ratio of the thermal center length to the velocity is 2.

7. INVESTIGATION OF TEMPERATURE DISTRIBUTION IN HTTF CORE FOR ASYMMETRIC UNIT CELLS

OSU is investigating various core designs with the intention of reducing the number of coolant channels and/or heaters. The OSU baseline design had six cooling channels adjacent to each heater rod and is identified in this chapter as Case 1. An OSU alternate to the baseline design is shown in Figure 7-1—which has alternatively four coolant channels per heater rod and six coolant channels per heater rod. The alternate design is identified as Case 2. The Case 2 unit cell that has only four coolant channels per heater rod is Case 2a and the other unit cell that has six coolant channels per heater rod is Case 2b.

The concern for the various HTTF core designs that have non-uniform numbers of coolant channels in an alternating fashion within the same core, per heater rod is the evenness of heat transfer (non-uniform temperature gradients from one unit cell to the next), the ability of RELAP5 to model the core heat transfer, and the potential for insufficient cooling of the heater rods which have fewer adjacent cooling channels. A first look at the non-uniformity of the heat transfer in the central region of the coolant channel lattice is addressed in the present calculations by comparing the temperature distributions for Case 1 and Case 2.

The calculations were performed by analyzing the temperature field in the HTTF core region for unit cells of single heater rods surrounded by first four coolant channels and then six coolant channels (Case 2a and Case 2b respectively). Subsequently, analyses were performed to characterize the temperature field in the HTTF core region unit cell that consists of a single heater rod surrounded by six cooling channels (Case 1). The calculational meshes of the models created to perform these analyses are shown in Figure 7-2 for Case 2a and in Figure 7-3 for Case 1. It should be noted that because the net number of coolant channels for an HTTF core that has a heater rod configuration that is alternately cooled by four and then six coolant (Case 2) has larger average coolant channel flow areas than the design with a uniform six cooling channels to heater rod configuration (Case 1)—since both HTTF core configurations have the same total flow area that consists of the sum of all the coolant channel areas.

The method of comparing the Case 2 core design with the Case 1 core design was to use the software FlexPdE[n] to analyze a unit cell containing one heater rod plus the surrounding coolant channel segment. The software solves the transient conduction equation in two dimensions with the heat source assumed to be suddenly applied at time t=0 as a boundary condition. The initial temperature of the core is assumed to be equal to the (constant) coolant temperature. Heat transfer to the coolant channel is assumed to occur with constant convection coefficient, h. Parameters used in the calculations are listed below.

Core material properties (preliminary values provided by OSU):

- Density = 2,300 kg/m^3
- Specific heat = 1,000 J/kg K
- Thermal conductivity = 4 W/m K
- Heater rod power/ length = 600 kW/(282 rods*1.98m) = 1.08 kW/m
- Rod diameter = 19.05 mm (0.75 in.)
- HTTF core design with heater rod unit cells that have alternating four and six cooling channels per heater rod (Case 2) = 16.76 mm (0.66 in.)
- Baseline HTTF (Case 1) core design coolant channel diameter = 14.99 mm (0.59 in.)
- Coolant channel temperature = 800°C.

n. PdE Solutions, Inc., Spokane Valley, Wa, 2009.

The same heater rod diameter and power are assumed for Case 1 and Case 2 for comparison. It is assumed that the total core flow area is the same for both designs. Therefore, the flow area per channel is smaller by a factor of approximately 0.8 for the original design since two out of ten lattice positions for coolant channels in the alternate design are blank (this does not consider possible diameter design differences in the outer flow channels adjacent to the reflector). The Reynolds number for flow in the Case 1 design (which is proportional to diameter) is therefore smaller by a factor of the square root of 0.8 (assuming equal velocity) compared with the Case 2 design and the convection coefficient, assuming that the Dittus-Boelter (1930) correlation is applicable, is smaller by a factor of the square root of 0.8 raised to the power of 0.8 = 0.9146. The convection coefficients used in the calculations (typical values for natural convection) are h = 36.58 W/m^2 K for the Case 1 design and h = 40 W/m^2 K for the Case 2 design.

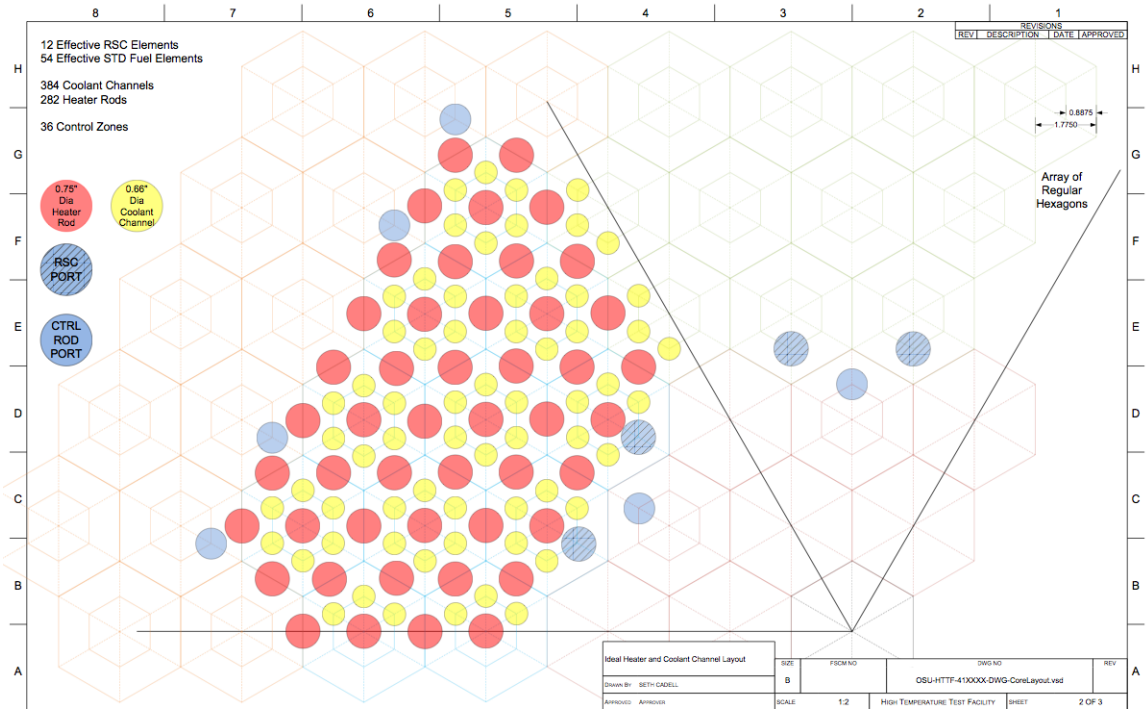

Figure 7-1. Case 2 HTTF core layout.

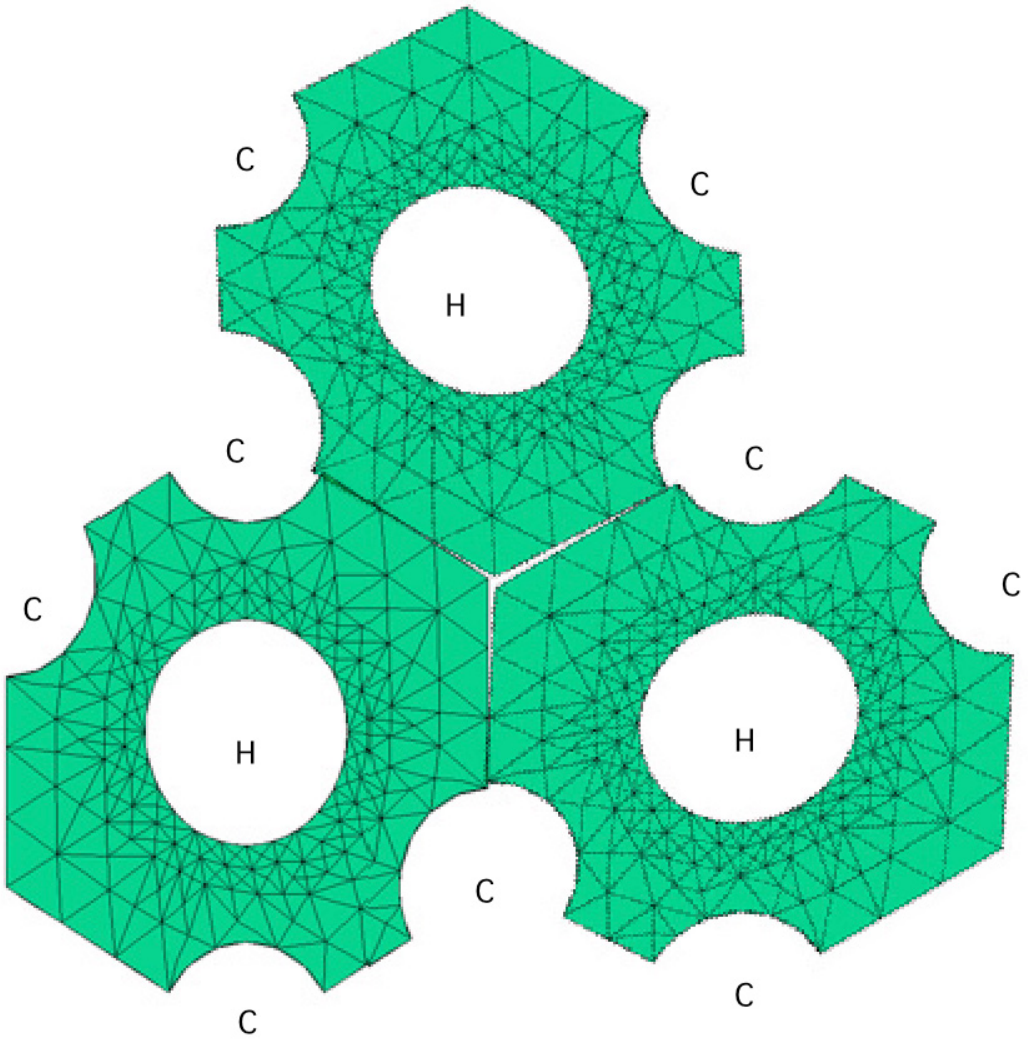

Figure 7-2. Case 2a core design nodalization (four cooling channels per heater rod).

The Case 2a core design nodalization, as shown above, has three adjacent cells in which each heater rod transfers heat to four coolant channels. Cell boundaries are assumed to be adiabatic outside boundaries with coolant channels. For coolant channels, heat flux is assumed to be = -h(Temperature-$T_{coolant}$) with both h and $T_{coolant}$ set as constant. Heater power is assumed to be constant. H indicates heater rod position and C indicates coolant channel. A similar approach was used for Case 1 (see Figure 7-3) and Case 2b.

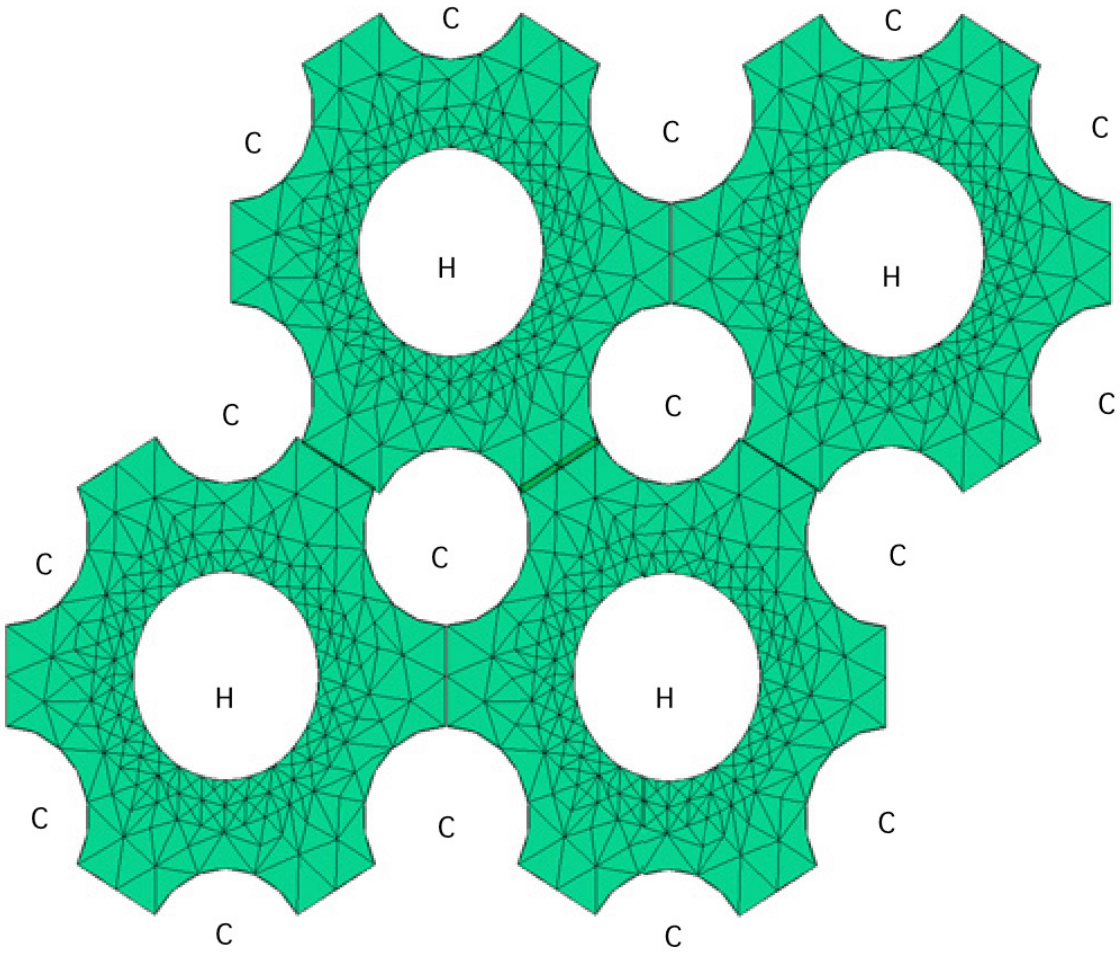

Figure 7-3. Case 1 design showing four cells where each heater rod transfers heat to six coolant channels. H indicates heater, C indicates coolant channel.

The Case 1 analysis is shown in Figures 7-4 and 7-5. The calculated temperature distribution is shown in Figure 7-4 while calculated temperatures, normalized on the basis of the maximum calculated temperature are shown in Figure 7-5. Because of the symmetric distribution of cooling channels about the heater rod, the calculated Case 1 temperature profiles show a uniform distribution that is defined on the basis of the cooling channel location. The maximum calculated temperature is 819.23 ºC.

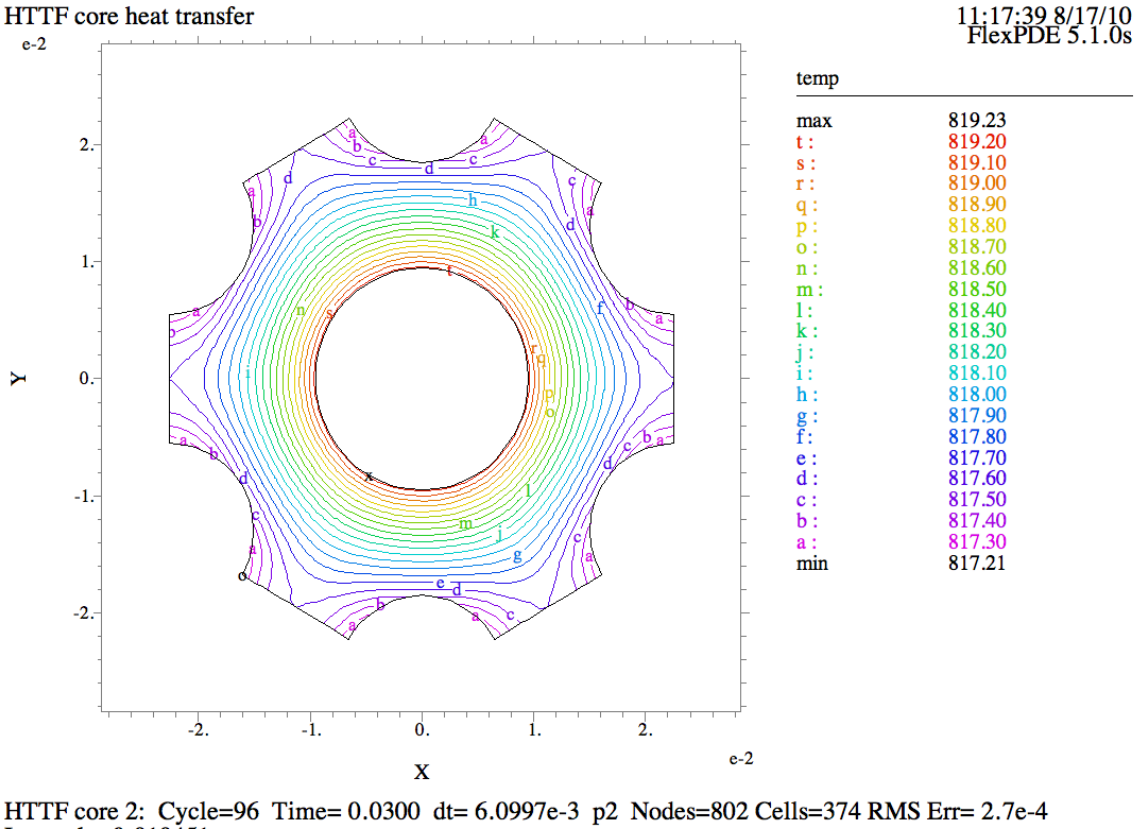

Figure 7-4. Calculated final temperature profile for Case 1 design.

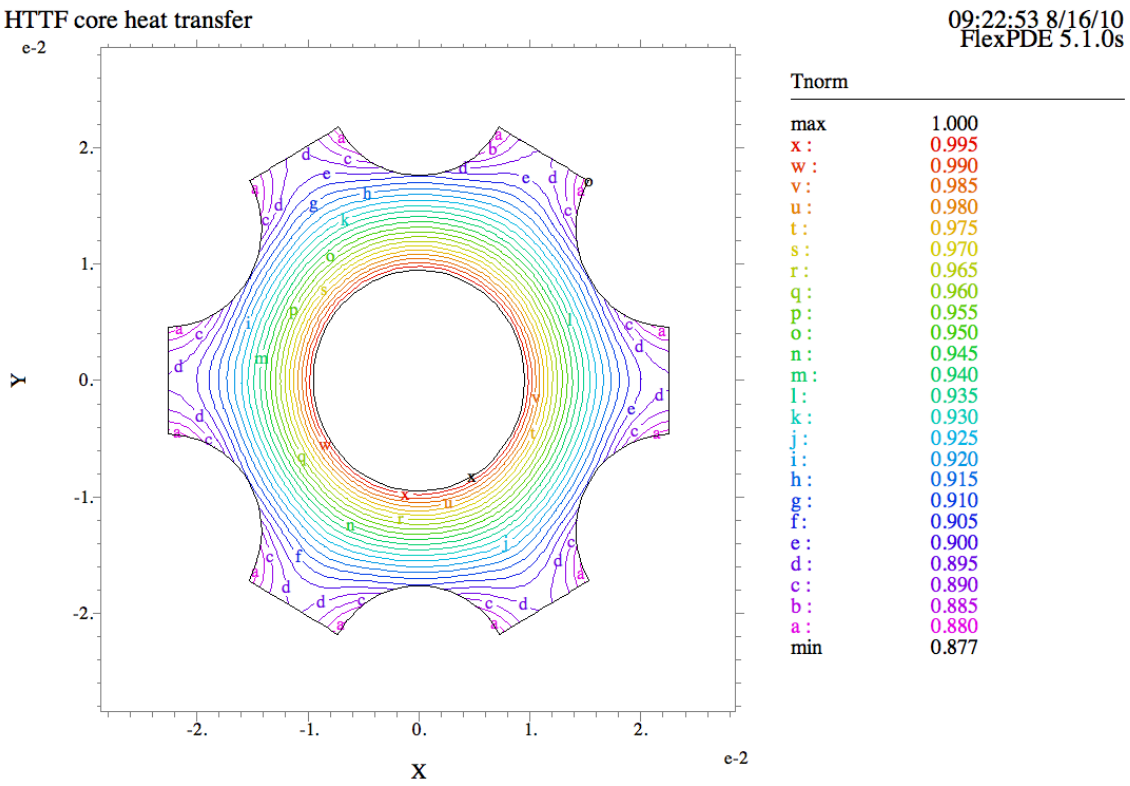

Figure 7-5. Normalized temperature distribution for Case 1 design.
(Tnormalized = T-Tcoolant)/(Tmax-Tcoolant)

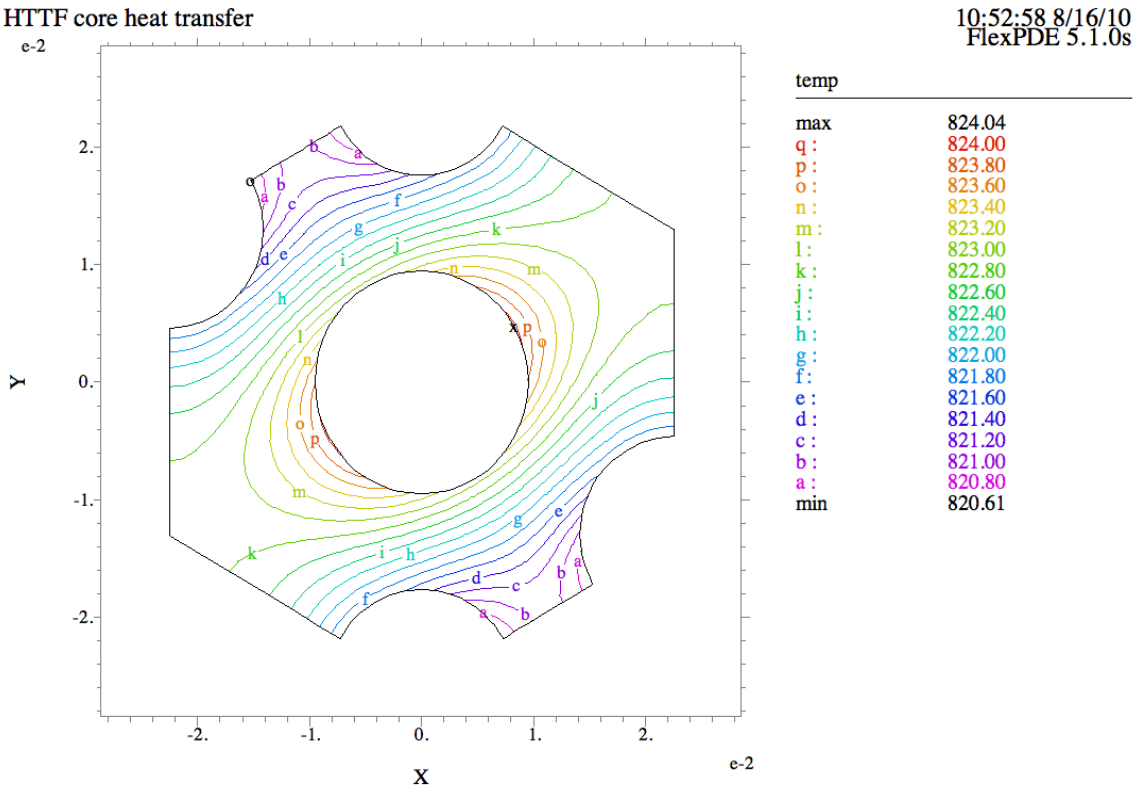

HTTF core 2-2: Cycle=94 Time= 0.0300 dt= 5.2163e-3 p2 Nodes=803 Cells=375 RMS Err= 0.0011

Figure 7-6. Calculated final temperature profile for Case 2a design for a cell surrounded by four coolant channels.

The results of similar calculations, performed to study the Case 2a and Case 2b configurations, are shown in Figures 7-6 and 7-7 respectively. The maximum calculated temperature for Case 2a is 824.04 ºC while the maximum calculated temperature for Case 2b is 815.95 ºC. The maximum temperature of Case 2b is somewhat lower than that for Case 1 because the convective heat transfer is larger for Case 2b than for Case 1—as noted in the discussion in the above paragraphs. The differences in the maximum temperatures between Cases 2a and 2b are indicative of the sort of temperature variations that will be experienced in the Case 2 design, i.e., less than 10 ºC for a similar radial location with respect to the heater rod periphery.

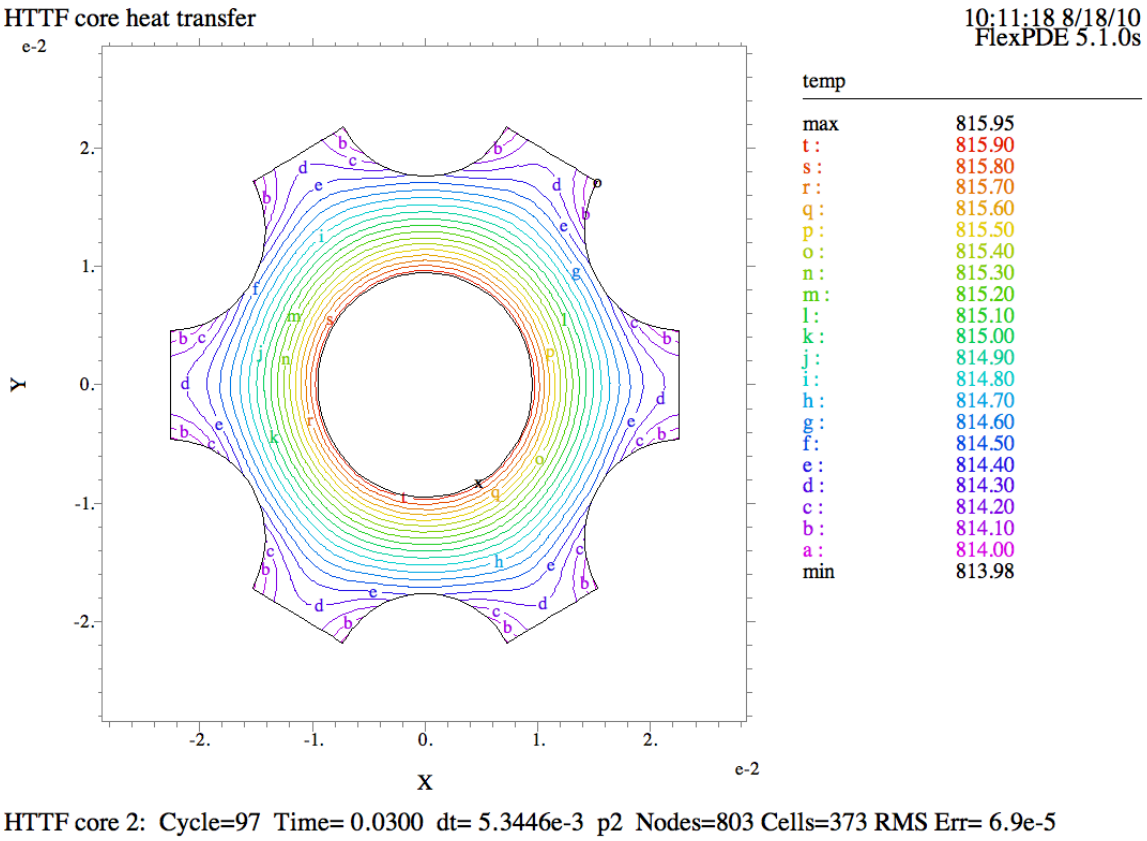

Figure 7-7. Calculated final temperature profile for Case 2b design for a cell surrounded by six coolant channels.

Concluding remarks: These preliminary calculations show that there is distortion of the temperature profile of the Case 2 design compared with the Case 1 design, although the maximum calculated temperatures of the Case 2 design for this example (approximately 824°C for the cells surrounded by four coolant channels and 816°C for cells surrounded by six coolant channels) are not greatly different than that calculated for the equivalent Case 1design (approximately 819°C) and the averages of the maximum temperatures for the Case 2 design is approximately equal to the maximum temperature of the Case 1 design.

These preliminary results give a qualitative indication that the Case 2 core design approach may be a viable option. However, before any definitive conclusions are reached concerning the core design that is chosen to build, a more complete CFD analysis needs to be undertaken to study the complete core (or a symmetric pie section representation) over a representative range of powers and convection coefficients. Also, the suitability of modeling the final core design with RELAP5 and other systems' codes should be addressed by using CFD studies in conjunction with RELAP5 studies since the RELAP5 model will lump cells surrounded by six coolant channels and four channels into annular rings. The approximately 5°C maximum temperature variation between cells for this example would not be seen in the RELAP5 calculations.

8. STUDIES OF STEADY-STATE BEHAVIOR IN MHTGR AND HTTF USING RELAP5-3D AND CFD

Thermal-hydraulic analyses of the HTTF were performed to support the design of the facility. Of particular interest was how the facility scaling may result in behavior different from the reference nuclear reactor (distortions). To address this concern, scoping models for both the reference MHTGR and HTTF were developed using the RELAP5-3D computer code. Computational fluid dynamics (CFD) simulations of the HTTF were also performed using the STAR-CCM+ computer code.

8.1 MHTGR Modeling and Analysis

A scoping RELAP5-3D model of a portion of the MHTGR was developed to provide an indication of how the core would respond to conduction cooldown transients. Steady state and transient simulations were performed that included uncertainties in certain geometric design parameters.

8.1.1 RELAP5-3D Input Model Description

The RELAP5-3D input model for the MHTGR was developed as a scoping model to provide reference simulations to compare with HTTF simulations. The model included the reactor vessel, the reactor cavity atmosphere, and the RCCS. Boundary conditions were applied where the cross vessel connects to the reactor vessel flow inlet and outlet. Information used to develop the model was obtained from the MHTGR Preliminary Safety Information Document (PSID).[1]

Figure 8-1 shows the reactor vessel nodalization for the model. Cold helium enters the reactor vessel, flows into a region below the outlet plenum, then passes into the coolant riser channels on the outside of the core barrel. This flow enters the upper plenum before passing through a number of parallel channels in the core and reflectors. Flow exiting these paths is collected in the outlet plenum before flowing back out of the reactor vessel into the hot duct. The helium between the core barrel and reactor vessel, outside of the riser channels, was also included in the model.

A cross section of the MHTGR reactor vessel in the core region is shown in Figure 8-2, and the corresponding RELAP5-3D modeling approach is presented in Figure 8-3. Each reflector ring was modeled as a separate heat structure, with a gap in between rings through which helium flows. The central reflector ring closest to the core was further divided into inner and outer halves. The inner half is solid, and the outer half contains the control rod hole and related coolant holes; Figure 8-4 illustrates the modeling. Radiative and convective heat transfer was modeled between the reflector rings.

Three core rings were modeled using representative unit cells, which are shown in Figure 8-5. A coolant hole is in the center, surrounded by concentric rings of graphite, fuel, and more graphite. Heat is transferred from the core to the adjacent reflector rings via conduction. The coolant gaps in the core are only connected to the middle core ring; this was done with the expectation that modeling a convective path between the core and reflector would result in an uncharacteristically large radial heat transfer, because the actual block surface area in contact with the coolant gaps is much smaller than the modeled surface area in the core rings.

Radiation and convection were modeled from the side reflector to the core barrel, from the barrel to the riser channels and reactor vessel, and from the reactor vessel to the air-cooled RCCS. Radiation was also modeled from the top reflector to the upper plenum shield, and from the shield to the upper head. Axial conduction was modeled in all of the vertical structures except the confinement wall.

Steady state calculations were performed at the rated core power of 350 MW. A constant radial power density was assumed in the fuel blocks, with a chopped cosine axial power shape with a peak-to-average

ratio of 1.2. All of the power was deposited in the fuel; gamma heating of the reflector blocks was not modeled. The model was adjusted as necessary to obtain a total bypass flow of about 11%. Figure 8-1 presents the calculated initial conditions compared to the operating conditions provided in the PSID. While more model adjustments could have been made to achieve a higher core pressure drop, the lower resistance will not have a significant effect on the transients of interest, in which there is no forced flow through the core.

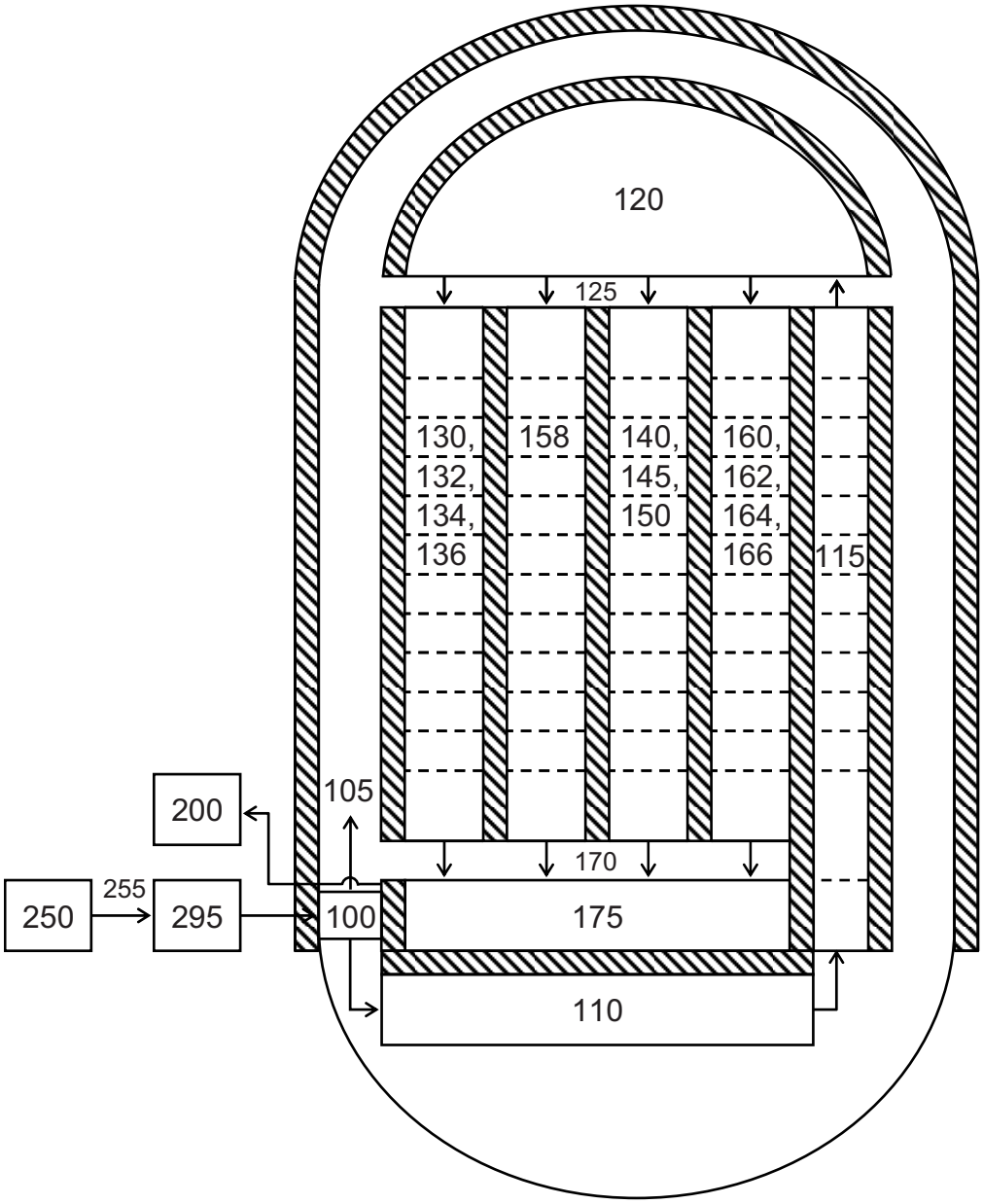

Figure 8-1. RELAP5-3D nodalization of the MHTGR reactor vessel.

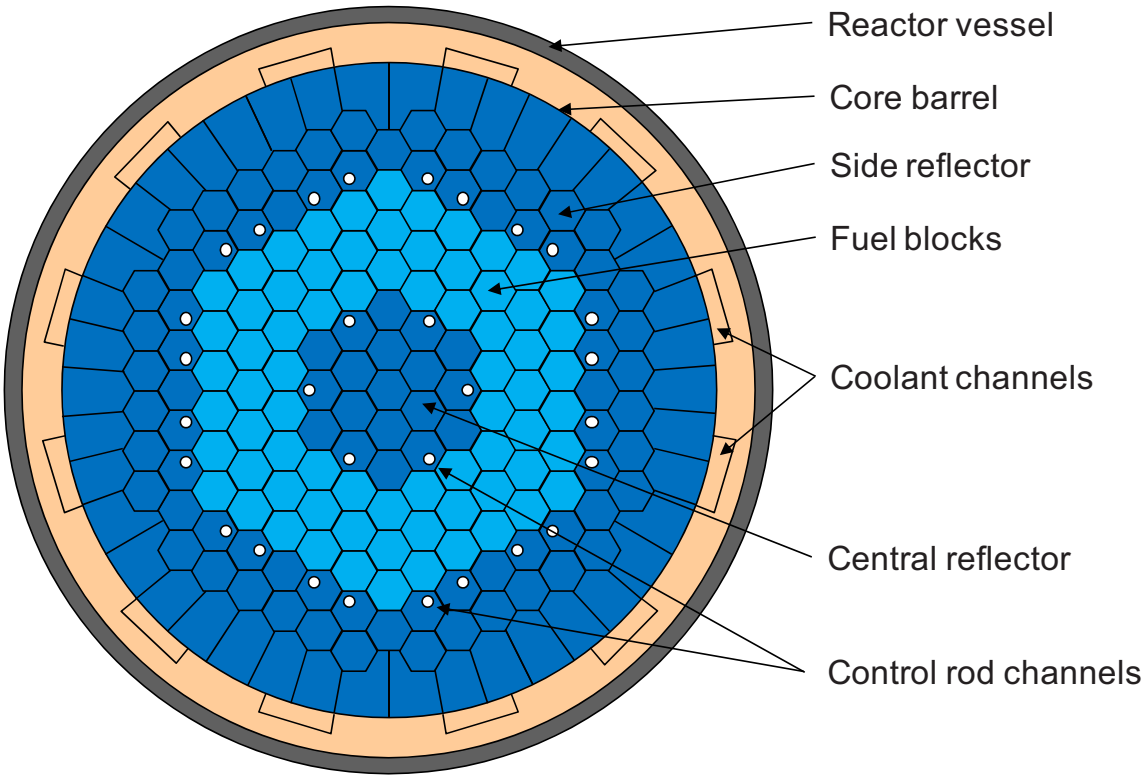

Figure 8-2. Cross section of the MHTGR reactor vessel in the core region.

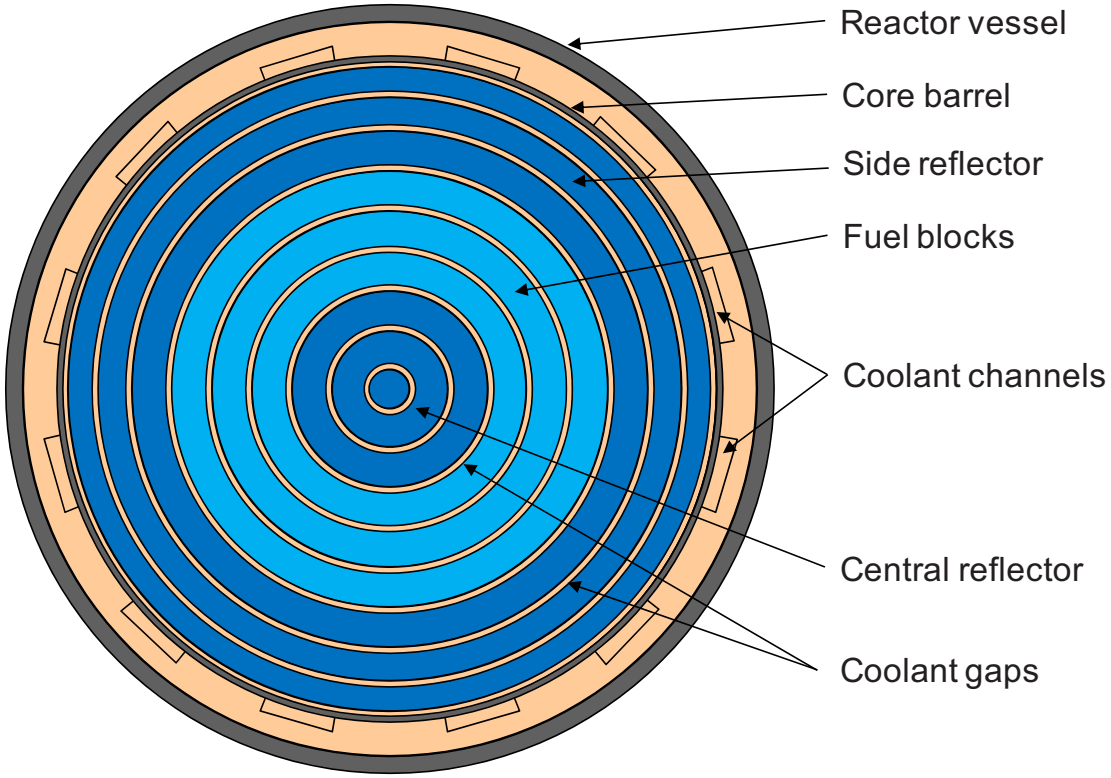

Figure 8-3. Cross-section of the RELAP5-3D model of the MHTGR reactor vessel.

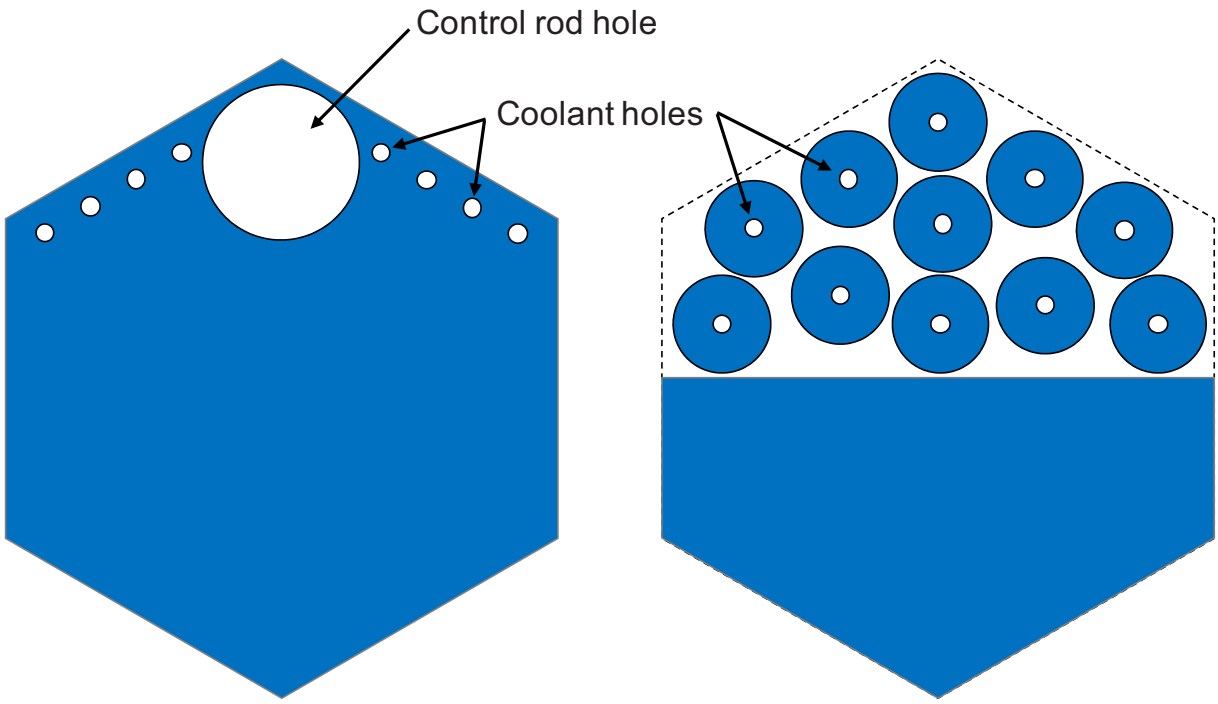

Figure 8-4. RELAP5-3D modeling of the MHTGR central reflector outer ring.

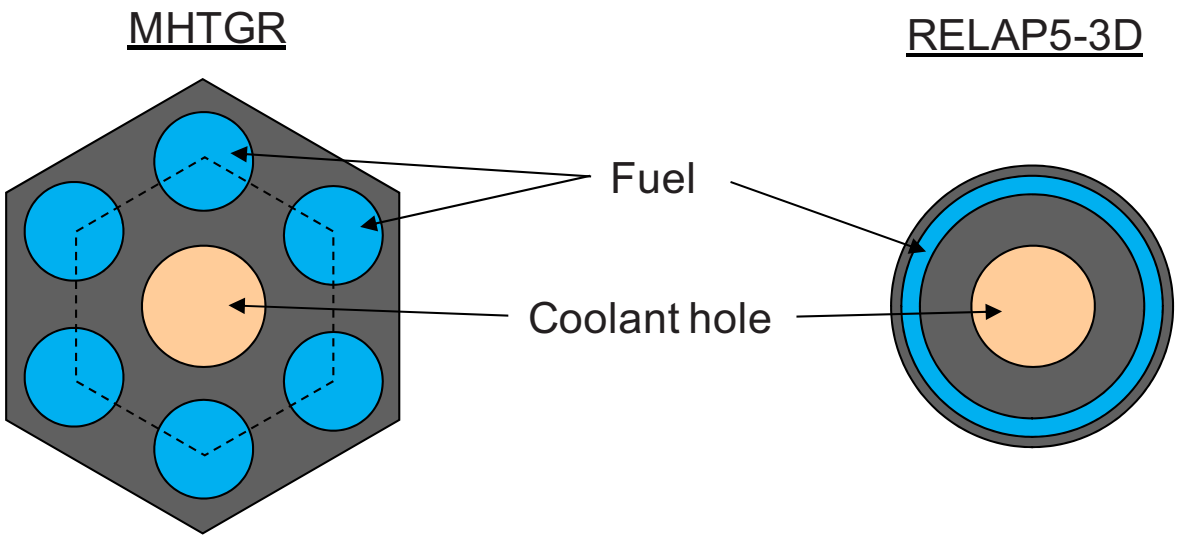

Figure 8-5. Unit cell for the core rings in the RELAP5-3D MHTGR model.

Table 8-1. Desired and calculated MHTGR steady state conditions.

Parameter	Desired	Calculated
Reactor power (MW)	350	350
Helium inlet temperature (°C)	258.6	258.6
Helium outlet temperature (°C)	687	687
Coolant flow rate (kg/s)	157.05	156.66
Total bypass flow	11	10.8
Inlet pressure (MPa)	6.38	6.38
Core pressure drop (kPa)	31.4	25.8
RCCS heat removal (MW)	0.7	0.69

8.1.2 Base Transient Simulations

After the desired steady state conditions were achieved, simulations of two base conduction cooldown transients were performed. The DCC was modeled by imposing a 10-s depressurization to atmospheric pressure, after which both the reactor vessel inlet and outlet were open to helium-filled volumes at atmospheric pressure. The PCC was simulated by a 60-second forced flow coastdown with the reactor vessel outlet maintained at normal operating pressure and the reactor vessel inlet isolated. In both transients, a reactor scram signal was assumed to be generated at transient initiation.

Figure 8-6 presents the peak fuel temperatures calculated for the base DCC and PCC transients. The peak temperature initially decreased in the PCC transient because the flow coasted down slower than the power; the forced convection heat transfer was sufficient to remove some of the stored energy in the core. As the forced convection cooling was lost as the flow coastdown ended, energy was moved from the hotter parts of the core both radially and axially to cooler parts of the reactor. After about 4 hours, the core and reflectors began a gradual heatup. By contrast, the rapid depressurization in the DCC transient resulted in little heat transfer in the core, and the peak temperatures rose as the transient began. The temperature increase slowed after 1-2 hours as energy was redistributed in the core and reflectors, then increased more rapidly after about 10 hours. The temperatures in both cases continued to rise until reaching maximum values, then slowly decreased as the RCCS heat removal exceeded the decay heat generation. In the DCC case the peak temperature of 935°C occurred at 36 h, while in the PCC transient the peak temperature of 844°C occurred at 42 hours.

Reactor vessel temperatures for these two cases are shown in Figure 8-7 from the location that had the highest peak temperature. In both cases, the temperatures decreased at the beginning of the transient, as the reactor scram reduced the amount of heat being generated in the core. The temperature then increased earlier in the PCC case, because natural convection within the reactor vessel was effective in moving heat from the fuel regions to the core periphery; with the vessel inlet blocked in the model, the hot helium rising through the hotter portions of the core was forced back down through gaps between cooler reflector blocks, such as between the permanent reflector and the core barrel. The heatup of the vessel lagged that of the core, continuing for a much longer time before the RCCS was able to remove more heat than was being transferred from the vessel interior. The DCC case peak vessel temperature of 320°C occurred at 110 hours, and the PCC case peak temperature of 310°C occurred at 84 hours.

Figure 8-8 shows the RCCS heat removal for the two conduction cooldown transients. The heat removal closely followed the axial average reactor vessel temperatures throughout the simulation. The heat removal dropped at the beginning of the transient as core power was reduced and less heat was transferred out to the reactor vessel. As the transient progressed, increased temperatures in the core and

reflectors resulted in increased reactor vessel temperatures, which in turn resulted in increased radiation heat transfer to the RCCS. Overall, component temperatures in the reactor vessel decreased after the RCCS heat removal rate exceeded the decay heat generation rate; this occurred near 11 hours in the DCC and near 77 hours in the PCC.

One notable difference from the point design analyses[2] is the much lower peak fuel temperatures, which were close to 1600°C for the gas turbine modular helium reactor. Several factors contribute to this reduction, including a 150°C lower helium outlet temperature and a 10% lower core power density. The steady state (initial) temperature of the reflectors was also much lower than in the earlier analyses because of the more detailed modeling of the inter-block gap flow paths. The flow in the gaps was calculated to be in turbulent flow, resulting in reasonably convective heat transfer coefficients that helped cool the reflectors. The two-dimensional nature of the RELAP5-3D input model does not allow for azimuthal variations in the reflector and core to be accounted for. This would tend to reduce the predicted temperature of the central reflector because the entire outer portion of that reflector is modeled as being in reasonable proximity to control rod or coolant holes; the reflector blocks without control rod holes are not modeled separately. A three-dimensional model that accounted for the difference in reflector blocks would likely see more heat transfer from the core into the central reflector. Another factor that may contribute to lower reflector temperatures is that direct heat transfer between the core and reflector heat structures in the RELAP5-3D code is limited to either radiation or conduction, not both.

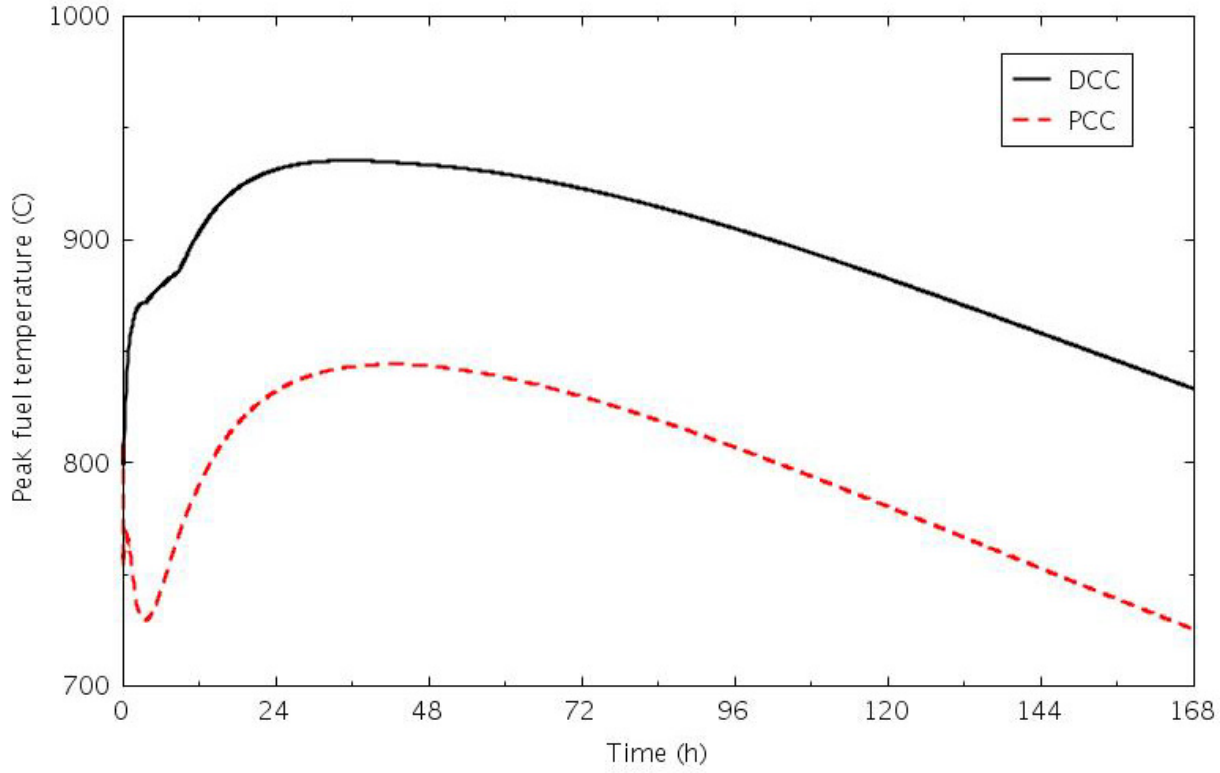

Figure 8-6. Peak fuel temperatures for the MHTGR base case DCC and PCC simulations.

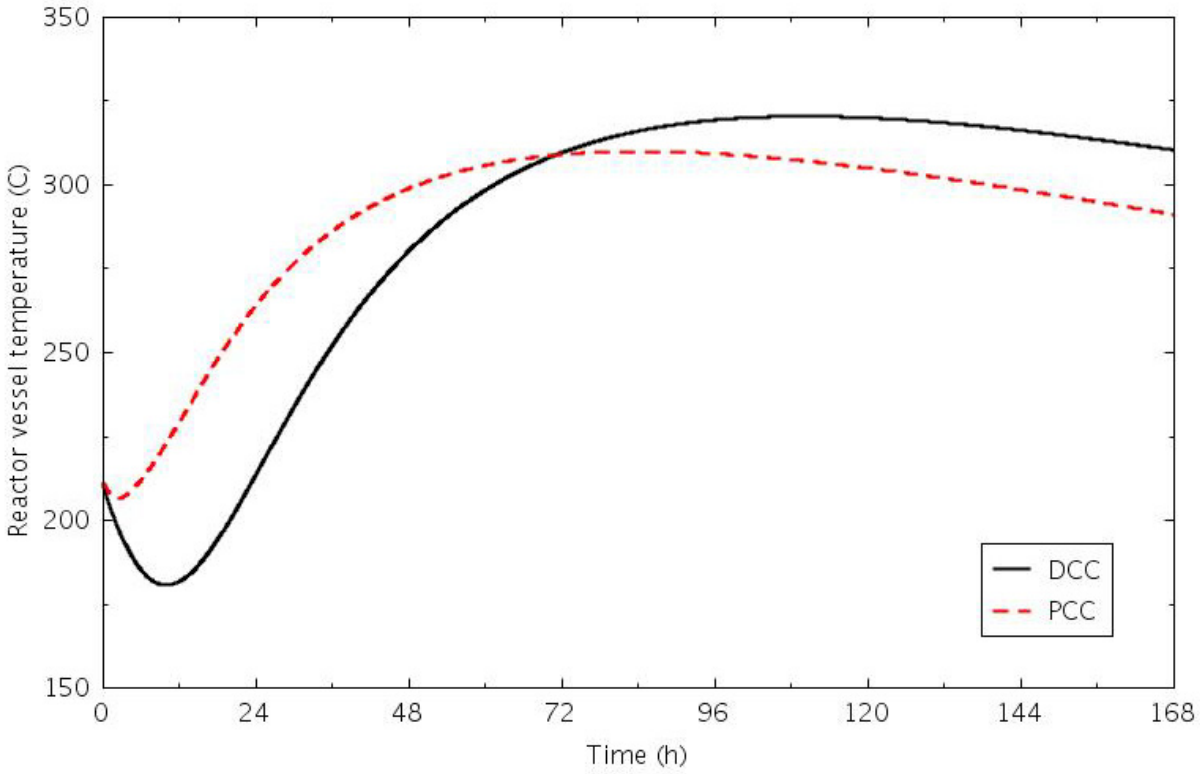

Figure 8-7. Reactor vessel temperatures for the MHTGR base case DCC and PCC simulations.

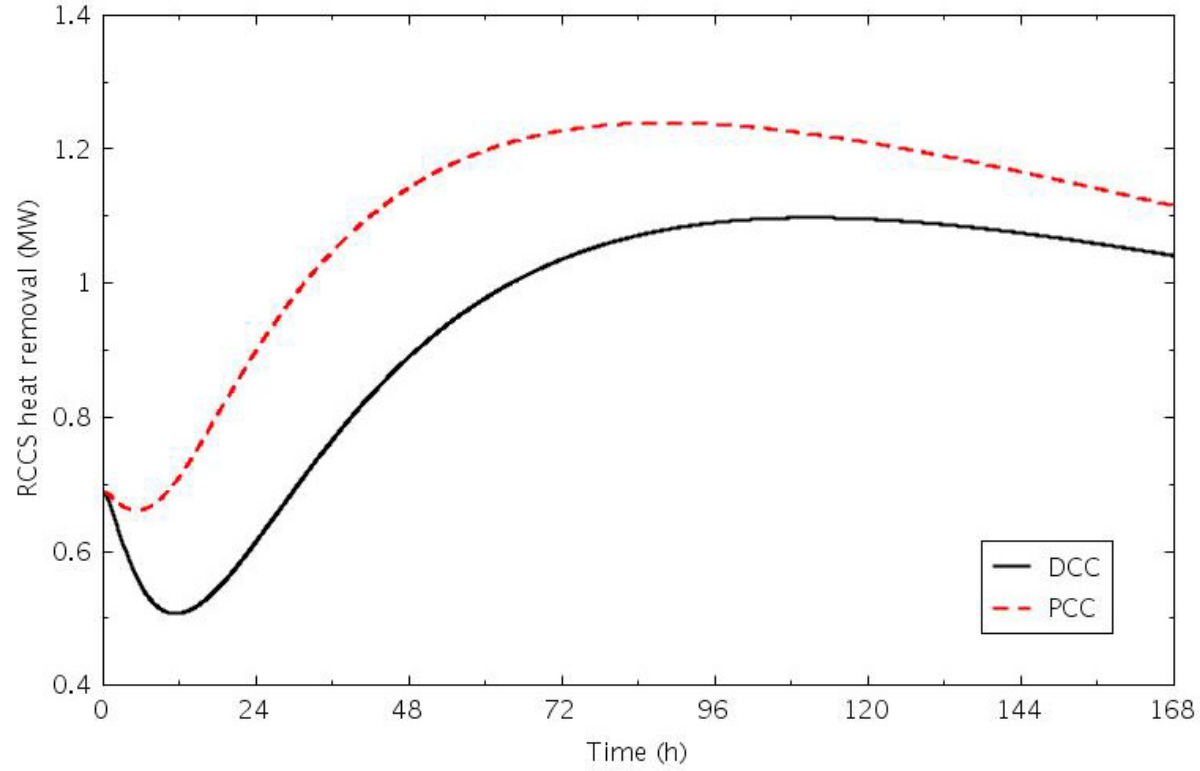

Figure 8-8. RCCS heat removal for the MHTGR base case DCC and PCC simulations.

8.1.3 Sensitivity Calculations

Several sets of sensitivity calculations were performed to investigate the effects of various geometric and phenomenological assumptions. Modeling the heat transfer across the gaps between the reflector blocks with radiation resulted in peak fuel temperatures less than 10°C higher than modeling the heat transfer with conduction. The peak reactor vessel temperatures were nearly the same.

PCC calculations were also performed in which the flow coastdown was followed by a 4-hour depressurization to either 3.0 or 0.7 MPa, as it is not known at what pressure the system will equilibrate during this event. The calculated peak fuel temperatures lay between the PCC and DCC values (Figure 8-9) with the peak temperature increasing as the pressure decreased. The peak reactor vessel temperatures were slightly lower than in the base case PCC calculation.

The most extensive sensitivity calculations looked at different gap sizes between the reflector blocks. The gap between the blocks is expected to change during an operating cycle because of irradiation and temperature effects. The base model assumed 1-mm gaps between the blocks; and the sensitivity calculations had both 3- and 4-mm gaps. This set of calculations also served as a sensitivity on the core bypass flow. While the bypass flow was 11% in the base model, it was 18% with 3-mm gaps and 25% with 4-mm gaps. During steady state, maintaining the same helium outlet temperature with higher core bypass flow rates resulted in cooler reflectors and hotter core blocks than in the base case calculations.

The higher initial fuel temperatures were carried through the transients as well. Figure 8-10 presents the peak fuel temperatures during the DCC transient for the base and bypass flow sensitivity cases. The maximum temperature increased and occurred later as the bypass flow increased, with peak values of 1038°C at 44 hours with 18% bypass flow and 1096°C at 48 hours with 25% initial bypass flow, compared with the base case peak of 935°C at 36 hours.

There was not a significant effect on the peak reactor vessel temperatures. Figure 8-11 and Figure 8-12 show the results from the DCC and PCC simulations, respectively. In the DCC, increasing bypass flow resulted in peak temperatures that were slightly lower and occurred later in the transient. The effect of the bypass flow was more pronounced in the PCC transient, where the higher bypass flows resulted in higher peak temperatures, although they occurred at about the same time in all three cases.

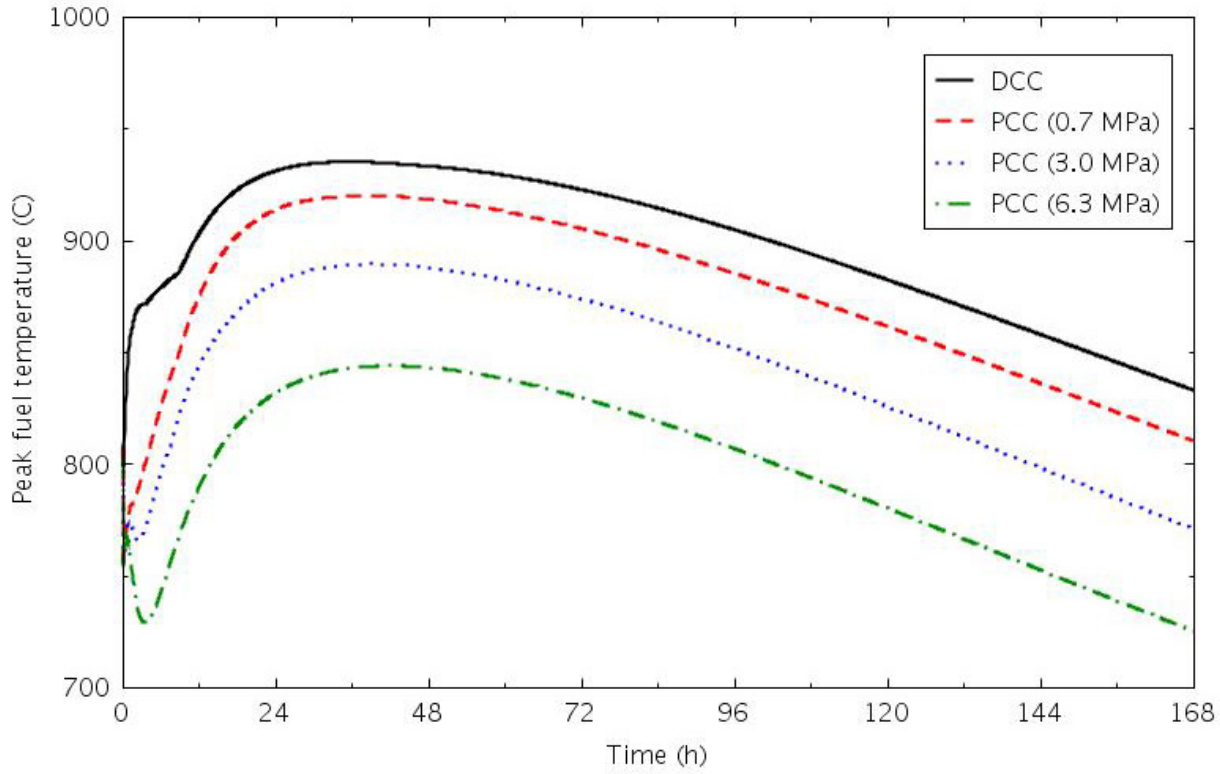

Figure 8-9. Peak fuel temperatures for the base and PCC pressure sensitivity cases.

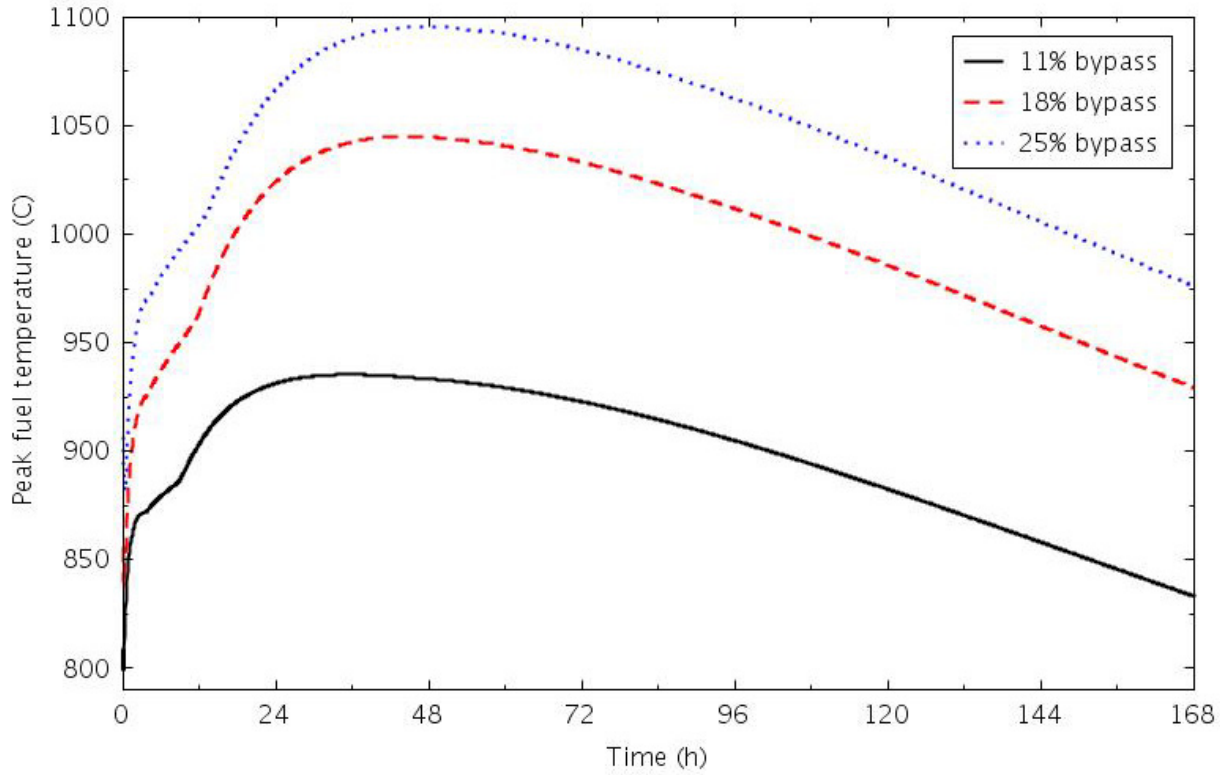

Figure 8-10. DCC transient peak fuel temperatures for the base and bypass flow sensitivity calculations.

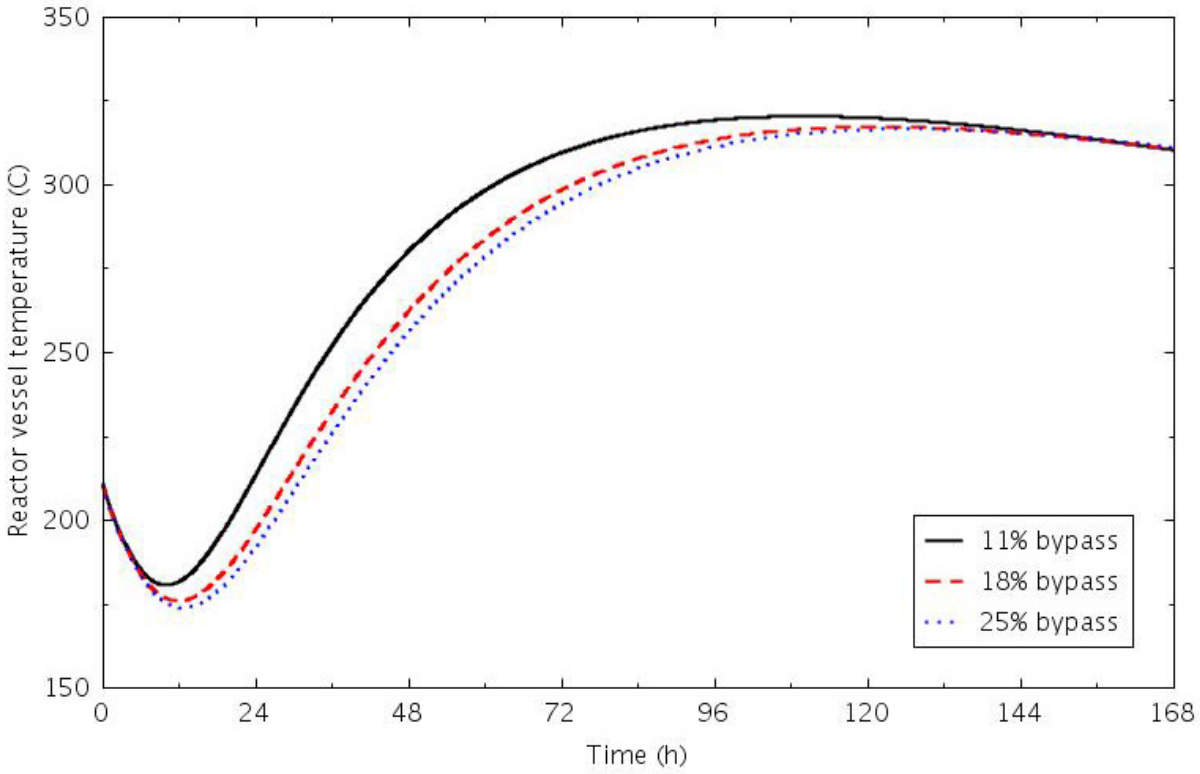

Figure 8-11. PCC transient reactor vessel temperatures for the base and bypass flow sensitivity calculations.

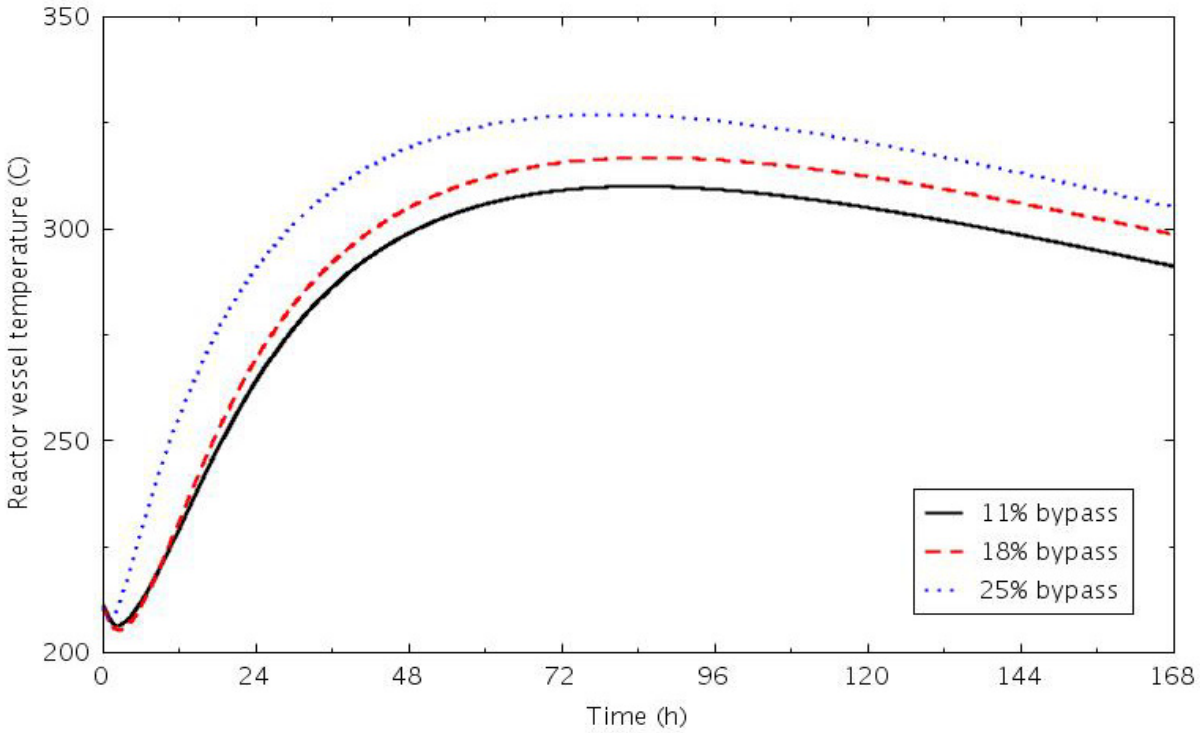

Figure 8-12. PCC transient reactor vessel temperatures for the base and bypass flow sensitivity calculations.

8.2 HTTF Modeling and Analysis

Two approaches were used in the modeling and analysis of the HTTF. Initial investigations of the transient response of the HTTF were performed while the facility design was still being developed. These investigations used modified versions of the MHTGR model described above. The second set of analyses evolved as the facility design developed, and included both thermal-hydraulic and CFD simulations of the experiment facility.

8.2.1 Scoping Analyses Using the MHTGR Model

Two major simulations were performed with RELAP5-3D: one with a reduced operating power and one with a scaled-down model of the MHTGR.

8.2.1.1 Reduced Power Simulation

One scaling compromise in the HTTF is that it cannot run at full-scaled power, although it can model full-scale decay power. To investigate the potential impact of the reduced power, DCC and PCC simulations were performed with the MHTGR model at 10% power but with decay power based on 100% operation. The full power coolant inlet and outlet temperatures were also maintained by reducing the coolant flow rate approximately 90% as well. This resulted in a core bypass flow reduction to less than 7% of the total flow.

The flow reduction also caused a significant change in the initial temperature distribution in the core and reflectors. Table 8-2 presents axial average temperatures of the principal heat structures in the reactor vessel, where it can be seen that the core temperatures have been reduced by 50-70°C while the reflector temperatures have increased by 80–150°C. The lower flow rate required to keep the steady state helium outlet temperature at 687°C resulted in the flow in the gaps around the reflector blocks changing from turbulent to laminar flow, with a consequential reduction in the convective heat transfer. Flow through the coolant holes in the core blocks remained turbulent.

Transient calculations were then performed in which the steady state power was held constant until the (350 MW) decay power dropped below 35 MW, after which the power followed the decay curve. Figure 8-13 compares peak fuel temperatures from the base and 10% power DCC calculations, and Figure 8-14 compares them for the PCC calculations. In both cases, the higher initial reflector temperatures resulted in higher, earlier peak fuel temperatures.

Reactor vessel temperatures for the two conduction cooldown transients are shown in Figure 8-15 and Figure 8-16. As for the fuel, the reduced power case peak vessel temperatures are higher and earlier in the sensitivity calculation than in the base case.

While the peak fuel and vessel temperatures were shifted higher and earlier, the calculated trends of the curves were similar for both the DCC and PCC transients. The results of these simulations show that at reduced operating power, a full decay power model can produce representative transient response.

Table 8-2. Calculated MHTGR steady state structure average temperatures at 350 and 35 MW.

Structure	350 MW Case	35 MW Case
Central reflector, Ring 1	305°C	458°C
Central reflector, Ring 2	315°C	459°C
Fuel Ring 3	635°C	565°C
Fuel Ring 4	626°C	577°C
Fuel Ring 5	631°C	564°C
Side reflector, Ring 6	309°C	466°C
Side reflector, Ring 7	283°C	417°C
Side reflector, Ring 8	267°C	347°C
Core barrel	285°C	309°C
Reactor vessel cylinder	218°C	231°C

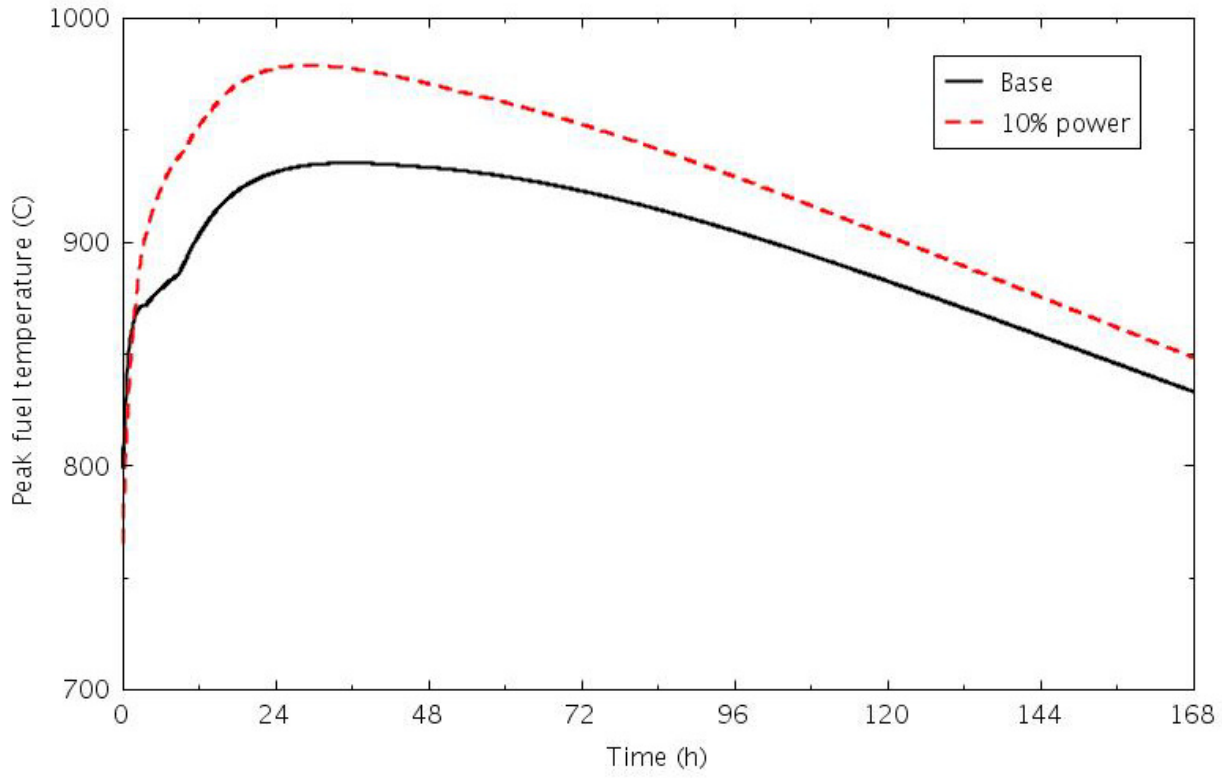

Figure 8-13. Peak fuel temperatures for the DCC base and 10% power cases.

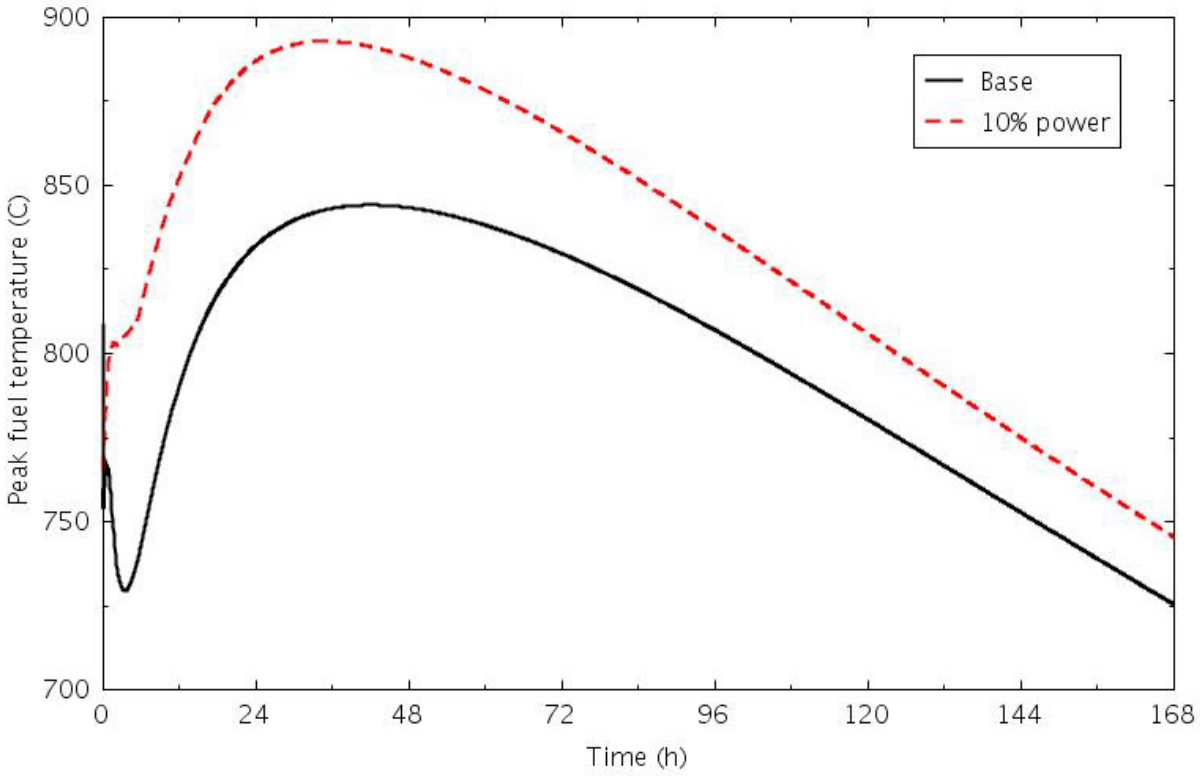

Figure 8-14. Peak fuel temperatures for the PCC base and 10% power cases.

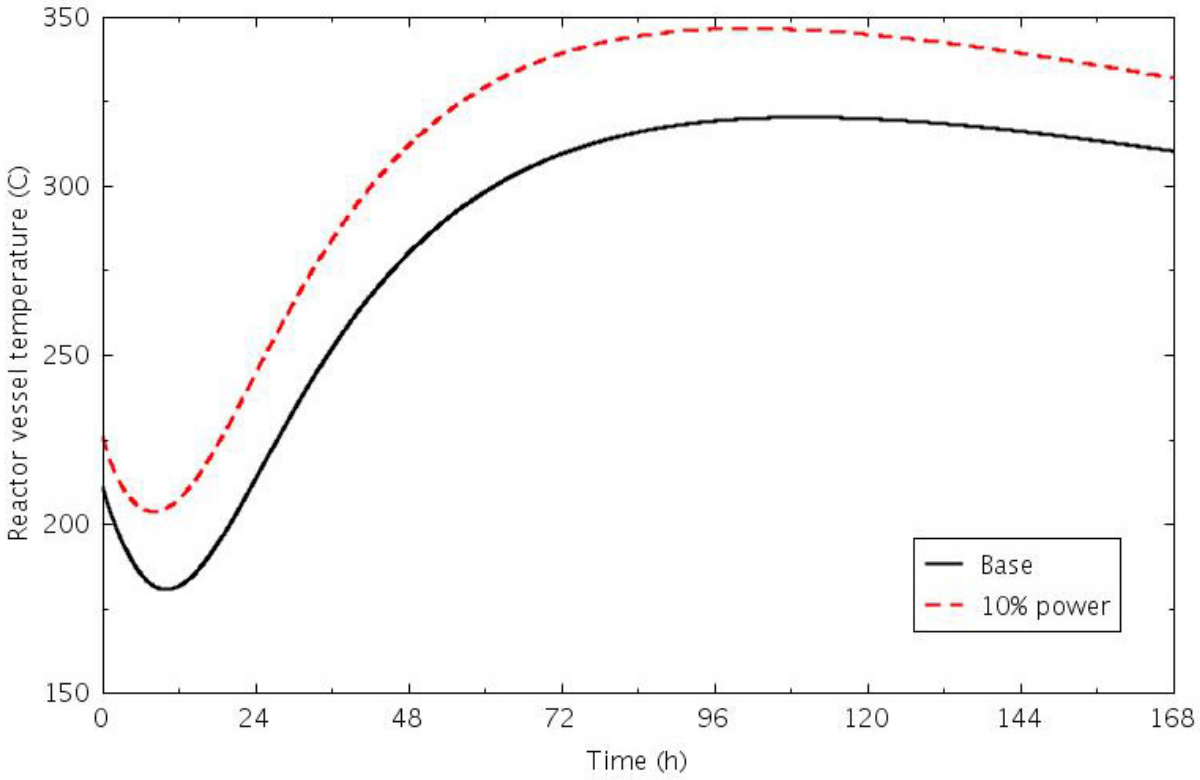

Figure 8-15. Reactor vessel temperatures for the DCC base and 10% power cases.

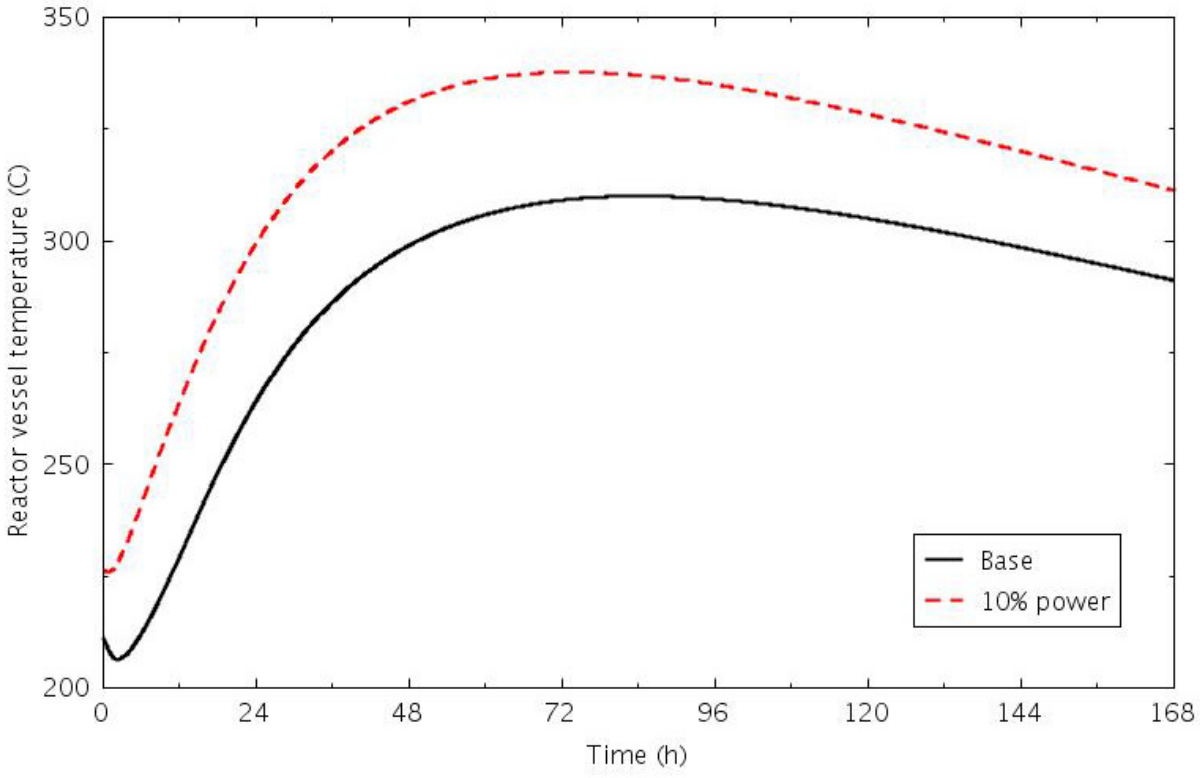

Figure 8-16. Reactor vessel temperatures for the PCC base and 10% power cases.

8.2.1.2 Scaled Model Simulation

Seeing that reasonable transient response could be obtained for the full scale model running at reduced operating power, the next step was to develop a model closer in physical dimensions to what the HTTF will be. A second sensitivity study was therefore performed in which the radial and axial scaling factors of 0.25 were applied to most of the modeled components. The fuel block coolant hole diameters were maintained at prototypic dimensions, as they will be in HTTF. The fuel and reflector block thermal properties were changed to those of a ceramic material, and the decay power used was 1/32 that of the MHTGR.

Steady state calculations were performed at several different operating power levels (the power level in HTTF was expected to be around 600 kW) with the coolant flow rate adjusted to maintain the prototypic helium inlet and outlet temperatures of 259°C and 687°C, respectively. Table 8-3 shows the axial average temperatures for the major structures in the reactor vessel. The temperatures in the scaled model were significantly higher than in the prototype, especially in the reflectors. The reason for this is that the flow in the gaps in the reflectors is laminar; the flow in the coolant holes is also laminar in the 500 and 700 kW cases. Reynolds numbers in the various coolant flow paths inside the core barrel are provided in Table 8-4. Using linear interpolation, it is estimated that the power would need to be above 1250 kW to have turbulent flow in the coolant channels. The flow in the gaps will remain laminar at any reasonable extrapolated power, but this is unimportant as the HTTF will not have gaps in the reflectors, only control rod coolant holes.

Table 8-3. Calculated steady state structure temperatures for the scaled MHTGR model.

		Scaled Model Power			
Structure	MHTGR	500 kW	700 kW	1500 kW	2000 kW
Ring 1	305°C	600°C	594°C	589°C	581°C
Ring 2	315°C	613°C	607°C	604°C	598°C
Fuel Ring 3	635°C	684°C	685°C	710°C	731°C
Fuel Ring 4	626°C	687°C	691°C	717°C	737°C
Fuel Ring 5	631°C	646°C	653°C	694°C	714°C
Ring 6	309°C	530°C	531°C	544°C	541°C
Ring 7	283°C	460°C	458°C	462°C	455°C
Ring 8	267°C	368°C	364°C	361°C	355°C
Core barrel	285°C	322°C	315°C	313°C	311°C
Reactor vessel	218°C	198°C	197°C	200°C	201°C

Table 8-4. Calculated steady-state Reynolds numbers for the scaled MHTGR model.

		Scaled Model Power			
Flow Channel	MHTGR	500 kW	700 kW	1500 kW	2000 kW
Gap 0-1	2367	2	3	10	21
Gap 1-2	2317	2	3	10	20
Reflector holes	18755	241	335	868	1264
Fuel Ring 3	37171	779	1162	2670	3570
Fuel Ring 4	37849	781	1162	2683	3578
Fuel Ring 5	37314	844	1231	2696	3630
Gap 5-6	2108	2	3	10	20
Gap 6-7	2372	2	3	13	25
Gap 7-8	2408	3	4	16	31
Core barrel gap	12592	4	6	25	49

Figure 8-17 presents the peak fuel temperatures from DCC calculations at four different power levels. The peak temperature is considerably higher than in the MHTGR simulations because the vessel structures started at much higher temperatures. The reactor vessel temperature at the location of the highest temperature is shown in Figure 8-18. The peak temperatures are somewhat lower than for the MHTGR. In both figures, little difference in response is seen among the initial power levels. PCC simulations with these initial powers showed similar responses.

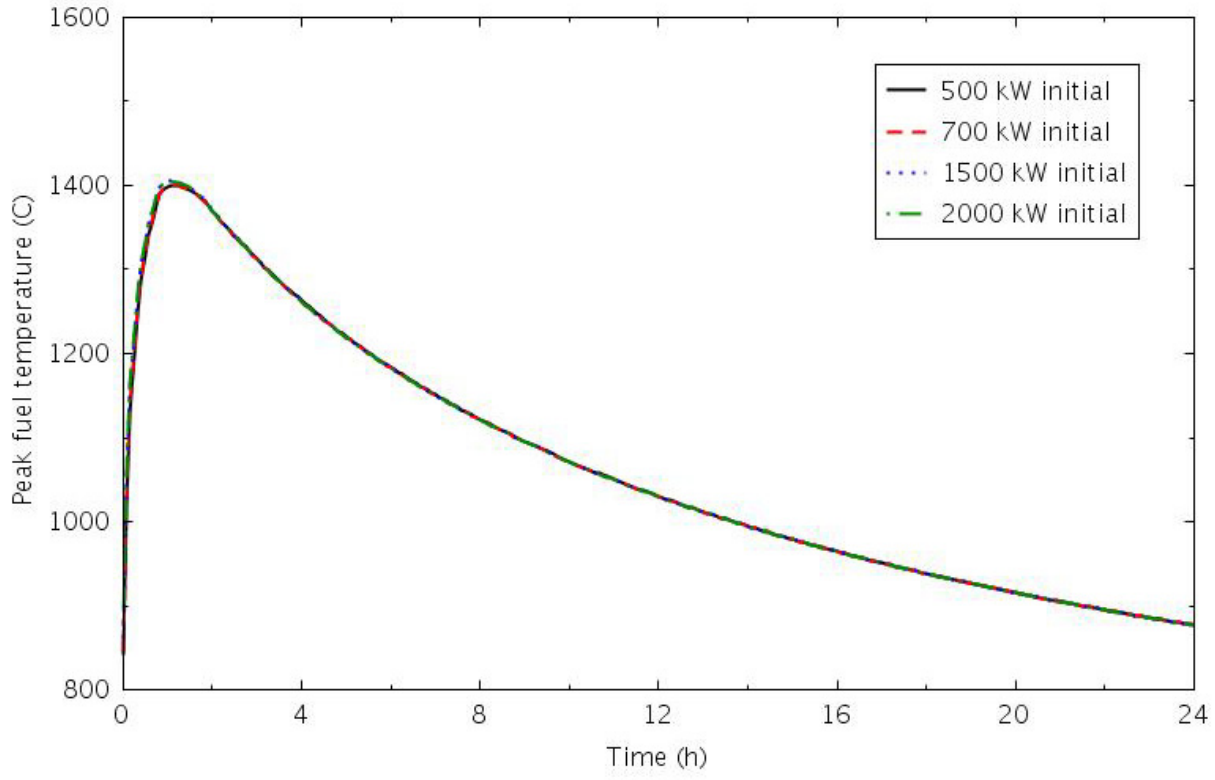

Figure 8-17. DCC transient peak fuel temperatures for the scaled MHTGR model.

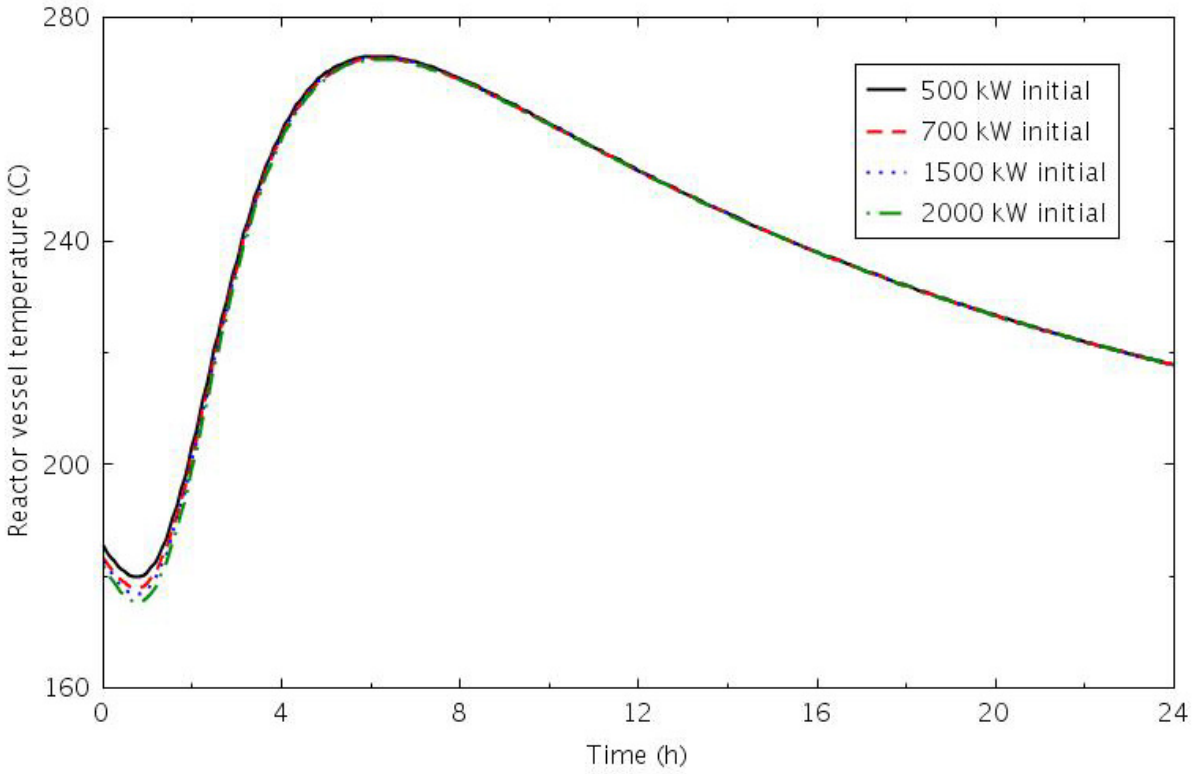

Figure 8-18. DCC transient reactor vessel temperatures for the scaled MHTGR model.

8.2.2 Scoping Analyses Using HTTF Models

The scoping analyses using the MHTGR model showed that a scaled facility operating at reduced steady state power may be able to produce transient response similar to that of the reference reactor system. However, concerns about the steady-state temperatures in the reactor vessel components were identified, particularly with respect to laminar flow in the core. Since the scaled MHTGR model contained core bypass flow paths that will not exist in the HTTF, and preliminary drawings of the HTTF were now available, the next step in the process was to model the HTTF. Both RELAP5-3D and STAR-CCM+ models were developed.

8.2.2.1 RELAP5-3D Input Model Description

The RELAP5-3D input model for the HTTF was developed with the objective of being as consistent with the MHTGR input model as practical, just as the objective of the facility is to be as representative of the reference plant as scaling will allow. The focus of the model was the reactor vessel; a simplified RCCS was modeled as a heat structure with a constant surface temperature. Flow boundary conditions were applied at the reactor vessel flow inlet and outlet.

Figure 8-19 shows the reactor vessel nodalization for the model. The model is similar to the MHTGR model, but with fewer flow paths inside the core barrel. Note that the gaps on either side of the permanent reflector (Components 164 and 166) are only connected to the outlet plenum, as the upper plenum plate prevents flow from entering the tops of these channels.

A cross-section of the model in the core region is shown in Figure 8-20. The central reflector is modeled in two parts, a solid-center cylinder surrounded by a ring with six (6) 0.938-in.-diameter control rod holes. Figure 8-21 shows how this outer region is modeled, as a number of coolant holes are surrounded by a proportional amount of ceramic material. The core region is modeled as three rings containing heater rods, coolant holes, and ceramic. The unit cell modeled in these regions is also shown in Figure 8-21. The heater rod is modeled as a heat structure that radiates to the ceramic surrounding a coolant hole. The side reflector was modeled similarly to the central reflector, with a ring of ceramic containing twenty-four (24) 0.938-in.-diameter control rod holes next to the core region with an outer ring of solid material. One-mm gaps were assumed to separate the permanent reflector from the side reflector and the core barrel. Heat transfer between the core and central and side reflectors was modeled using conduction enclosures, with radiation modeled across the gaps between the other structures.

The heater rods were all assumed to have the same power and a flat axial power shape. Flow resistance through the reflector cooling holes was adjusted to provide a total core bypass flow of about 11%. The ceramic material was assumed to have a thermal conductivity of 4W/m-K and a volumetric heat capacity of 2.3e6 J/m^3-K.

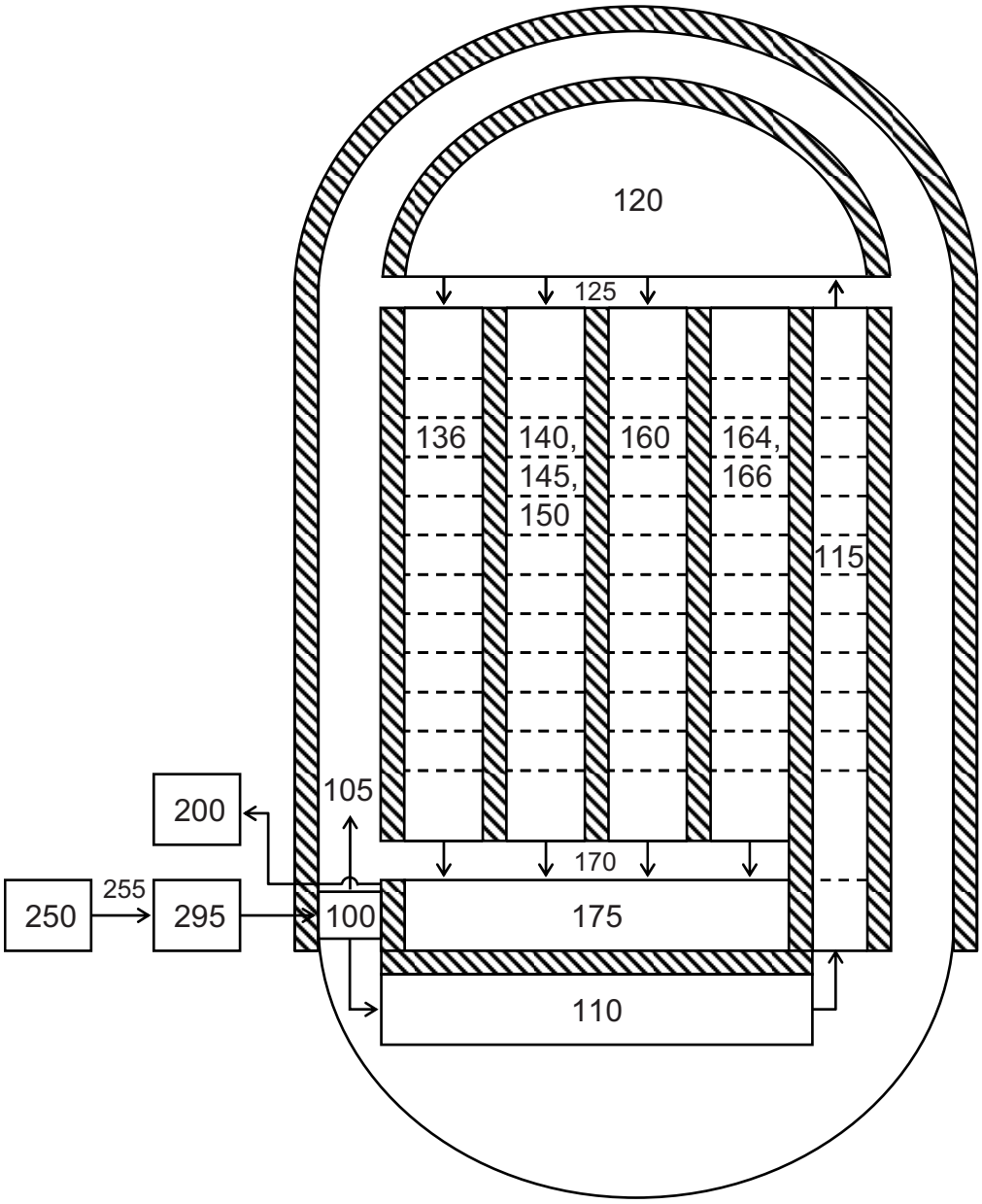

Figure 8-19. RELAP5-3D nodalization of the HTTF reactor vessel.

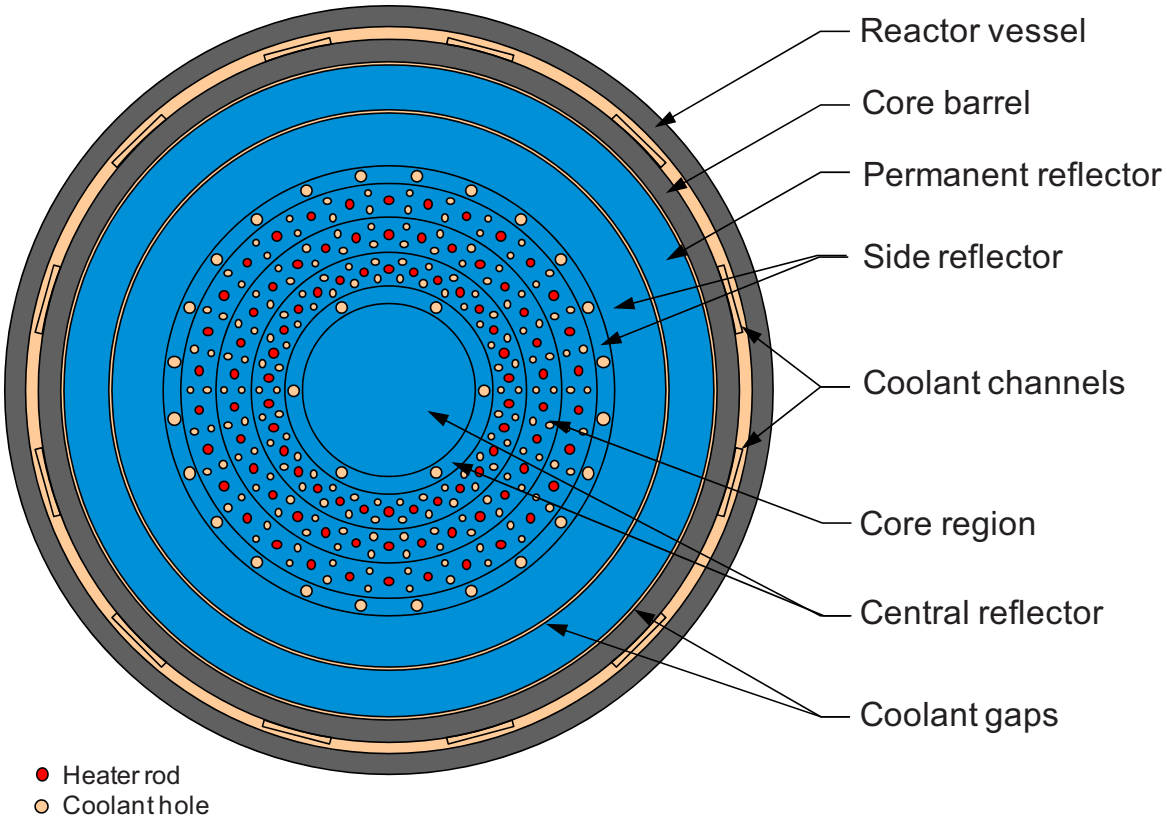

Figure 8-20. Cross-section of the RELAP-3D model of the HTTF reactor vessel.

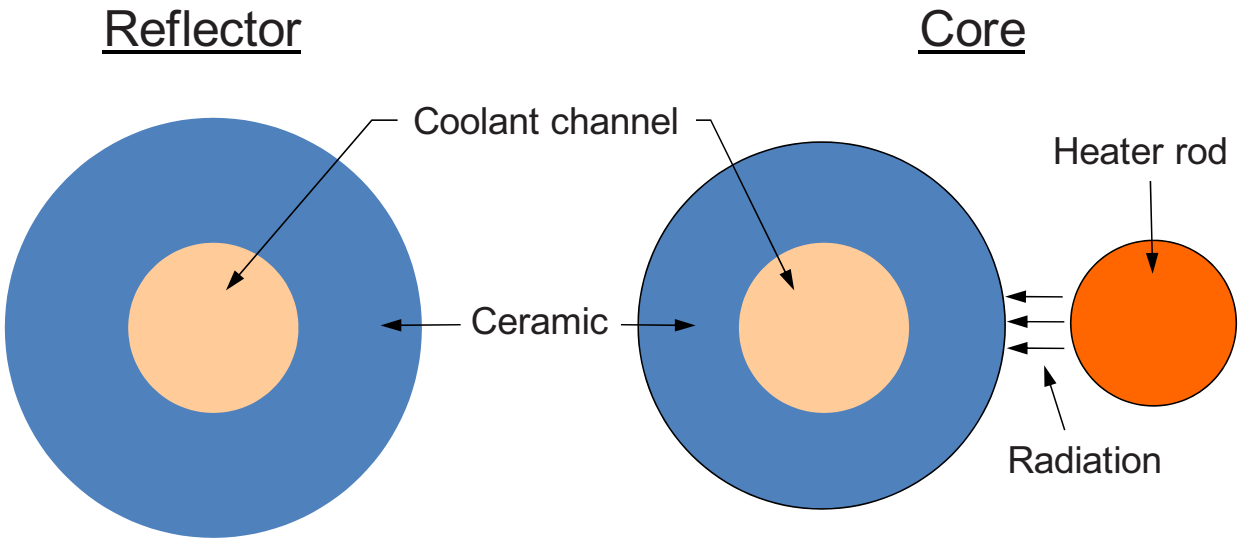

Figure 8-21. Unit cells used in the RELAP5-3D model of the HTTF reactor vessel.

8.2.2.2 STAR-CCM+ Input Model Description

A STAR-CCM+ model of the HTTF core and reflectors was developed to provide a more detailed prediction of the steady state temperature distribution. This three-dimensional model can preserve azimuthal variations in the facility that the RELAP5-3D model two-dimensional approach loses.

The model included the central and side reflectors and the heater rod region in the radial direction, and the upper reflector, heated region, and lower reflector in the axial direction. A 1/6 symmetry model was used that included the cooling holes, heater rods and surrounding helium gap, the control rod holes in the central and side reflectors, and the bulk ceramic material.

Three different reflector control rod hole geometries were modeled: the base geometry, a model with twice as many holes but half the diameter, and a model with one additional large hole in the central reflector and two additional large holes in the side reflector. The mesh for these three geometries is shown in Figure 8-22 (on the left, right, and center, respectively). An unstructured tri- and quad-mesh was generated on the cross-sectional face, and extruded to generate a structured mesh in the axial direction; Figure 8-23 shows a sample of the axial mesh.

Each heater rod was modeled as having the same power with a flat axial power shape. Heat generated in the heater rods was conducted across the helium gap to the surrounding ceramic, and from there to the rest of the model. Heat transfer to the helium flowing through the core was through convection and conduction. The radial and azimuthal edges of the model were modeled as adiabatic.

The pressure boundary conditions applied at the top and bottom of the model were taken from the RELAP5-3D steady-state calculations. The inlet temperature was specified to be 259°C. A k-ε turbulence model was used for the helium flowing through the core.

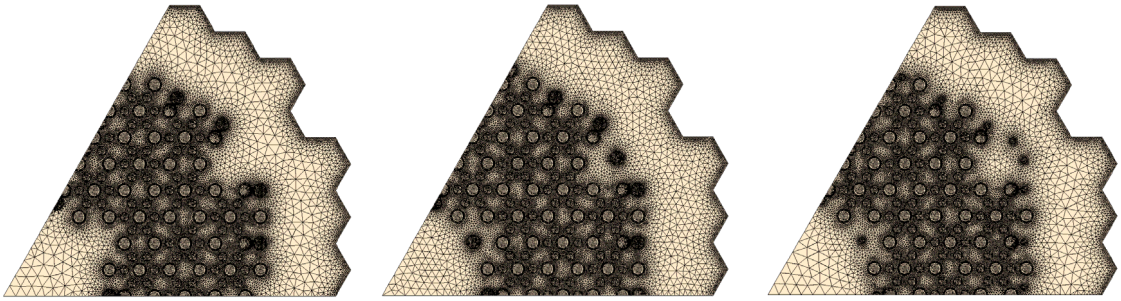

Figure 8-22. Cross section of the STAR-CCM+ HTTF model for three control rod hole configurations.

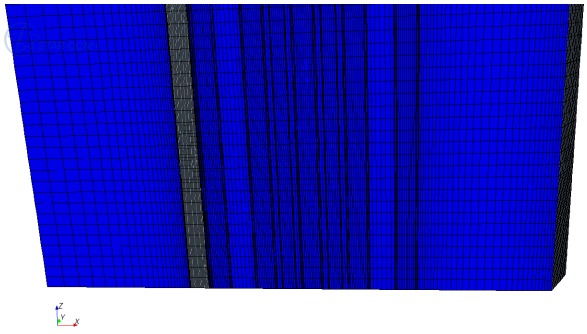

Figure 8-23. Lower block axial mesh of the STAR-CCM+ HTTF model (1.27-cm mesh height).

8.2.2.3 Steady-State Simulations

Preliminary steady-state calculations were run with a smaller RELAP5-3D model to investigate the effect of different control rod hole configurations on the core temperatures; this model assumed adiabatic conditions on the outside of the core barrel. These simulations showed that more, smaller holes may be able to provide reflector temperatures that were close to the nominal configuration, but with less bypass flow. These calculations had the drawback that the two-dimensional modeling approach results in the reflector rings with the control rod holes acting as thermal shields for the rest of the reflector. The azimuthal variations in the heater rod and coolant channel placement suggest that locally hotter reflector temperatures are likely to occur. Therefore, STAR-CCM+ calculations were also performed for two control rod hole configurations: the base case, and one in which the number of holes in both the central and side reflectors was doubled, but the hole diameter was reduced to 0.5 in. Figure 8-22 showed the location of the additional holes.

Steady-state calculations were performed at core power levels of 0.6, 1.5, and 2.0 MW. Since the current estimate of the HTTF power is 2.2 MW, the results from the 2.0 MW case will be presented. Table 8-5 contains the steady-state flow parameters from the calculations. Figure 8-24 and Figure 8-25 present the temperatures calculated by STAR-CCM+ near the core axial midplane for the base and sensitivity calculations. Figure 8-26 andFigure 8-27 show temperatures lower in the core for the same cases. Both sets of figures showed that the reduced flow in the coolant holes, despite being more distributed around the heater rods, was not as effective in cooling either the inner or outer reflector. The hole added in the central reflector did effectively reduce the hot spot between the four heater rods.

STAR-CCM+ calculations were also performed with a total core power of 2.2 MW for the base control rod hole configuration and for the configuration with one additional control rod hole in the central reflector and two additional holes in the side reflector (18 additional holes in a full core model), as shown in the middle drawing of Figure 8-22. The additional holes added were identical to those in the base model, with no adjustments made to increase the flow resistance so that the ~11% bypass flow would be maintained. Results of these steady state calculations are provided in Table 8-6, where it is seen that the higher bypass flow resulted in a coolant outlet temperature that was a bit lower than desired, although it was considered adequate for the scoping analyses being performed.

Temperatures near the core midplane for the base and sensitivity cases are shown in Figure 8-28 and Figure 8-29, respectively; temperatures in the bottom portion of the core are presented in Figure 8-30 and Figure 8-31. Near the core midplane, which is close to a surrogate for the axial average temperature, the additional coolant holes have eliminated the hot spots in the middle of the inner core periphery and at the edges of the outer core periphery. The central reflector temperature has been reduced by about 200°C, and the side reflector by about 100°C. The reductions are about twice as large in the bottom portion of the core. Figure 8-31 shows that the highest ceramic temperatures have been localized around the heater rods and that they are around 1150°C, compared to around 1340°C in the base case.

These sensitivity calculations have shown that changing the configuration of the control rod (coolant) holes in the reflectors can have a significant impact on the initial temperatures in the reflectors. Further analyses should be performed to determine the configuration and flow rates that would provide the desired initial temperature distribution in HTTF.

Table 8-5. Calculated HTTF steady-state values for the control rod hole sensitivity at 2.0 MW.

Parameter	RELAP 5-3D	STAR-CCM+	RELAP 5-3D	STAR-CCM+
Number of control rod holes	30	30	60	60
Control rod hole diameter (in.)	0.938	0.938	0.5	0.5
He flow rate (kg/s)	0.897	0.966	0.898	0.884
He inlet temperature (°C)	259	259	259	259
He outlet temperature (°C)	687	675	687	666
Bypass fraction	0.18	0.15	0.08	0.07

Table 8-6. STAR-CCM+ calculated HTTF steady-state values for the control rod hole sensitivity at 2.2 MW.

Parameter	Base case	Sensitivity case
Central reflector control rod holes	6	12
Side reflector control rod holes	24	36
He flow rate (kg/s)	1.10	1.15
He inlet temperature (°C)	259	259
He outlet temperature (°C)	661	644
Bypass fraction	0.10	0.14

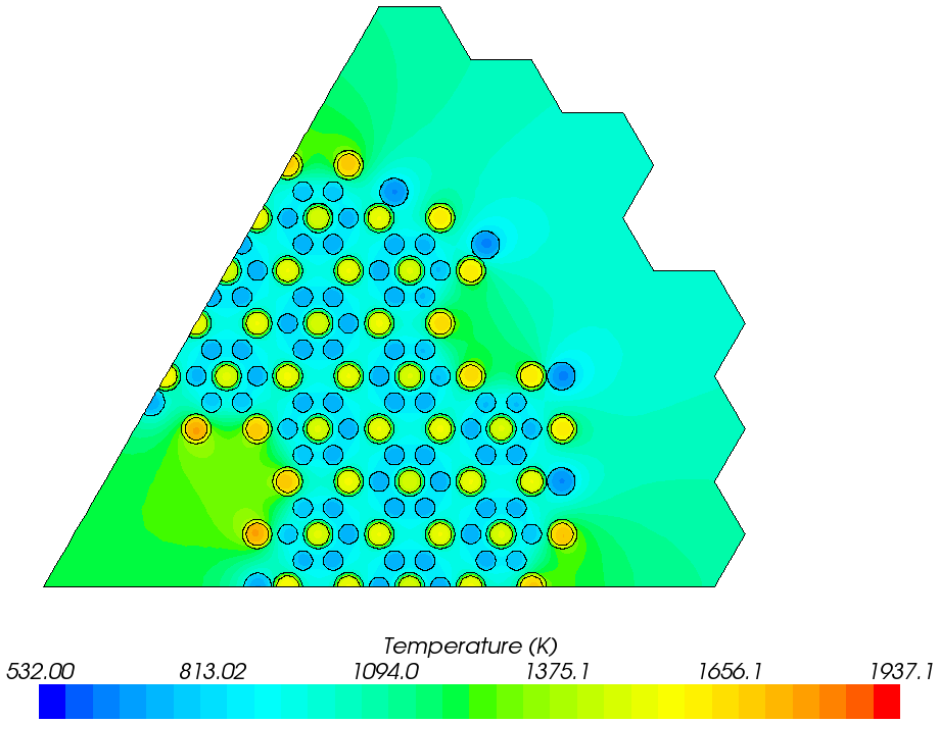

Figure 8-24. Calculated HTTF temperatures near the core midplane for the 2.0 MW base case.

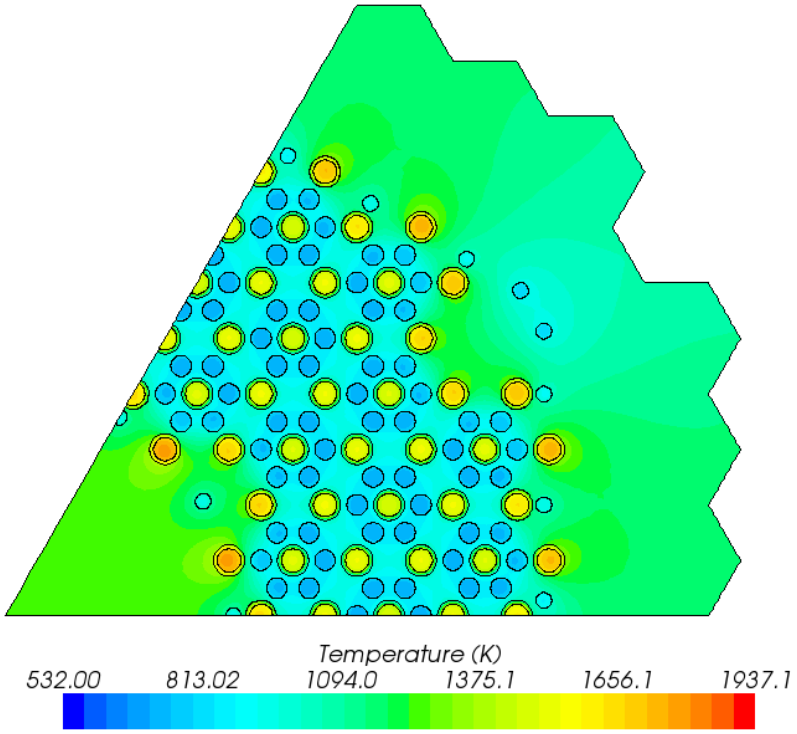

Figure 8-25. Calculated HTTF temperatures near the core midplane for the 2.0 MW control rod hole sensitivity case.

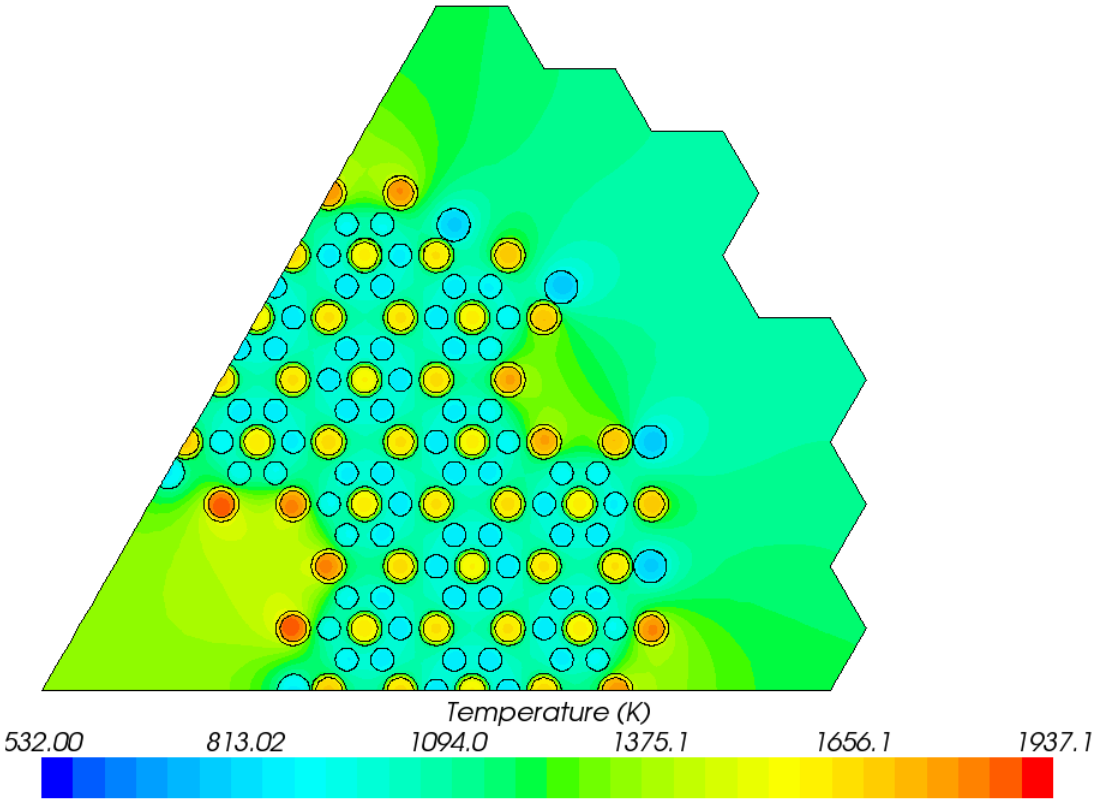

Figure 8-26. Calculated HTTF temperatures in the bottom portion of the core for the 2.0 MW base case.

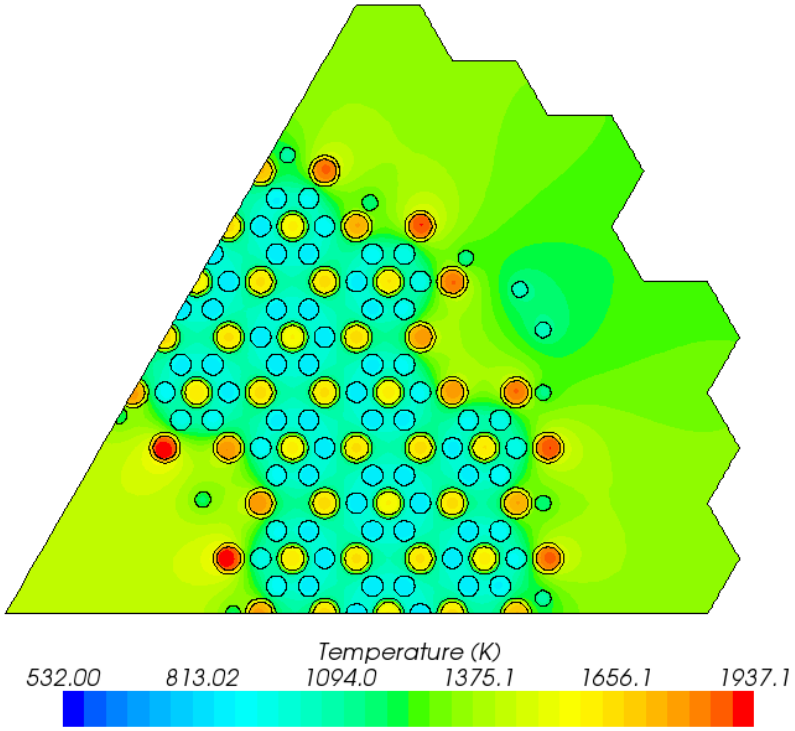

Figure 8-27. Calculated HTTF temperatures in the bottom portion of the core for the 2.0 MW control rod hole sensitivity case.

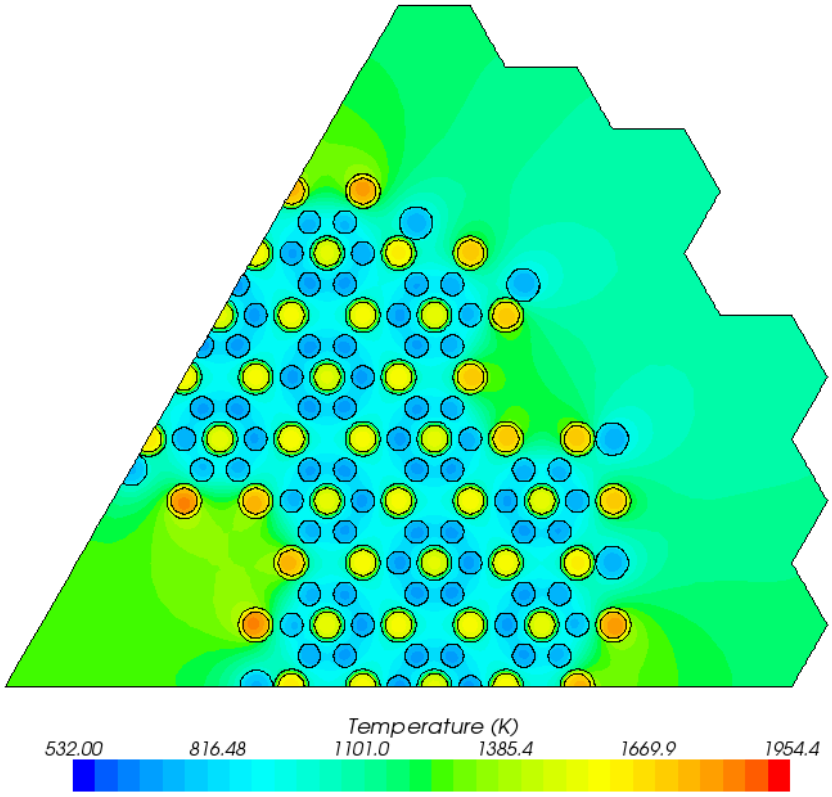

Figure 8-28. Calculated HTTF temperatures near the core midplane for the 2.2 MW base case.

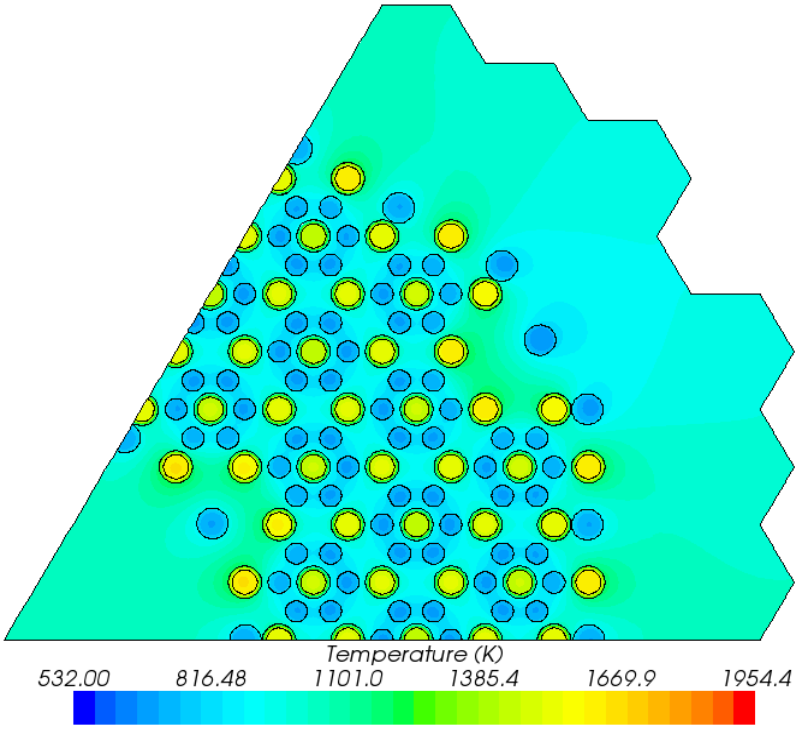

Figure 8-29. Calculated HTTF temperatures near the core midplane for the 2.2 MW control rod hole sensitivity case.

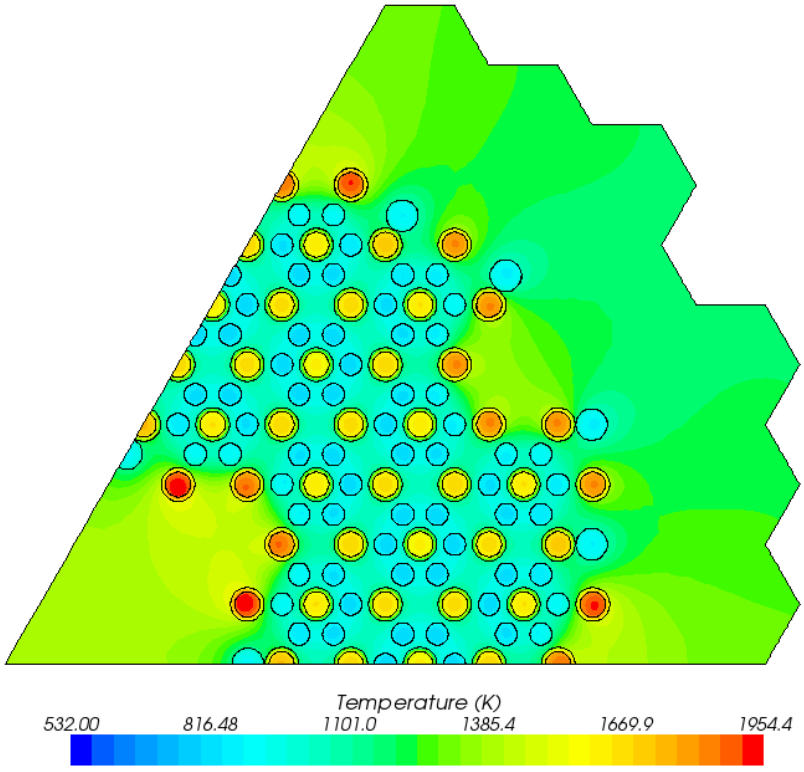

Figure 8-30. Calculated HTTF temperatures in the bottom portion of the core for the 2.2 MW base case.

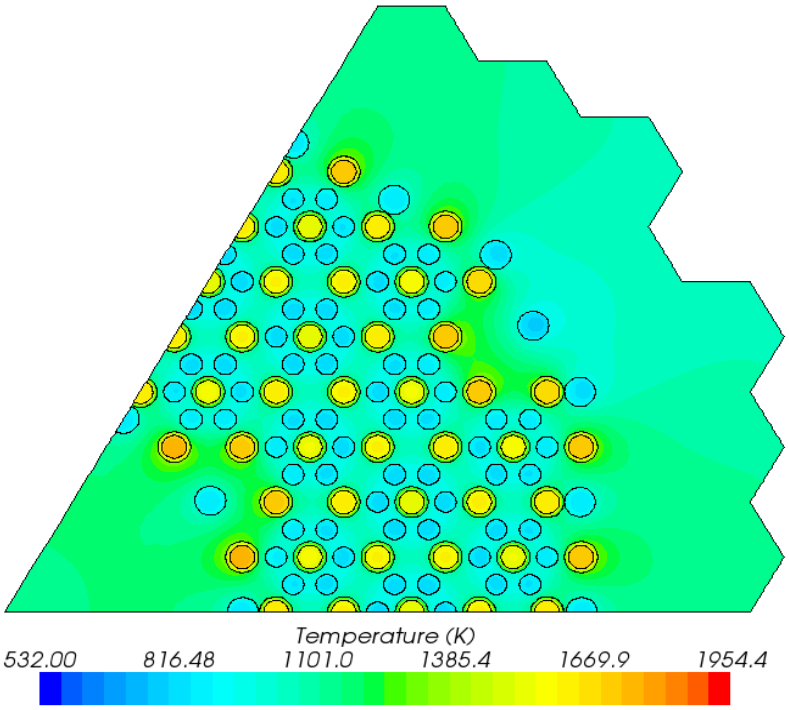

Figure 8-31. Calculated HTTF temperatures in the bottom portion of the core for the 2.2 MW control rod hole sensitivity case.

8.3 Summary

A number of computer simulations have been performed to support the design of the HTTF. Scoping RELAP5-3D calculations of the MHTGR were performed to provide a reference case for investigations of the HTTF. The initial calculations of the HTTF used a reduced scale model of the MHTGR. Subsequent simulations used facility drawings to develop preliminary RELAP5-3D and STAR-CCM+ models of the experiment.

Two principal issues were identified in the course of the analyses. The first is the flow rate through the core during steady-state operation. Initial investigations showed that maintaining the reference plant core inlet and outlet helium temperatures at reduced power requires a much lower flow rate. At the initial HTTF power level of about 600 kW, this would result in all of the flow paths through the core being in laminar, rather than turbulent, flow. The associated reduction in the convective heat transfer coefficient resulted in all of the core and reflectors being much hotter than in the MHTGR. The higher initial temperatures will lead to much higher temperatures during the transient experiments, which besides being atypical of the plant response, may pose challenges to the material integrity of the facility. It was estimated that the transition to turbulent flow would occur at a power level of about 1250 kW.

The second issue identified is the steady-state temperature of the central and side reflectors, which were much colder in the MHTGR simulations than in the HTTF. The lack of convective cooling provided by the helium flow in the gaps between the blocks in the MHTGR was the primary reason, as the HTTF is mostly a solid block of ceramic in which the control rod holes provide the only flow path for cooling the reflectors. Since there are no control rods in these holes (they are there for similarity with the MHTGR, which has control rods in the reflectors), the number, size, and location of the holes should be designed to provide sufficient cooling so that the initial reflector temperature distribution is representative of that in the reference plant.

9. References

Dittus, F.W., and Boelter, L.M.K., 1930, "Heat transfer in automobile radiators of the tubular type," *U. California Publ. Engr*., Vol 2, p. 443.

Kreith, F., 1958, *Principles of Heat Transfer,* second edition, International Textbook Co., Scranton, Pa.

Lewis, E.E., 1977, *Nuclear power reactor safety*, John Wiley, New York, pp. 398-302.

Math Soft., 2001, *MathCad 2001 User's Guide*, Math Soft, Inc.

McAdams, W.H., 1954, *Heat Transmission*, 3rd ed., McGraw-Hill, New York.

National Institute of Standards and Technology (NIST) Webbook, http://webbook.nist.gov, accessed September 13, 2010.

DOE/HTGR-86-024, 1986, *Preliminary Safety Information Document for the Standard MHTGR*, 1986, Stone & Webster Engineering Corp, HTGR-86-024.

Shapiro, A.H., 1953, *The dynamics and thermodynamics of compressible fluid flow-volume*, Vol. 1, Ronald Press, New York, p. 84.

Weinberg, G. M, 1975, An Introduction to General Systems Thinking, J. Wiley & Sons, New York.

Woods, et al., 2009, *Scaling analysis for the very high temperature reactor test facility at Oregon State University*, OSU-HTTF-000000-TECH-oo1-R0/DRAFT.

Zuber, N., 1991, "Appendix D: A Hierarchical, Two-Tiered Scaling Analysis," *An Integrated Structure and Scaling Methodology for Severe Accident Technical Issue Resolution*, NUREG/CR-5809; EGG-2659, November.

Appendix A

Computer Code Quality Assurance

Appendix A

Computer Code Quality Assurance

Table A-1. Quality assurance information for the computer codes used for the computer simulations.

Computer Code	Version	Vendor	V&V Status	INL Computer	Computer Operating System
FlexPdE[o]	Student	PdE Solutions Inc., Spokane Valley, WA.	Unknown	Macintosh G5	OSX10.4.11
FLUENT	6.3.26	FLUENT Inc./Ansys Inc., 10 Cavendish Court, Centerra Resource Park, Lebanon, NH, 03766 USA	Vendor holds ISO 9001 certification	Dell PowerEdge 1950 distributed memory cluster (Helios)	OpenSUSE 11.1
GAMBIT	2.4.6	FLUENT Inc./Ansys Inc., 10 Cavendish Court, Centerra Resource Park, Lebanon, NH, 03766 USA	Vendor holds ISO 9001 certification	Dell PowerEdge 1950 distributed memory cluster (Helios)	OpenSUSE 11.1
MathCad	2001	Mathsoft, Inc, 101 Main St, Cambridge, MA 02142	Vendor holds ISO9001 certification	Macintosh G5	OSX10.4.11
RELAP5-3D	2.95is	Idaho National Laboratory	INL controlled.	Macintosh GSI	Suse Linux 1X9
STARCCM+	3.04.20	CD-adapco, 60 Broadhollow Road, Melville, NY 11747	Vendor holds ISO 9001 certification	SGI Altix ICE 8200 distributed memory blade cluster (Ice Storm)	SUSE Linux Enterprise Server 10 Service Pack 2, with SGI Propack 6
STARCCM+	5.02.009	CD-adapco, 60 Broadhollow Road, Melville, NY 11747	Vendor holds ISO 9001 certification	SGI Altix ICE 8200 distributed memory blade cluster (Ice Storm)	SUSE Linux Enterprise Server 10 Service Pack 2, with SGI Propack 6

o. PdE Solutions, Inc., Spokane Valley, Wa, 2009.